



University of Bradford eThesis

This thesis is hosted in [Bradford Scholars](#) – The University of Bradford Open Access repository. Visit the repository for full metadata or to contact the repository team



© University of Bradford. This work is licenced for reuse under a [Creative Commons Licence](#).

**ANALYSIS OF ANTI-CANCER DRUG PENETRATION THROUGH
MULTICELL LAYERS *IN VITRO*.**

**The development and evaluation of an *in vitro* model for assessing the
impact of convective fluid flow on drug penetration through avascular
cancer tissues.**

Hafiz Antar Mohammad MAKEEN

**Submitted for the degree of
Doctor of Philosophy (PhD)**

**Institute of Cancer Therapeutics (ICT),
University of Bradford**

2012

Abstract:

Analysis of anti-cancer drug penetration through multicell layers *in vitro*.

Hafiz A. M. Makeen,

Key words: Drug penetration, Drug delivery, Solid tumours, Multicell layers, Interstitial fluid pressure, Convective fluid flow, Convection, Hydrostatic pressure, Chemotherapy resistance.

High interstitial fluid pressure (IFP) in tumours is recognized as a barrier to drug delivery resulting in reduced efficacy. High IFP impedes the normal process of convective fluid flow (CFF) from blood vessels into the interstitium. The aim of this study was to develop an *in vitro* model that could be used to measure CFF and to study its effects on drug delivery. The model consists of a transwell cell culture insert which supports the growth of multicell layers (MCL) on collagen coated membranes. A graduated tube is inserted into the transwell and a pressure gradient is applied across the membrane by raising the volume of medium in the tube above that of the bottom chamber. CFF is determined by measuring the weight of medium in the bottom chamber as a function of time. CFF was inversely proportional to MCL thickness and 41.1±3.6µm thick MCL has completely stopped CFF. Using a physiologically relevant hydrostatic pressure of 28mmHg, a CFF of 21µL/min was recorded using a DLD-1 MCL that was 12.21±3.2µm thick. Under these conditions, the rates of penetration of doxorubicin, imatinib and gefitinib were respectively 42, 26 and 13 folds greater than when no CFF exists. Reversing the CFF so that it opposed the drug diffusion gradient significantly impairs drug penetration. In conclusion, a novel *in vitro* model for assessing the impact of CFF on drug delivery has been developed. This model could be used to evaluate strategies designed to increase drug delivery to solid tumours by modifying the CFF.

Acknowledgements:

I am heartily thankful to my supervisors, Dr. Roger M. Phillips and Dr. Paul M. Loadman, who have supported me throughout my thesis with their patience and knowledge. I would like to thank them for their encouragement and efforts. Without them, this project and this thesis would not have been completed. One simply could not wish for better or friendlier supervisors.

I would like to express my gratitude to everyone at the Institute of Cancer Therapeutics for their help and support. I offer my regards and blessings to all of those who supported me in any respect during the completion of the project.

I would like to thank my parents, family members and friends for their support and understanding throughout my studies.

Lastly, I would like to express my appreciation to my wife Amna whose dedication, love and persistent confidence in me, has taken the load off my shoulder. I would like also to thank my sons Moaaz and Murad. Albeit their distraction, they were always filling my heart with encouragement, love and happiness.

Table of contents:

ABSTRACT:	II
ACKNOWLEDGEMENTS:	III
TABLE OF CONTENTS:	IV
LIST OF FIGURES:	VIII
LIST OF TABLES:	XII
LIST OF ABBREVIATIONS:	XIV
1. INTRODUCTION:	19
1.1 GENERAL INTRODUCTION TO THE CANCER PROBLEM:	19
1.2 TREATMENT MODALITIES OF CANCER:	26
1.3 LIMITATIONS OF CHEMOTHERAPY:	33
1.4 LIMITED DRUG DELIVERY TO SOLID TUMOURS AS A FORM OF DRUG RESISTANCE:	37
1.5 FACTORS INFLUENCING DRUG PENETRATION INTO SOLID TUMOURS:	40
1.6 IMPACT OF (IFP), (HP) AND (CFF) ON DRUG PENETRATION:	48
1.7 METHODS USED TO STUDY DRUG PENETRATION INTO SOLID TUMOURS:	53
1.7.1 <i>In vitro techniques:</i>	53
1.7.2 <i>In vivo techniques:</i>	57
1.8 STRATEGIES USED TO IMPROVE DRUG PENETRATION INTO SOLID TUMOURS:	60
1.8.1 <i>Manipulating tumour vasculature:</i>	60
1.8.2 <i>Reducing interstitial fluid pressure (IFP):</i>	63
1.8.3 <i>Manipulation of tumour pH:</i>	68
1.8.4 <i>Remodelling the extracellular matrix (ECM):</i>	69
1.8.5 <i>Modifying drug administration technique:</i>	72
1.8.6 <i>Modifying drug pharmacokinetics and nanoparticle delivery:</i>	73
1.9 SYNOPSIS AND OBJECTIVES OF THE PROJECT:	74
2. MATERIALS AND METHODS:	77
2.1 CHEMICALS AND REAGENTS:	77
2.2 CELL LINES AND CELL CULTURE CONDITIONS:	77
2.3 GROWTH CURVES:	79

2.4	GROWTH CHARACTERISTICS OF CELLS ON TRANSWELL MEMBRANES:	80
2.4.1	<i>Apparatus characteristics and MCLs formation:</i>	80
2.4.2	<i>Processing MCLs for thickness measurement:</i>	81
2.4.3	<i>Ability of cell lines to form MCLs:</i>	84
2.4.4	<i>Collagen expression in the MCL using immunohistochemistry:</i>	85
2.4.5	<i>Testing the ability of the MCL to form a barrier using trypan blue:</i>	87
2.5	ANALYSIS OF DOXORUBICIN:	88
2.5.1	<i>HPLC analysis of doxorubicin:</i>	88
2.5.2	<i>Extraction techniques and extraction efficiency test:</i>	89
2.5.3	<i>Extraction efficiencies, intra-day and injection reproducibilities:</i>	91
2.5.4	<i>Calibration curves and limit of detection:</i>	92
2.5.5	<i>Doxorubicin stability at 37°C:</i>	93
2.6	ANALYSIS OF IMATINIB AND GEFITINIB:	94
2.6.1	<i>HPLC, LC/MS, and LC/MS/MS analysis of imatinib and gefitinib:</i>	94
2.6.2	<i>Extraction of imatinib and gefitinib from TCM:</i>	96
2.6.3	<i>Calibration curves and limits of detection:</i>	96
2.6.4	<i>Stability test of imatinib and gefitinib at 37°C:</i>	97
2.7	DRUG PENETRATION ASSAYS USING MODEL-1:	97
2.7.1	<i>Drug penetration assays using (VCG) technique:</i>	98
2.7.2	<i>Calculating drug penetration rates using (VCG) technique:</i>	99
2.7.3	<i>Drug penetration assays using (CCG) technique:</i>	99
2.7.4	<i>Calculating drug penetration rates using (CCG) technique:</i>	100
2.8	IMPACT OF (HP), ON (CFF) AND DRUG PENETRATION USING MODELS 2 AND 3:	101
2.8.1	<i>Model 2, convection plus diffusion ($C \downarrow D \downarrow$):</i>	102
2.8.2	<i>Model 3, diffusion opposing convection ($D \downarrow C \uparrow$):</i>	106
2.8.3	<i>Modified model 3, diffusion opposing convection ($D \uparrow C \downarrow$):</i>	107
2.9	PENETRATION ASSAY DETAILED METHODOLOGY FOR ALL MODELS AND DRUGS:	109
2.10	INFLUENCE OF PENETRATION ASSAYS CONVECTION VERSUS EXPOSURE TIME ON CELL SURVIVAL:	109
3.	RESULTS	111
3.1	GROWTH CURVES IN MONOLAYER SETTING:	111
3.2	GROWTH OF CELL LINES ON THE TRANSWELL'S MEMBRANE AND MCL THICKNESS MEASUREMENTS:	111
3.2.1	<i>Growth characteristics and thicknesses of DLD-1 and MCF-7 MCLs:</i>	111

3.2.2	<i>The ability of a panel of cell lines to form MCLs:</i>	114
3.2.3	<i>Testing the ability of the MCL to form a homogenous barrier using trypan blue:</i>	116
3.3	ANALYSIS OF DOXORUBICIN:	118
3.3.1	<i>HPLC analysis of doxorubicin:</i>	118
3.3.2	<i>Calibration curves, limits of detection, extraction efficiencies, intra-day variations and injection reproducibility:</i>	119
3.3.3	<i>Doxorubicin stability at 37°C:</i>	122
3.4	ANALYSIS OF IMATINIB AND GEFITINIB:	122
3.4.1	<i>HPLC, LC/MS and LC/MS/MS analysis of imatinib and gefitinib:</i>	122
3.4.2	<i>Calibration curves and limits of detection:</i>	128
3.4.3	<i>Stability of imatinib and gefitinib at 37°C:</i>	131
3.5	DRUG PENETRATION ASSAYS USING MODEL-1:	132
3.5.1	<i>Drug penetration assay using variable concentration gradient (VCG) technique:</i>	132
3.5.2	<i>Drug penetration assay using constant concentration gradient (CCG) technique:</i>	142
3.6	DRUG PENETRATION ASSAYS USING MODELS 2 AND 3:	151
3.6.1	<i>Model 2: Convection plus diffusion ($C \downarrow D \downarrow$) penetration assay:</i>	151
3.6.2	<i>Model 3, diffusion opposing convection ($D \downarrow C \uparrow$):</i>	154
3.6.3	<i>Modified model 3, diffusion opposing convection ($D \uparrow C \downarrow$):</i>	155
3.7	IMPACT OF CFF ON DRUG PENETRATION THROUGH MCLs USING DOXORUBICIN, IMATINIB AND GEFITINIB:	159
3.8	INFLUENCE OF CONCENTRATION VERSUS EXPOSURE TIME ON CELL SURVIVAL:	169
3.9	COLLAGEN EXPRESSION IN THE MCL USING IMMUNOHISTOCHEMISTRY (IHC):	172
4.	DISCUSSION AND CONCLUSION:	174
4.1	GROWTH CHARACTERISTICS OF CELLS IN MONOLAYER AND MCL SETTINGS:	175
4.1.1	<i>Growth curves in monolayer settings:</i>	175
4.1.2	<i>Growth characteristics of cell lines on the transwell membrane and MCL thickness:</i>	176
4.2	EXTRACTION TECHNIQUES AND THEIR EFFICIENCIES:	178
4.3	EVALUATING AND VALIDATING SAMPLING METHODS:	178
4.4	EVALUATING AND VALIDATING ANALYSIS METHODS:	181
4.5	EVALUATING DRUGS STABILITY AT 37°C:	181
4.6	IMPACT OF (CFF) AND DIFFUSION ON DRUG PENETRATION USING THE THREE DIFFERENT PENETRATION MODELS:	182
4.6.1	<i>Diffusion only penetration assays, model-1 ($D \downarrow$):</i>	182

4.6.2	<i>Convection plus diffusion penetration assays, model-2 ($D \downarrow C \downarrow$):</i>	186
4.6.3	<i>Diffusion opposing convection penetration assays, model-3 ($D \downarrow C \uparrow$):</i>	189
4.7	CONCENTRATION VERSUS TIME EFFECT ON CELL SURVIVAL:	191
4.8	MODIFYING ECM COMPONENTS AS A STRATEGY TO IMPROVE CFF:	192
4.9	LIMITATIONS OF THE STUDY:	194
4.10	CONCLUSION:	195
5.	REFERENCES	197
6.	APPENDICES:	229
6.1	APPENDIX 1: CHEMICAL STRUCTURES AND MOLECULAR WEIGHTS OF DOXORUBICIN, IMATINIB AND GEFITINIB:	229
6.2	APPENDIX 2: VARIOUS ANALYSIS CONDITIONS USED FOR DOXORUBICIN, IMATINIB AND GEFITINIB	230
7.	CONFERENCE ABSTRACTS:	231
7.1	ABSTRACT-1	231
7.2	ABSTRACT-2	232

List of figures:

FIGURE 1-1: ESSENTIAL HALLMARKS OF CANCER CELLS	20
FIGURE 1-2: EMERGING HALLMARKS AND ENABLING CHARACTERISTICS OF CANCER	21
FIGURE 1-3: CANCER STATISTICS IN EUROPE	24
FIGURE 1-4: TEN LEADING CANCER TYPES IN 2010 IN THE UNITED STATES	25
FIGURE 1-5: EFFECTS OF CYTOTOXIC DRUGS ON PHASES OF THE CELL CYCLE	28
FIGURE 1-6: FACTORS DETERMINING DRUG DISTRIBUTION IN TISSUE	40
FIGURE 1-7: DIFFERENCES BETWEEN THE VASCULATURE OF NORMAL AND MALIGNANT TISSUE	44
FIGURE 1-8: REASONS WHY CELLS DISTANT FROM BLOOD VESSELS MIGHT BE RESISTANT TO TREATMENT	45
FIGURE 1-9: FACTORS REGULATING DRUG TRANSCAPILLARY TRANSPORT IN NORMAL AND CANCEROUS TISSUE	49
FIGURE 1-10: MULTICELLULAR MODELS USED TO STUDY DRUG PENETRATION	56
FIGURE 1-11: DOXORUBICIN DISTRIBUTION INTO SECTIONS OF TUMOUR TISSUE	58
FIGURE 1-12: DOXORUBICIN DISTRIBUTION IN HUMAN TISSUE	58
FIGURE 2-1: MODEL 1 (DIFFUSION ONLY $D \downarrow$), DRUG PENETRATION SYSTEM	81
FIGURE 2-2: MODEL 2 (CONVECTION PLUS DIFFUSION $C \downarrow D \downarrow$), DRUG PENETRATION SYSTEM	103
FIGURE 2-3: MODEL 3 (DIFFUSION OPPOSING CONVECTION $D \downarrow C \uparrow$), DRUG PENETRATION SYSTEM	107
FIGURE 2-4: MODIFIED MODEL 3	108
FIGURE 3-1: GROWTH CURVES OF DLD-1 AND MCF-7	112
FIGURE 3-2: HISTOLOGICAL SECTIONS THROUGH MCLs OF DLD-1 AND MCF-7	113
FIGURE 3-3: THICKNESSES OF DLD-1 AND MCF-7 MCLs	114
FIGURE 3-4: HISTOLOGICAL SECTIONS THROUGH OTHER CELL LINES	115
FIGURE 3-5: MCL THICKNESSES OF OTHER CELL LINES	116
FIGURE 3-6: CALIBRATION CURVES USED TO CALCULATE PENETRATING TRY PAN BLUE	117
FIGURE 3-7: CONCENTRATIONS (% W/V) OF PENETRATING TRY PAN BLUE	118
FIGURE 3-8: HPLC CHROMATOGRAMS OF DOXORUBICIN AND EPIRUBICIN	119
FIGURE 3-9: DOXORUBICIN CALIBRATION STANDARDS USED FOR SAMPLES CREATED BY MODEL 3	120

FIGURE 3-10: DOXORUBICIN STABILITY AT 37°C	122
FIGURE 3-11: DETECTION OF IMATINIB AND GEFITINIB USING HPLC	125
FIGURE 3-12: DETECTION OF IMATINIB USING LC/MS	126
FIGURE 3-13: DETECTION OF GEFITINIB USING LC/MS	127
FIGURE 3-14: CHROMATOGRAPHIC TRACES OF IMATINIB AND GEFITINIB USING LC/MS/MS	128
FIGURE 3-15: IMATINIB CALIBRATION STANDARDS USED FOR SAMPLES CREATED USING MODEL 3	130
FIGURE 3-16: GEFITINIB CALIBRATION STANDARDS USED FOR SAMPLES CREATED USING MODEL 3	130
FIGURE 3-17: STABILITY OF IMATINIB AND GEFITINIB AT 37°C	131
FIGURE 3-18: PENETRATION OF DOXORUBICIN (100, 50 AND 25 µM) THROUGH NON HYDRATED BLANK MEMBRANES USING VCG-TECHNIQUE	133
FIGURE 3-19: PENETRATION OF DOXORUBICIN (100 µM) THROUGH HYDRATED AND NON-HYDRATED BLANK MEMBRANES USING VCG-TECHNIQUE	134
FIGURE 3-20: PENETRATION OF DOXORUBICIN (100 µM) THROUGH A TRYPSINIZED AND NON- TRYPSINIZED BLANK MEMBRANE USING VCG-TECHNIQUE.	135
FIGURE 3-21: PENETRATION OF DOXORUBICIN (100, 50 AND 25 µM) THROUGH BLANK AND THROUGH DLD-1 MCL USING VCG-TECHNIQUE	138
FIGURE 3-22 : PENETRATING AMOUNTS OF DOXORUBICIN (100 µM), THROUGH BLANK AND THROUGH DLD-1 MCL USING VCG-TECHNIQUE	139
FIGURE 3-23: PENETRATION RATES OF DOXORUBICIN (100, 50 AND 25 µM) THROUGH BLANK AND THROUGH DLD-1 MCLs USING VCG-TECHNIQUE.	142
FIGURE 3-24: PENETRATION OF DOXORUBICIN (100, 50 AND 25 µM) THROUGH BLANK MEMBRANES USING CCG-TECHNIQUE	143
FIGURE 3-25: PENETRATION OF DOXORUBICIN (100 µM) THROUGH DLD-1 MCLs USING CCG- TECHNIQUE	144
FIGURE 3-26: PENETRATION OF DOXORUBICIN (100 µM) THROUGH MCF-7 MCLs USING CCG- TECHNIQUE	144
FIGURE 3-27: PENETRATION RATES OF DOXORUBICIN (100, 50 AND 25 µM) THROUGH BLANK MEMBRANE USING CCG-TECHNIQUE	146

FIGURE 3-28: CUMULATIVE PENETRATING AMOUNTS OF DOXORUBICIN (100 μ M) THROUGH DLD-1 MCLS USING CCG-TECHNIQUE	147
FIGURE 3-29: CUMULATIVE PENETRATING AMOUNTS OF DOXORUBICIN (100 μ M) THROUGH MCF-7 MCLS USING CCG-TECHNIQUE	147
FIGURE 3-30: PENETRATION RATES OF DOXORUBICIN (100, 50 AND 25 μ M) THROUGH DLD-1 MCL USING CCG-TECHNIQUE	150
FIGURE 3-31: PENETRATION RATES OF DOXORUBICIN (100, 50 AND 25 μ M) THROUGH MCF-7 MCL USING CCG-TECHNIQUE	150
FIGURE 3-32: CONVECTIVE FLUID FLOW (CFF) THROUGH DLD-1 MCL (DAY-1)	152
FIGURE 3-33: CONVECTIVE FLUID FLOW (CFF) THROUGH SEVERAL THICKNESSES OF DLD-1 MCL	153
FIGURE 3-34: PENETRATION OF DOXORUBICIN (100 μ M) THROUGH DLD-1 MCL USING MODEL 2	154
FIGURE 3-35: DOXORUBICIN (100 μ M) PENETRATION THROUGH DLD-1 MCL USING MODEL 3	155
FIGURE 3-36: CUMULATIVE AMOUNTS OF DOXORUBICIN (100 μ M) THROUGH DLD-1 MCL USING ORIGINAL AND MODIFIED MODEL 3	156
FIGURE 3-37: DOXORUBICIN PENETRATION THROUGH DLD-1 MCL USING MODIFIED MODEL 3	157
FIGURE 3-38: DOXORUBICIN (100 μ M) PENETRATION RATES THROUGH DLD-1 MCL USING MODIFIED MODEL 3 COMPARED TO OTHER MODELS	158
FIGURE 3-39 : CUMULATIVE CFF CALCULATED FOR DOXORUBICIN, IMATINIB AND GEFITINIB PENETRATION THROUGH DLD-1 MCL USING MODELS 2 AND 3	161
FIGURE 3-40: CONVECTIVE FLUID FLOW (CFF) CALCULATED FOR CONTROL (DRUG-FREE MEDIUM) AND FOR DOXORUBICIN, IMATINIB AND GEFITINIB PENETRATION THROUGH DLD-1 MCL USING MODELS 2 AND 3	163
FIGURE 3-41: DOXORUBICIN (100 μ M) PENETRATION RESULTS THROUGH DLD-1 MCL USING THE THREE DIFFERENT PENETRATION MODELS	164
FIGURE 3-42: IMATINIB (100 μ M) PENETRATION RESULTS THROUGH DLD-1 MCL USING THE THREE DIFFERENT PENETRATION MODELS	165
FIGURE 3-43: GEFITINIB (100 μ M) PENETRATION RESULTS THROUGH DLD-1 MCL USING THE THREE DIFFERENT PENETRATION MODELS	166

FIGURE 3-44: DOXORUBICIN, IMATINIB AND GEFITINIB PENETRATING AMOUNTS THROUGH DLD-1 MCL USING THE THREE DIFFERENT PENETRATION MODELS	167
FIGURE 3-45: PENETRATION RATES OF DOXORUBICIN, IMATINIB AND GEFITINIB (100 μ M) USING THE THREE DIFFERENT PENETRATION MODELS	168
FIGURE 3-46: EFFECT OF 30 MIN. EXPOSURE OF DLD-1 CELLS TO DOXORUBICIN ON SURVIVAL	170
FIGURE 3-47: EFFECT OF 30 MINUTES EXPOSURE OF DLD-1 CELLS TO IMATINIB ON SURVIVAL	171
FIGURE 3-48: EFFECT OF 30 MINUTES EXPOSURE OF DLD-1 CELLS TO GEFITINIB ON SURVIVAL	171
FIGURE 3-49: COLLAGEN EXPRESSION IN DLD-1 XENOGRAFT TUMOUR AND IN DLD-1 MCL	173

List of tables:

TABLE 1-1: LIST OF SOME MOLECULAR TARGETED AGENTS CURRENTLY IN THE CLINIC	32
TABLE 1-2: HOST FACTORS INFLUENCING PK PROFILES AND DRUG SUPPLY TO TUMOURS	42
TABLE 1-3: VALUES OF IFP IN NORMAL AND NEOPLASTIC TISSUES.	50
TABLE 2-1: LIST OF USED CANCER CELL LINES AND THEIR TISSUE OF ORIGINS	78
TABLE 2-2: DOXORUBICIN, IMATINIB AND GEFITINIB CUMULATIVE CONCENTRATIONS RETRIEVED FROM PENETRATION MODELS .	110
TABLE 3-1: EXTRACTION EFFICIENCIES, LIMITS OF DETECTION AND PRECISION	121
TABLE 3-2: PENETRATION RATES OF DOXORUBICIN (100 μM) THROUGH DLD-1 MCLS USING VCG-TECHNIQUE.	137
TABLE 3-3: PENETRATION RATES OF DOXORUBICIN (50 μM) THROUGH DLD-1 MCL USING VCG-TECHNIQUE.	137
TABLE 3-4: PENETRATION RATES OF DOXORUBICIN (25 μM) THROUGH DLD-1 MCL USING VCG-TECHNIQUE.	137
TABLE 3-5: PENETRATION RATES OF DOXORUBICIN (100 μM) THROUGH DLD-1 MCL USING CCG-TECHNIQUE.	148
TABLE 3-6: PENETRATION RATES OF DOXORUBICIN (50 μM) THROUGH DLD-1 MCL USING CCG-TECHNIQUE.	148
TABLE 3-7: PENETRATION RATES OF DOXORUBICIN (25 μM) THROUGH DLD-1 MCL USING CCG-TECHNIQUE.	148
TABLE 3-8: PENETRATION RATES OF DOXORUBICIN (100 μM) THROUGH MCF-7 MCL USING CCG-TECHNIQUE.	149
TABLE 3-9: PENETRATION RATES OF DOXORUBICIN (50 μM) THROUGH MCF-7 MCL USING CCG-TECHNIQUE.	149
TABLE 3-10: PENETRATION RATES OF DOXORUBICIN (25 μM) THROUGH MCF-7 MCL USING CCG-TECHNIQUE.	149
TABLE 3-11: CFF CALCULATED FOR DOXORUBICIN, IMATINIB AND GEFITINIB (100 μM) PENETRATION THROUGH DLD-1 MCL USING THE THREE DIFFERENT PENETRATION MODELS	163

TABLE 3-12: PENETRATION RATES OF DOXORUBICIN, IMATINIB AND GEFITINIB (100 μ M) THROUGH DLD-1 MCL USING THE THREE DIFFERENT PENETRATION MODELS	168
TABLE 3-13: DOXORUBICIN, IMATINIB AND GEFITINIB CUMULATIVE CONCENTRATIONS USED FOR TESTING CONCENTRATION VS TIME EFFECT ON DLD-1 SURVIVAL RATES USING MTT ASSAY	170

List of abbreviations:

5-FU	5-Flourouracil
786-0	Human renal cell adenocarcinoma
A-2780	Human ovarian carcinoma
A549	Human lung carcinoma
ALL	Acute lymphoblastic leukaemia
ATCC	American Type Culture Collection
BBB	Blood brain barrier
BC	Breast cancer
BLD	Below the limit of detection
C	Convection
C↓D↓	Convection plus diffusion
Caski	Human cervix epidermoid carcinoma
CA4P	Combretastatin A-4 phosphate CA4P
CAM	Cell adhesion molecule
CAP	Capillary
CCG	Constant concentration gradient
CFF	Convective fluid flow
CML	Chronic myelogenous leukaemia,
CNS	Central nervous system
COP	Colloidal osmotic pressure
CRC	Colorectal cancer
CV	coefficient of variation
D	Diffusion

D↓	Diffusion only
D↓C↑	Diffusion opposed by convection
DLD-1	Human colorectal adenocarcinoma
ECACC	European Collection of Cell Culture
ECM	Extracellular matrix
EE	Extraction efficiency
EGFR	Epidermal growth factor receptor
EPR	Enhanced permeability and retention effect
FBS	Foetal bovine serum
GIST	Gastro intestinal stromal tumour
HBSS	Hanks Balanced salt solution
HCC	Hepatocellular carcinoma
HER-2	Human epidermal growth factor-2
HP	Hydrostatic pressure
HPLC	High performance liquid chromatography
Hsts26t	human soft tissue sarcomas xenografts
HT29	Human colorectal adenocarcinoma
HUVEC	Human umbilical vein endothelial cells
i.d.	Inner diameter
IARC	International Agency for Research on Cancer
IF	Interstitial fluid
IFP	Interstitial fluid pressure
IHC	Immunohistochemistry
IL	Interleukin

LC	Liquid chromatography
LLOQ	Lower limit of quantification
LOD	Limit of detection
m/z	Mass to charge ratio
M14	Human melanoma
mBC	Metastatic breast cancer
MCF-7	Human breast adenocarcinoma
MCL	Multi cell layer
MCS	Multicell spheroid
MDR	Multiple drug resistance
M-IHP	Melphalan-based isolated hepatic perfusion
mmHg	millimetre mercury
MPA	Mobile phase-A
MPB	Mobile phase-B
MRI	Magnetic resonance imaging
MRM	Multiple reaction monitoring
MS	mass spectrometry
mTOR	Mammalian target of rapamycin
MTT	3-(4,5-dimethylthiazole-2-yl)-2,5-diphenyltetrazolium bromide
NHL	Non-Hodgkin's lymphoma
NO	Nitric oxide
NSCLC	Non-small-cell lung carcinoma
P	Pressure
Panc-1	Human Pancreatic adenocarcinoma

PBS	Phosphated buffer saline
PC3	Human prostate adenocarcinoma
PDGFR	Platelet derived growth factor receptor
PD	Pharmacodynamic
PET	Positron emission tomography
PGE	Prostaglandin E
pH	power of hydrogen
PK	Pharmacokinetic
PT	Protein precipitation
PT-evap	Protein precipitation and evaporation
PTFE	Polytetrafluoroethylene
r^2	Correlation coefficient
RCC	Renal cell carcinoma
SiHa	Human cervix carcinoma
SIR	Selected ion reading
SK-MEL 23	Human melanoma
S/N	Signal to noise ratio
SPE	Solid phase extraction
TCM	Tissue culture medium
TGF	Transforming growth factor
TKI	Tyrosine kinase inhibitor
TNF	Tumour necrosis factor
TPZ	Tirapazamine
UPLC	Ultra high pressure liquid chromatography

V/V	Volume per volume
VCG	Variable concentration gradient
VEGF	Vascular endothelial growth factor
W/V	Weight per volume
WHO	World Health Organization

1. INTRODUCTION:

1.1 General introduction to the cancer problem:

Cancer is a cellular disease characterized by a shift in control mechanisms that govern the balance between cell proliferation, cell death and differentiation. In this disease, cancer cells grow abnormally and form a mass or tumour (Weinberg, 1996). Tumours can be benign or malignant. Benign tumours may grow but they do not invade surrounding normal tissue, spread to other tissues and are usually not life threatening. On the other hand, malignant tumours are life threatening. They grow, invade and spread (metastasise) to other tissues in the body.

In comparison to normal cells, cancer cells acquire six essential hallmarks or traits (Figure1-1). The first hallmark is self-sufficiency in growth signals, the second is insensitivity to growth-inhibitory (antigrowth) signals, the third is evasion of programmed cell death (apoptosis), the fourth hallmark is limitless replicative potential, the fifth is sustained angiogenesis and finally the sixth hallmark is tissue invasion and metastasis, (Hanahan and Weinberg, 2000).

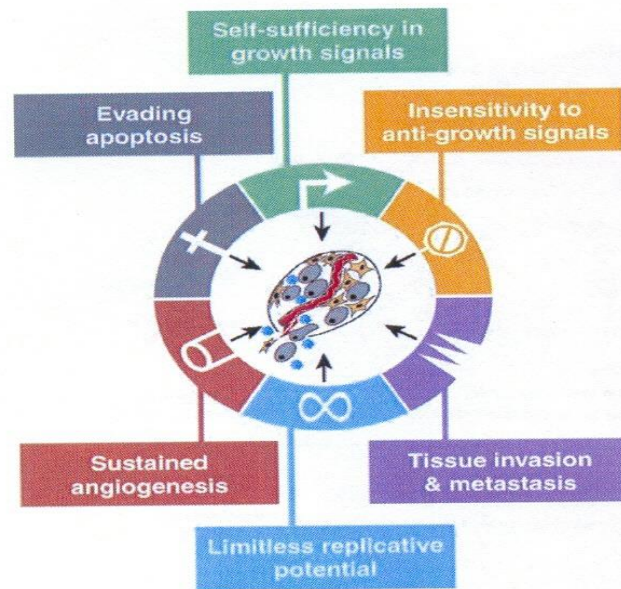


Figure 1-1: Essential Hallmarks of Cancer Cells (Hanahan and Weinberg, 2000).

These hallmarks were updated in 2011. Two emerging hallmarks and two enabling characteristics were added to the current hallmarks (Figure1-2). The emerging hallmarks are the ability of cancer cells to avoid immune destruction and their ability to deregulate cellular energetics. The first of the enabling characteristics is the development of genomic instability in cancer cells which generates random mutations and the second is tumour-promoting inflammation. Tumour microenvironment plays a major role in enabling cancer cells to acquire these hallmarks (Hanahan and Weinberg, 2011).

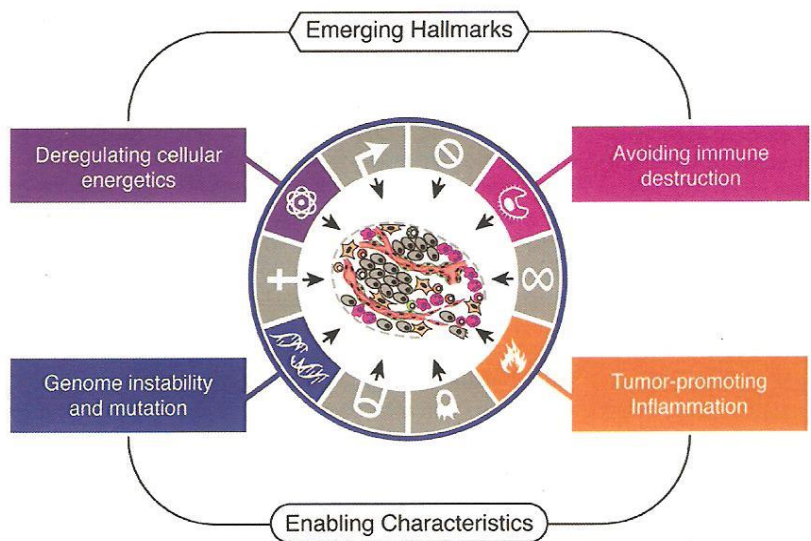


Figure 1-2: Emerging hallmarks and enabling characteristics of cancer (Hanahan and Weinberg, 2011).

Several factors may cause cancer. Environmental factors (Montesano and Hall, 2001), heredity, immune deficiency, some viral infections and carcinogenic agents are all linked to various cancers (Fagan-Dubin, 1979). Doll and Peto have listed various factors that may lead to cancer. These factors included tobacco, alcohol, diet, food additives, reproductive and sexual behaviour, occupation, pollution, industrial products, medicines and medical procedures and infections (Doll and Peto, 1981). Knowledge of and a close understanding of how exposure to these risk factors can be reduced is an important weapon in the war on cancer. A detailed account of this is however beyond the scope of this thesis.

Overview of the molecular basis of cancer:

Cancer can be considered a genetic disease. Oncogenes and tumour suppressor genes play a major role in the pathogenesis of cancer. DNA damage can lead to the activation of oncogenes and loss of tumour suppressor genes. Oncogenes can be considered tumour inducing factors and they develop from normal genes called proto-oncogenes. They have important roles in all phases of carcinogenesis. Activated oncogenes can produce excessive amounts of the normal gene product or an abnormal gene product. This can result in an abnormal cell growth and proliferation. The platelet derived growth factor receptor (PDGFR), epidermal growth factor receptor (EGFR), tyrosine kinases and apoptosis regulator BCL2 are examples of oncogenic proteins. These oncogenes can be targeted by cancer therapies (Croce, 2008). Imatinib is a prime example of a cancer therapy that targets a cancer causing oncogene in order to treat chronic myelogenous leukaemia. Imatinib is a small molecule that targets the tyrosine kinases ABL and C-KIT and the PDGFR. It is used in the treatment of chronic myelogenous leukaemia (Goldman and Melo, 2001) and gastrointestinal stromal tumours (GIST) (Cohen et al., 2010). Cetuximab is a monoclonal antibody which targets EGFR and is used in the treatment of colorectal cancer (Scartozzi et al., 2011). In contrast, tumour suppressor genes regulate and inhibit inappropriate cellular growth and proliferation. Mutation or loss of this gene can result in loss of normal cell growth control. P53 is an example of a tumour suppressor gene.

Mutation of P53 is one of the most common genetic changes associated with cancer. In addition, alteration in DNA repair genes can lead to cancer. DNA repair genes encode for protein that corrects errors that may occur during DNA duplication (Weinberg, 1996). Cancers evolve as a result of a series of mutations in both oncogenes and tumour suppressor genes, the classic example of this being the Fearon-Vogelstein model of colorectal cancer (Fearon and Vogelstein, 1990).

Incidence and Mortality Figures of cancer:

About 12.7 million cancer cases and 7.6 million cancer death are estimated to have occurred in 2008 according to GLOBOCAN 2008. GLOBOCAN is an estimate of cancer incidence and mortality worldwide produced by the International Agency for Research on Cancer (IARC), which is a part of the World Health Organization (WHO). According to the same agency, the most frequently diagnosed and the leading cause of cancer death in female is the breast cancer which accounts for 23% of the total cancer cases and 14% of cancer death. However, in males, lung cancer was the leading cancer site accounting for 17% of total new cancer cases and 23% of the total cancer death (Jemal et al., 2011).

In the European Union (EU), 1,281,436 is the predicted total number of cancer deaths in 2011. As the total number of cancer deaths in the (EU) was 1,256,071 in 2007, there is an increase in the number of cases by 25,365. In 2011, the estimated standardized cancer death rates in (EU) also are expected to be 142.8/100,000 men and 85.3/100,000 women compared with

153.8/100,000 men and 90.7/100,000 women in 2007 (figure 1-3) (Malvezzi et al., 2011).

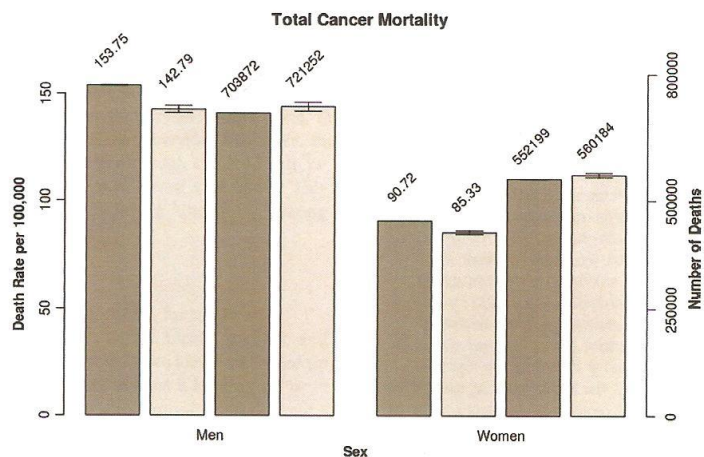


Figure 1-3: Cancer statistics in Europe: Bar plots of standardized death rates per 100 000 population and certified deaths for the year 2007 (dark grey) and the predicted death rates and number of deaths for 2011 (light grey) for total cancer mortality in the (EU) in men and women (Malvezzi et al., 2011).

In the United States, cancer is considered the second leading cause of death after cardiovascular disease. In 2010, more than 1.5 million new cancer cases were predicted to be diagnosed and about 569,490 cancer deaths are expected to be recorded in the United States. The overall survival rate from 1999 to 2005 for all types of cancer was 68% and the five most common causes of death from cancer in men in the United States in 2007 were lung, prostate, colorectal, pancreas and leukaemia and in women they were lung, breast, colorectal, pancreas and ovarian cancer. Figure-1-4 represents the ten leading cancer types for the estimated new cancer cases and deaths in male and female in 2010 in the United States (Jemal et al., 2010).

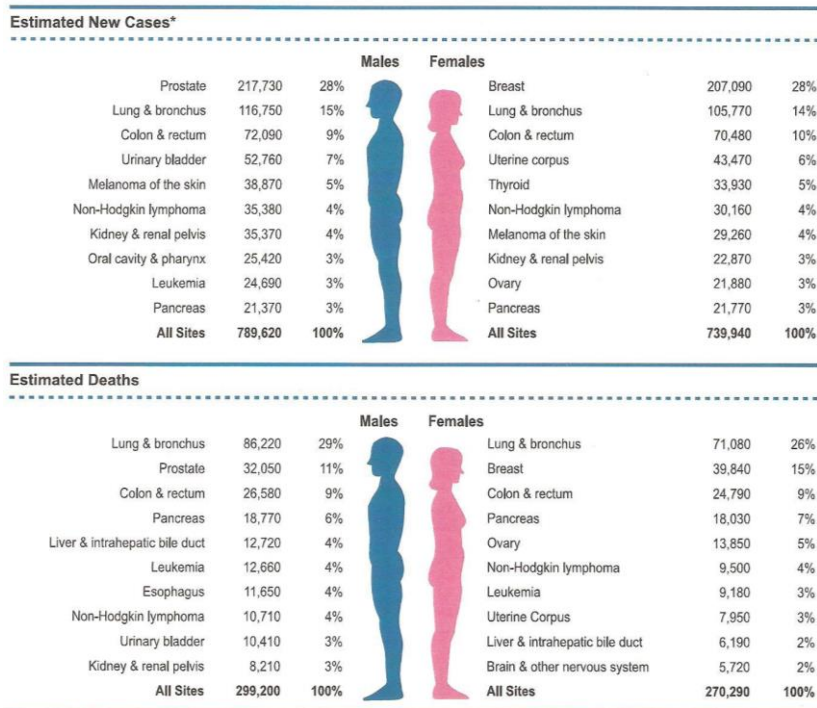


Figure 1-4: Ten leading cancer types for the estimated new cancer cases and deaths in men and women in 2010 in the United States (Jemal et al., 2010).

These statistics are essential for evaluating the current cancer prevention and management strategies. It is clear from the current statistics that there is a real need for new therapies for treating cancer and/or new strategies to make the current available treatment modalities work better.

1.2 Treatment modalities of cancer:

Surgery, radiotherapy and systemic therapy are the main cancer treatment modalities.

Surgery: Surgery is the oldest modality available to treat patients with cancer. It is highly effective at treating cancer that have not metastasized and in these cases, treatment can be curative. Catching the disease early therefore is important but for many cancers, the disease has already disseminated at the time of diagnosis. Patients with limited metastatic disease may still benefit from surgical resection of the metastasis. Furthermore, in patients with advanced metastasis, surgery can be used to relieve pain, improve functional abnormalities (e.g. gastrointestinal obstruction) and may improve the patient's quality of life (Nagula et al., 2010).

Radiation therapy: Radiation therapy can be used to eradicate localized tumour masses or disseminated disease (leukaemia) with bone marrow or stem cell transplants. Radiation can also be used for tumours located at non-operable areas of the body. The usefulness of radiation can be limited by its toxic effects on normal tissues that are located beside the tumour (Camma et al., 2000; Higgins et al., 1986).

Systemic therapy: Not all cancers can be cured by surgery or radiation therapy, especially metastatic cancers. In these cases, systemic treatment is essential. These include chemotherapy (both traditional cytotoxics and molecularly targeted therapies), hormonal therapy and biological therapy.

Chemotherapy is the mainstay of systemic therapies and its origins go back to observations made in the middle 1940s, when mustard gas was shown to produce bone marrow suppression and lymphoid hypoplasia in service men exposed to the gas. This incident led to the use of mustard gas derivatives (nitrogen mustard alkylating agents) in the treatment of Hodgkin's disease and other lymphomas (Joensuu, 2008). Since the use of nitrogen mustards emerged, a series of cytotoxic agents were developed, the vast majority of which kill cancer cells mainly by damaging DNA, interfering with DNA synthesis or inhibiting cell division. Cytotoxic chemotherapy agents have been classified by their effect on the cell cycle or their mechanism of action (Gilman, 2006). Agents that affect the cell only during a specific phase of the cell cycle often are referred to as phase specific agents or schedule dependent agents. On the other hand, agents that affect the cell during any phase of the cell cycle are often referred to as phase non-specific agents or dose dependent agents. Figure 1-5, shows the mechanism of action and the effects of the cytotoxic drugs on phases of cell cycle. It does also show examples of phase specific and phase non-specific cytotoxic agents (Kimble, 2004).

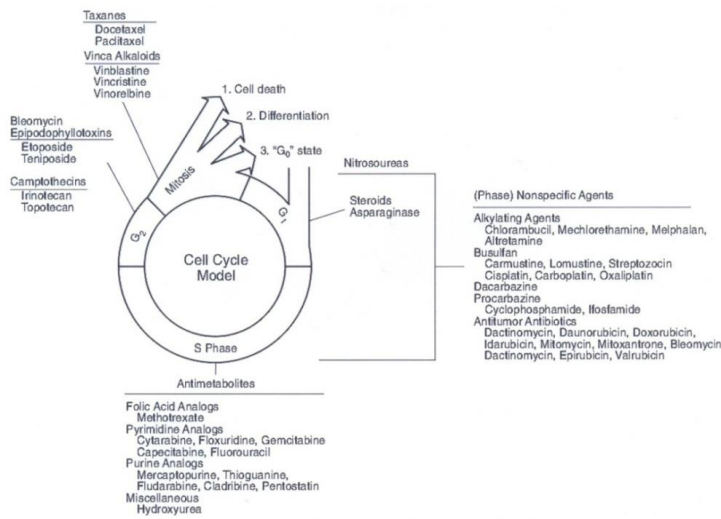


Figure 1-5: Effects of cytotoxic drugs on phases of the cell cycle (Kimble, 2004).

Cancer chemotherapy may be used as a primary, palliative, adjuvant or neoadjuvant treatment modality. It is considered a primary or a curative modality in some diseases like leukaemias, lymphomas and testicular cancer. Chemotherapy is initiated for palliative purposes in most of solid tumours to relieve symptoms either because of the nature of the tumour or because of advanced disease at time of treatment (Sepulveda et al., 2002). Adjuvant therapy is defined as the use of systemic chemotherapy to eradicate micro-metastatic disease following surgery or radiotherapy or both of them. The main purpose of chemotherapy in this situation is to reduce tumour recurrence rates and prolong patient's long term survival (Mazzeo et al., 2003). Chemotherapy may also be given in neoadjuvant or preoperative setting. The purpose in this case is to make other treatment modalities like surgery more effective by reducing tumour burden and to destroy micro-metastases (Mauriac et al., 1999).

With increased understanding of cancer cell biology, other systemic therapeutic agents have been introduced. The following section describes the key mechanisms of action and provides a few examples of hormonal, biological and molecular targeted agents used for the treatment of cancer.

Hormonal therapy is type of anti-neoplastic therapy currently in the clinic. The drugs related to this group oppose or alter the effect of male or female hormones in hormone dependent tumours. This group of drugs inhibits tumour growth by blocking the receptors or by eliminating the endogenous hormone which feeds the tumour. The problem with this group is resistance where not all the tumours arising from hormone sensitive tissue respond to hormonal therapy. Examples of hormones used as anti-neoplastic drugs include the progestin hydroxyprogesterone, the anti-estrogen tamoxifen and the anti-androgen flutamide (Ali and Coombes, 2002).

Biological therapy is another form of systemic cancer therapy. In this group a protein, antibody or gene can be administered to the cancer patient in order to kill cancer cells or to support the patient immune system (Mihich, 2000; Rochlitz, 2001). The immune system plays an important role in determining cancer development. Immune-suppressed patients like AIDS patients face an increased risk of developing cancer compared to immune-competent individuals (Franceschi et al., 1998). Supporting the immune system can help prevent or treat cancer. Biological therapies aim to support individual immune response as well as providing selective anti-tumour effects. Immunotherapy is an example on biological systemic therapy and it usually involves stimulating

the host's immune system to fight the cancer cells. The agents used in immunotherapy are naturally occurring cytokines which have been produced by the aid of the recombinant DNA technology. Examples of agents used in immunotherapy include interferons and interleukins (ILs). The proposed mechanism of action of Interferon- α for example is direct anti-proliferative efficacy, an immunomodulatory effect on natural killer cells, T cells, B cells and macrophages, anti-angiogenic efficacy and a differentiating effect on tumour cells (Kirkwood, 2002). Interleukin-2 (IL-2) is a recombinantly produced lymphokine with an immunoregulatory action and its use in patients with advanced renal cell carcinoma has induced tumour regression and increased patient survival with a favourable toxicity profile when used in low doses (Bleumer et al., 2006).

The new generation of targeted therapeutic drugs:

By understanding the mechanisms by which cancer cells exhibit abnormal growth, angiogenesis, apoptosis and metastasis, it has been possible to design drugs that inhibit these processes (Hanahan and Weinberg, 2011). Molecular targeted therapeutic agents were introduced to kill tumour cells without disrupting the physiological functions of normal cells (Eckhardt, 2006). Bevacizumab, cetuximab, trastuzumab, erlotinib, gefitinib and dasatinib are examples of clinically used molecular targeted agents (Soria et al., 2011). A list of them and other molecular targeted agents, their targets and clinical uses is available in table 1-1. Bevacizumab is a monoclonal antibody with antiangiogenic activity. It targets the vascular endothelial growth factor (VEGF)

(Zondor and Medina, 2004). Bevacizumab is available in the clinic for the treatment of non-small-cell lung cancer (Herbst et al., 2011) and colorectal cancer (Tol and Punt, 2010). The other monoclonal antibodies cetuximab and trastuzumab are also used clinically (Syed et al., 2004) for the treatment of solid tumours including colorectal cancer and breast cancer. They inhibit growth factor receptors leading to decreasing cell proliferation and increasing death of tumour cells (Yarden, 2001). Cetuximab targets the epidermal growth factor receptor (EGFR). It was reported as active and save option for the treatment of colorectal cancer (Roca et al., 2010). Trastuzumab is now a standard drug for Her-2 positive breast cancer patients (Slamon et al., 2011). Other examples of targeted drugs are erlotinib and gefitinib which inhibit the epidermal growth factor receptor tyrosine kinase (EGFR). They are used for the treatment of different types of solid tumours including non-small cell lung cancer (Herbst et al., 2011; Maemondo et al., 2010). Dasatinib also is another example of molecular targeted agents. It has the advantage of being used for the treatment of leukemias. It targets and inhibits the BCR-ABL tyrosine kinase. Dasatinib can be used for the treatment of patients with chronic myelogenous leukaemia (CML) or Philadelphia positive acute lymphoblastic leukaemia (ALL). It has shown efficacy in patients with CML or Philadelphia-positive (ALL) patients who are resistant to imatinib as it inhibits imatinib BCR-ABL mutations (Kantarjian et al., 2010; Talpaz et al., 2006).

Table 1-1: List of some molecular targeted agents currently in the clinic:

Generic name	Trade name	Molecular Target	Clinical use	Reference
Bevacizumab	Avastin	VEGF	CRC, NSCLC, mBC, RCC	1, 2, 3
Cetuximab	Erbix	EGFR	CRC	4, 5, 6
Panitumumab	Vectibix	EGFR	CRC	11
Trastuzumab	Herciptin	HER-2	BC	4, 5, 7
Imatinib	Glivec	PDGFR	ALL, CML, GIST	9, 10
Gefitinib	Iressa	EGFR	NSCLC	2, 8
Erlotinib	Tarceva	EGFR	NSCLC	2, 8
Dasatinib	Sprycel	BCR-ABL	ALL, CML	9, 10
Sorafenib	Nexavar	EGFR	HCC, RCC	12, 13
Sunitinib	Sutent	PDGFR, VEGF	GIST	11
Lapatinib	Tyverb	HER-2	NSCLC	14

VEGF= Vascular endothelial growth factor, EGFR= Epidermal growth factor receptor, PDGFR= Platelet derived growth factor receptor, ALL= Acute lymphoblastic leukaemia, BC= Breast cancer, mBC= Metastatic breast cancer, HER-2= Human epidermal growth factor 2, CML= Chronic myelogenous leukaemia, CRC= Colorectal cancer, HCC= Hepatocellular carcinoma, RCC= Renal cell carcinoma, GIST= Gastro intestinal stromal tumour, NSCLC= Non-small-cell lung carcinoma.

References: 1= (Zondor and Medina, 2004), 2= (Herbst et al., 2011), 3= (Tol and Punt, 2010), 4= (Syed et al., 2004), 5= (Yarden, 2001), 6= (Roca et al., 2010), 7= (Slamon et al., 2011), 8= (Maemondo et al., 2010), 9= (Kantarjian et al., 2010), 10= (Talpa et al., 2006), 11= (Soria et al., 2011), 12= (Kane et al., 2009), 13= (Chowdhury et al., 2008), 14= (Kim et al., 2008).

Current cancer treatment modalities can produce good cure and survival rates in some types of cancers such as certain types of leukaemia and testicular cancer (Brenner, 2002). But unfortunately, limitations that reduce the effectiveness of systemic therapy exist and these are discussed in the following section.

1.3 Limitations of chemotherapy:

Cancer chemotherapy can be limited by several factors. These factors include administration technique problems, adverse effects, patient performance status and resistance, details of which are summarised below.

Administration techniques: Administration techniques including dose intensity and the schedule of chemotherapy are considered among the limitations of the efficacy of cancer therapy. Dose intensity is defined as the amount of drug administered per unit of time. (Gianni and Piccart, 2000). Lengthening the interval between successive courses of chemotherapy or decreasing the dose can negatively affect treatment outcomes. The dose intensity for most chemotherapy regimens is limited by major dose-related toxicities such as bone marrow suppression (Lewis et al., 1997).

The schedule of chemotherapy administration is also an important determinant of response. The optimal schedule is influenced by the pharmacokinetic properties of the anticancer agent. For example, phase-specific agents have cytotoxic effects only when the cell is in a particular phase of the cell cycle. If a phase-specific agent with a short half-life is administered by a bolus injection, it may not affect all the cells. On the other hand, if it was given by continuous infusion, more cancer cells may be exposed to its cytotoxic effect (Lokich and Anderson, 1997). Increasing the duration of exposure is of course limited by toxicity to normal tissues.

Adverse effects: Adverse effects of systemic therapy are among the most important treatment limitation factors. Several adverse effects are common to most conventional chemotherapeutic agents. These adverse effects include nausea, vomiting, myelosuppression (including anaemia, neutropenia and thrombocytopenia), mucositis, alopecia, infertility and secondary malignancies. Some of these adverse effects like myelosuppression for example and some drug specific cytotoxicities like cardiotoxicity induced by doxorubicin, are dose limiting side effects (Gharib and Burnett, 2002). Compared to conventional therapy, molecular targeted agents on the other hand, offer potential for improved efficacy and less toxicity as they act more selectively against cancer cells than normal cells (Soria et al., 2011).

Patient performance status: Patient performance status, tolerance and specific factors also can play a major role in the usefulness of a chemotherapeutic course. Patient specific factors (e.g. performance status, co-morbidities, renal and hepatic function, and pharmacogenomics), tumour-specific factors (e.g. pathology, stage, and molecular profile), and treatment goals (e.g. palliation or cure) in addition to the cost of the treatment are all considered when determining the treatment option (Wedding et al., 2007).

Resistance: Cancer cell resistance to systemic therapy is one of the most important limitation factors of cancer chemotherapy. Resistance can be classified into primary, acquired or multi drug resistance (MDR) and apparent resistance caused by limited drug delivery to the solid tumour. Drug resistance may be either inherent in cancer cells (primary) or acquired i.e. develop over

time during chemotherapy even after dramatic initial response. Some cell lines that became resistant to single chemotherapy agents may also be resistant to other agents that can be structurally non-related. This phenomenon is called multidrug resistance (MDR). The primary mechanism believed to be responsible for MDR is an increase in P-glycoprotein in the cell membrane. This protein mediates efflux of the chemotherapy agent causing a decreased accumulation of drug within the cells (Gottesman, 1993). Other mechanisms of resistance include alterations in metabolic pathways that influence drug metabolism, DNA repair, or apoptosis (Regev et al., 2007; Tannock and Rotin, 1989). As for conventional chemotherapy, molecular targeted agents have also shown to develop resistance (Nishida et al., 2008). The most widely studied cause of resistance is cell related. However, a neglected type of resistance is generated by the inability of drugs to penetrate into the solid tumour efficiently. Numerous studies support this proposal (Eytan, 2005; Hicks et al., 2003; Kyle et al., 2007; Sutherland et al., 1979; West et al., 1980) but the seminal work was done by Sutherland (1979).

Sutherland and his group studied resistance to doxorubicin using multicellular spheroids as an *in vitro* model. They used EMT-6 mammary tumour cell spheroids which were resistant to different exposure doses of doxorubicin. Compared to monolayer cultures, EMT-6 spheroids were exposed to different doxorubicin concentrations for different periods and a concentration gradient of fluorescence was observed from the outside to the centre of the intact spheroids. In addition, intact spheroids took up less doxorubicin compared with dissociated spheroids. Intact spheroid cells have also shown resistance

compared with dissociated cells when surviving fraction was plotted versus absorbed doxorubicin. Sutherland and his group also proved that the inner spheroid cells were the most resistant. They concluded that a diffusion barrier is present in the EMT-6 spheroids and they proposed that other factors related to the metabolic state of the cells, the microenvironment or the formation of different drug products must account for the observed resistance. (Sutherland et al., 1979).

This field has developed over the years and more recently, Hicks and colleagues (Hicks et al., 2003) developed a pharmacokinetic (PK)/pharmacodynamic (PD) model for the hypoxia selective drug tirapazamine (TPZ) which is currently in clinical trials (Rischin et al., 2010). Through this model, TPZ diffusion through HT-29 colon carcinoma multi-cell layers (MCL) was measured. In this model, TPZ PK was represented by its transport through the MCLs whereas its PD was represented by its cytotoxicity using the clonogenic assay. Cytotoxicity of transported TPZ through different thicknesses of anoxic HT-29 MCLs was proportional to the measured values of TPZ in the medium of the diffusion model. These values on the other hand were inversely proportional to the MCL thickness. Hicks and colleagues concluded that inefficient transport was responsible for tirapazamine resistance in multicell layers of HT-29 (Hicks et al., 2003).

Other studies have shown that drug resistance depends on the solid tumour microenvironment (Heldin et al., 2004) and pharmacological factors related to drug and/or on problems related to the delivery of anticancer drugs to the

tumour cells (Baxter and Jain, 1989; Cowan et al., 1996; Cowan and Tannock, 2001; Kyle et al., 2004; Kyle et al., 2007; Phillips et al., 1998; Primeau et al., 2005; Tannock et al., 2002; Tunggal et al., 1999). Details of some of these studies will be discussed later in this thesis. Results of all these studies suggest that optimization of transport properties of anticancer drugs may improve their therapeutic efficacy. Although the results of these studies have shown that limited drug delivery is one of the expected causes of chemotherapy resistance, an argument can be raised here that drugs such as doxorubicin are available in the clinic for treating several types of cancer so must be delivered well enough to have efficacy. The following section will discuss whether or not limited drug delivery to solid tumours is considered a clinical problem.

1.4 Limited drug delivery to solid tumours as a form of drug resistance:

To answer this question it is essential to consider specific therapeutic compounds, key questions to be addressed include; are the successful compounds able to efficiently penetrate their target tissue and is there evidence that ineffective agents fail due to limited penetration?

The best characterised drug in terms of its distribution is the anti-cancer agent doxorubicin, as its natural fluorescence facilitates its easy detection within tissues. A variety of different experiments show that doxorubicin penetrates tumours poorly. For example, the drug shows weaker activity against the cells in the centre of spheroid preparations (Durand, 1990; Kerr and Kaye, 1987)

and in the deeper layers of MCLs (Kyle et al., 2004). This is also the case *in vivo*, with Lankelma and colleagues (1999) showing with laser scanning microscopy that cells which are remote from the microvessels are exposed to lower doxorubicin concentrations (Lankelma et al., 1999).

The taxanes paclitaxel and docetaxel are microtubule-disrupting agents that are used to inhibit the growth of solid tumours. Similar distribution in tumours has been found for these drugs as for doxorubicin (Kuh et al., 1999; Kyle et al., 2007). Paclitaxel showed poor penetration in tumour sections which were incubated at 37°C in medium containing different paclitaxel concentrations for various times. (Kuh et al., 1999; Li et al., 2000) and both drugs showed inefficient distribution in MCL and tumour xenograft models (Kyle et al., 2007).

These results clearly demonstrate that at least several anti-cancer drugs penetrate solid tumours to a very limited degree. However, these agents are relatively successful in the treatment of cancer, questioning the necessity of efficient drug penetration in order to produce a therapeutic effect. It is still possible that these drugs could still be successful even if they cannot reach the cells that reside some distance from the blood supply (Minchinton and Tannock, 2006). For example, it may be that killing the cells that are close to blood vessels progressively renders more cells distant from blood vessel susceptible to the drug. Chemotherapy is typically given in repeated cycles, and so it could be that more and more of the tumour is destroyed with each treatment cycle (Minchinton and Tannock, 2006). Alternatively, it is possible that just killing the cells in the proximity to blood vessels is sufficient to result in tumour regression, possibly because the cells that are distant from blood

vessel are necrotic and therefore cannot sustain tumour growth. This might suggest that widespread distribution of chemotherapeutic agents throughout solid tumours is not critical for their therapeutic success.

In reality, it is hard to argue against the fact that these drugs would be considerably more effective if they were able to distribute more thoroughly throughout the tumour mass. This seems logically far more likely, and there are a few lines of evidence that may support this view. Some tumours develop resistance to these agents, and, although this is often attributed to efflux mechanisms or the acquisition of new mutations (McGrogan et al., 2008), it may be that inefficient killing of cells in the tumour interior allows the tumour to re-grow when the drug is removed. Moreover, there are many examples of anti-cancer compounds that are ineffective, and which can be demonstrated to penetrate tumours poorly. For instance, tirapazamine (TPZ), a drug designed to be activated once it reaches the hypoxic core of a tumour (Hicks et al., 2004) as mentioned above, is comparatively ineffective, probably because it cannot reach deep into tumours (Hicks et al., 2003). The other example is the well-known anti-cancer agent 5-fluorouracil (5-FU). It was proved that the concentration of 5-FU in tumour is directly proportional to its therapeutic effect (Muller et al., 1997; Presant et al., 1994). There is also evidence that efficient tissue distribution of drugs is crucial for successful treatment of other diseases. Drugs that act on the central nervous system (CNS) are an example (Upton, 2007). The inability of some of them to cross the blood brain barrier (BBB) and distribute through the cerebrospinal fluid makes the pharmacological targeting of the brain difficult (Liu et al., 2008).

Considering limited drug delivery to solid tumours as one of the causes of chemotherapy resistance, it is essential to be familiar with different factors which may interfere with drug delivery process. The following section discusses the factors which influence drug penetration into cancerous tissues and cause limited drug delivery.

1.5 Factors influencing drug penetration into solid tumours:

The effectiveness of cancer treatment depends on adequate delivery of the anticancer agent to tumor cells. Once it has reached the tumour cell, how it interacts with cellular macromolecules will also determine response. Many factors influence how much drug reaches tumours, the major ones have been summarized by Minchinton and Tannock (2006) into supply, flux and consumption (figure 1-6) (Minchinton and Tannock, 2006).

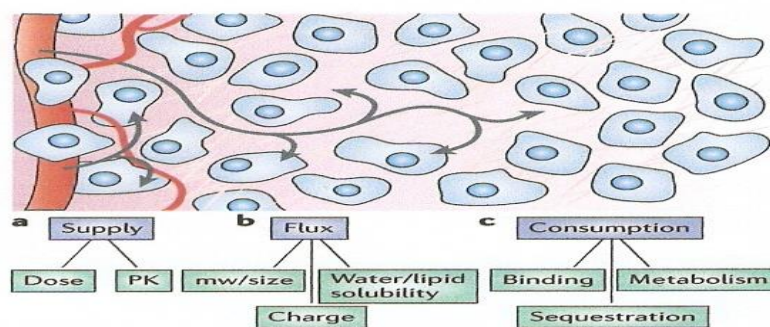


Figure 1-6: "Factors determining drug distribution in tissue. (a) Supply. The supply of a drug to the tissue will depend on its initial dose and its pharmacokinetics (PK). (b) Flux. After leaving the vasculature, flux through tissue can occur through extracellular or trans-cellular pathways, depending on relative solubility in water and lipids. Although diffusion through water will vary with size or molecular weight (mw), movement will be hindered by interactions with extracellular and cellular components, and the barrier posed by the cell membrane. (c) Consumption. Tissue penetration will be determined by the balance between delivery (supply and flux) and consumption. Cellular metabolism will reduce drug penetration and build-up within the tissue, and binding and sequestration can increase net tissue levels of a drug but limit its penetration." (Minchinton and Tannock, 2006).

Drug supply: The cytotoxic effects of chemotherapy agents are related to the time the tumour is exposed to an effective concentration of the agent (Alagkiozidis et al., 2011). A multitude of factors determine how much drug reaches the tumour. These include the dosage regimen or schedule employed, the actual dose administered, the type of administration (e.g. infusion or bolus) and route of administration. These factors can influence the concentration of the drug at the tumour site. In addition to the initial dose of administered drug, the pharmacokinetic (PK) processes of absorption, distribution, metabolism and excretion of the administered drug affect its concentration in the plasma (Rentsch et al., 1998). Some other pharmacological factors can also affect the drug distribution in normal or cancerous tissue. These factors are host related and they can affect the basic elements of pharmacokinetics and hence influence the supply of drugs to solid tumour, Table 1-2, (Garattini, 2007).

The vasculature of tumours is a critical factor that influences drug supply. It is well known that the vascular network which develops within tumours is poorly organised, inefficient and not extensive and this has a significant impact upon the supply of drugs to tumours (Brown and Wilson, 2004).

Table 1-2: Host factors influencing PK profiles and drug supply to tumours (Garattini, 2007).

- Age, Sex, Body weight, Race, Co-morbidity
- Genetic differences in cytochrome P450 and drug efflux and uptake transporters.
- Interactions with herbal remedies, food and drugs.

ABSORPTION

- Nausea, vomiting.
- Gastric acid secretion.
- Dissolution of tablets.

DISTRIBUTION

- Ascites or pleural effusion.
- Plasma albumins and α 1-acid-glycoprotein.
- Amount of body fat.
- Blood brain barrier (BBB).

METABOLISM

- Liver dysfunction.
- Altered hepatic blood flow.
- Reduced liver mass.
- Inflammation.

EXCRETION

- Altered biliary flow.
- Renal insufficiency.
- Urinary pH.

Drug flux through the tissue: Once a drug reaches the tumour, it has to leave the blood vessel (extravasate) and penetrate through several layers of cells. This process is called flux. There are two key processes by which drugs move through tissues; diffusion down a concentration gradient and convection which refers to the flow of fluid driven by differences in fluid pressure. Small molecules are mainly transported through tissue by diffusion whereas large molecules are transported by convection (Bobo et al., 1994). Drug diffusion depends mainly on the concentration gradient whereas convection depends on hydraulic conductivity and pressure differences (Jang et al., 2003). Drug flux through the tissue also depends on physicochemical properties such as

molecular weight, hydro or lipophilicity, and the charge of the drug. For example, the larger the drug molecule, its penetration through the extracellular matrix (ECM) is likely to be hindered. This applies to therapeutic agents such as antibodies (Garattini, 2007)

Drug consumption in the tissue: The last determinant factor of drug distribution in tissues is drug consumption, binding or sequestration in the targeted tissue. Drug can be consumed in the tissue in different ways. Consumption can occur through drug binding to receptor in the tissue. Whilst this type of binding can increase the deposition of the drug in the tissue, sequestered drugs will not be able to move to other cells within the tissue. Metabolism can lead to inactivation or degradation of the drug in preparation for it to be excreted. Consumption can also remove free drug by inhibiting further permeation (Baxter and Jain, 1991; Minchinton and Tannock, 2006).

In case of solid tumours, drug distribution in tissues can also be affected by other physiological factors related to the tumour microenvironment. These factors include irregular tumour vasculature, extracellular matrix (ECM) components, high interstitial fluid pressure (IFP) and cell to cell adhesion. The influence of physiological factors related to the characteristics of the tumour microenvironment on drug delivery and chemoresistance is discussed below.

Heterogenous angiogenesis and blood flow in tumours: Solid tumours have a unique physiology that is generated as a result of a chaotic and poor blood supply. During tumour development, the process of angiogenesis is “turned on” but the blood supply that develops is very different from that found

in normal tissues. Blood vessels in solid tumours are often highly abnormal with distended capillaries, leaky walls and sluggish flow (Figure-1-7) (Brown and Wilson, 2004; Shubik, 1982). In addition, the compression of blood vessels caused by cancer cells, increase resistance to blood supply and impair blood supply to the tumour. All this can result in reducing the delivery of nutrients and the clearance of metabolism products leading to hypoxic and acidic regions in the tumour, increased interstitial fluid pressure (IFP), abnormal extracellular matrix and establishing a microenvironment that has a direct impact on the delivery of anticancer drugs (Jain and Baxter, 1988; Padera et al., 2004).

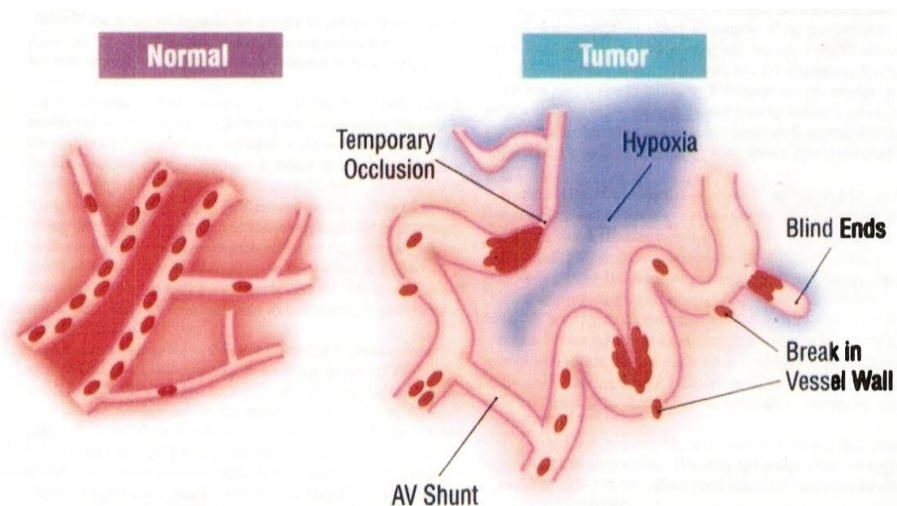


Figure 1-7: "The main differences between the vasculature of normal and malignant tissue. Whereas normal tissues have relatively uniform and well-ordered blood vessels that are sufficiently close together to oxygenate all of the tissues, blood vessels in tumours are tortuous, have incomplete vessel walls, have sluggish and irregular blood flow, and have regions of hypoxia between the vessels" (Brown and Wilson, 2004).

As stated above, poor and inefficient blood supply can lead to the presence of hypoxic regions within solid tumour tissues. In solid tumours, hypoxia has a significant role in enhancing resistance to both radiotherapy and chemotherapy (Brown, 1999). As the oxygen concentration decreases with increasing distances from the capillary, both cell proliferation rates and drug concentration also decrease (Figure 1-8). As a consequence of hypoxia, the fraction of proliferating cells will be decreased. The inhibition of cell proliferation can cause a decrease in the efficacy of most anticancer drugs because they are effective against rapidly dividing cells (Brown and Wilson, 2004; Minchinton and Tannock, 2006).

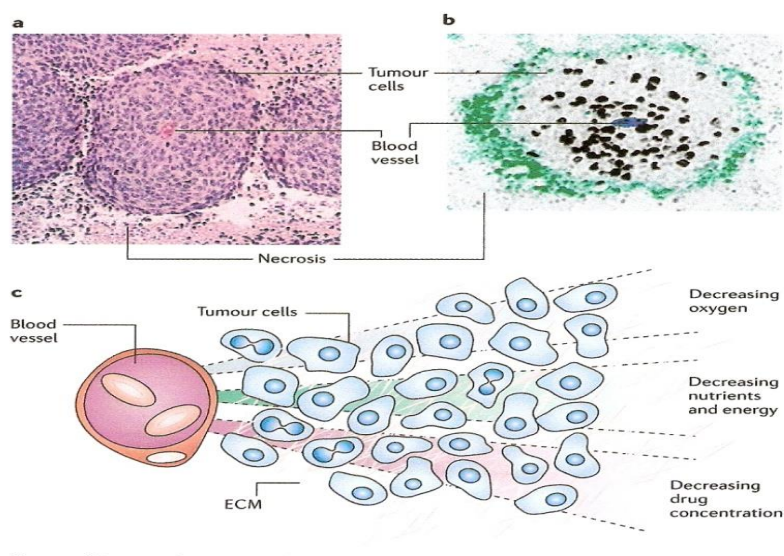


Figure 1-8: "Reasons why cells distant from blood vessels might be resistant to treatment. (a) Cords of cells surrounding a blood vessel in a xenograft of a cervix cancer. (b) Cords of cells surrounding a blood vessel in a xenograft of colon cancer. More cells are proliferating (bromodeoxyuridine-labelled black cells) close to the blood vessel. Green staining indicates hypoxic regions identified by pimonidazole. Proliferation occurs primarily close to blood vessels. Endothelial cells are coloured blue. (c) A diagrammatic representation illustrating the gradients in oxygen, nutrients and energy, and drug concentration." (Minchinton and Tannock, 2006).

The pH within the tumour microenvironment can also influence chemotherapy resistance or delivery of anticancer agents to cancer cells. Drug molecules depend mainly on passive diffusion to cross the cell membrane and diffusion will depend upon factors such as charge on the molecule. In the tumour microenvironment, the extracellular pH is low and the intracellular pH is neutral to alkaline (Kozin et al., 2001). Based on that, weakly basic drugs such as doxorubicin are protonated and show limited cellular uptake. On the other hand, weakly acidic drugs such as cyclophosphamide can be concentrated in the neutral intracellular space (Gerweck et al., 2006; Tannock and Rotin, 1989). In summary, a drug resistance in hypoxic and acidic regions of the solid tumour microenvironment may be related to a one of the following reasons, first, some drugs may be less effective in hypoxic, acidic, or nutrient deprived microenvironment, and second, cells in hypoxic areas may be exposed to low concentrations of drug because of limited drug access (Brown and Wilson, 2004; Tannock and Rotin, 1989).

Extracellular matrix (ECM) components: Solid tumours are composed of cancer cells and stromal cells including fibroblasts and inflammatory cells. Cancer cells and stromal cells are surrounded by an extracellular matrix (ECM) and are nourished by a vascular network. The ECM of solid tumours is composed of fibrous proteins such as collagen and polysaccharides like hyaluronan and proteoglycan. The role of ECM in normal tissue is to maintain homeostasis, generate tissue cohesiveness, act as a barrier to bacterial invasion and regulate macromolecule transport through interstitium (Heldin et al., 2004). Compared with normal tissues, tumour cells and stromal cells are

associated with an abnormal or altered ECM (Jang et al., 2003). The composition of extracellular matrix ECM in tumour can slow down the movement of molecules within the tumour and form a transport barrier against therapeutic drug penetration (Jain, 1998). Presence of glycosaminoglycan and collagen in the ECM can lower the hydraulic conductivity and lower convective fluid flow (CFF) through the interstitium (Netti et al., 2000).

Cell to cell adhesion: Cell-cell adhesion is another characteristic of the tumour microenvironment which acts as a barrier to drug delivery. The role of cell adhesion molecules (CAMs) in morphology, locomotion, mitosis, cytokinesis, phagocytosis and maintenance of cell polarity have been studied (Pavalko and Otey, 1994). CAMs are glycoproteins found on the cell surface and act as a receptor for cell-to-cell and cell-to-ECM adhesions (Hynes and Zhao, 2000). CAMs can be divided to integrins, cadherins, selectins and the immunoglobulin superfamily (Dunehoo et al., 2006). Targeting or modifying CAMs such as integrins to disrupt cell-cell adhesion can be exploited to enhance drug delivery to solid tumours (Chen and Chen, 2011).

High interstitial fluid pressure (IFP) and convective fluid flow (CFF): Another feature of solid tumours is the absence of a widespread lymphatic supply which is essential for returning the interstitial fluid to the blood circulation. In normal tissue, tissue fluid and macromolecules are drained via the lymphatic system. An impaired lymphatic system is a characteristic of solid tumours (Leu et al., 2000) which can lead to the retention of fluid and macromolecules in the tumour interstitium. The lack of a functional drainage

system causes the accumulation of fluids and contributes to increased interstitial fluid pressure (IFP) (Heldin et al., 2004; Hicks et al., 2006). This in turn can limit drug penetration into solid tumours in spite of leaky microvasculature because high IFP reverses the direction of CFF and fluid moves from the tumour into the blood vessel. This inhibits the transvascular transport of molecules and inhibits transport in the interstitial space (Jain, 1998; Padera et al., 2004). This issue will be discussed in detail in the following section as it is one of the key objectives of this project.

1.6 Impact of interstitial fluid pressure (IFP), hydrostatic pressure (HP) and convective fluid flow (CFF) on drug penetration:

One of the main objectives of this project is to assess the impact of convective fluid flow (CFF) on drug penetration. This section will discuss the impact of IFP, hydrostatic pressure (HP) and CFF on drug distribution in tissue as they are all related to each other. As explained earlier, one of the consequences of elevated IFP in solid tumours is that the normal process of CFF through tissue is impeded. This is now recognised as a major barrier to drug uptake leading to reduced drug efficacy (Heldin et al., 2004). Drugs are transported out of capillaries to the tissue by diffusion and/or convection. They are transported through the interstitial space then into the lymphatic system or venous part of the vasculature to be drained or excreted. Transcapillary pressure is determined by the HP and colloid osmotic pressure in capillaries and in the

interstitium, together with hydraulic conductivity and the plasma protein reflection coefficient (Figure 1-9) (Heldin et al., 2004).

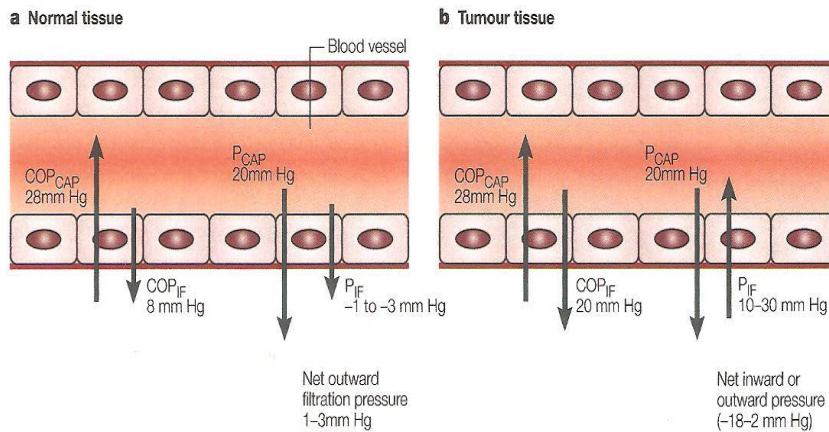


Figure 1-9: Factors regulating drug transcapillary transport in normal and cancerous tissue: In normal tissue, the hydrostatic pressure is greater than the IFP; therefore there is a net outward filtration of 1-3 mm Hg. In tumour tissue, the hydrostatic pressure is less than or slightly greater than the IFP therefore there is a net inward or outward pressure of -18-2mm Hg (Heldin et al., 2004). Figure's abbreviations: COP= Colloidal osmotic pressure, P= Hydrostatic pressure, IF= Interstitial fluid, CAP= Capillary.

In normal interstitium, the transcapillary flow is outward from the vessel into the interstitium. In case of tumour tissue however, the transcapillary flow or the filtration pressure is either inward or outward pressure. In case of solid tumour, HP and IFP are often increased (Jain, 1987b). This was noticed in breast cancer, colorectal cancer (Less et al., 1992) and head and neck cancer (Gutmann et al., 1992). IFP values in solid tumours may reach up to 38 mmHg (table 1-3) (Jain, 1998).

Table 1-3: Values of IFP (mmHg) in normal and neoplastic tissues, (Jain, 1998).

Tissue type	N	Mean IFP (mmHg)
Normal skin	5	0.4
Normal breast	8	0.0
Head/neck carcinomas	27	19
Cervical carcinomas	26	23
Lung carcinomas	26	10
Metastatic melanomas	14	21
Breast carcinomas	13	29
Brain tumours	17	7
Colorectal liver metastasis	8	21
lymphomas	7	4.5
Renal cell carcinoma	1	38

IFP can be measured using the wick-in needle technique or the micropuncture technique. Wick-in needle technique is performed by inserting a fine steel needle filled with a wick into the tissues to measure the fluid pressures. The needle is connected to pressure sensors that can read the pressure. The micropuncture technique is performed using a sharpened glass capillary. The capillary is connected to a counter pressure system to measure the fluid pressures in the tissues. This technique is more reliable than the wick-in needle as it is less traumatic. However, wick-in needle technique reserves the advantage of being able to measure fluid pressures in deep tissues (Aukland and Reed, 1993; Heldin et al., 2004).

Elevated IFP occurs in solid tumours due to blood-vessel leakiness, abnormal lymphatic system, interstitial fibrosis and contraction of the interstitial space caused by stromal fibroblasts (Heldin et al., 2004). High IFP which is a characteristic of solid tumours can limit drug delivery to solid tumours.

Evidence for this is provided in several studies. One of them revealed that patients with melanoma or lymphoma who showed low IFP responded better to the treatment whereas those with high IFP did not respond to the treatment (Curti et al., 1993). Resistance and bad progression in these tumours were expected by the author to be due to the high IFP. However, the author did not specify clearly that resistance noticed with high IFP was due to limited delivery of chemotherapeutic agents to these tumours. In another study, high IFP in patients with cervical cancer caused high recurrence rate and poor prognosis (Milosevic et al., 2001).

Large molecules such as proteins are transported in the interstitium by CFF. On the other hand, low molecular weight compounds such as oxygen and glucose are mainly transported by diffusion (Jang et al., 2003). High IFP can impede CFF and hence limit the delivery of drugs that depend on CFF to be delivered to the solid tumour. For this reason lowering IFP to turn CFF on again might be an effective strategy to improve drug delivery to solid tumours.

Utilizing convection (CFF) to deliver drugs to solid tumours has been tested in several studies (Baxter and Jain, 1989; Bobo et al., 1994; Chary and Jain, 1989; Mardor et al., 2005; Swabb et al., 1974). Chary and Jain (1989), used fluorescence photobleaching to measure interstitial convection and diffusion of albumin in normal and neoplastic tissues grown in a thin, transparent window chambers in the ear of a rabbit. Average albumin velocity and albumin diffusion coefficient were measured. The results of this study provided impetus for further investigation into convection and diffusion in different normal and

neoplastic tissues (Chary and Jain, 1989). Another study investigated the use of convection as a mean to enhance the distribution of the large and small molecules in the brains of anesthetized cats. Convection-enhanced distribution of transferrin as macro and sucrose as micro molecules into the white matter of these anesthetized cats was produced through maintaining a pressure gradient during interstitial infusion. Using interstitial infusion to enhance drug delivery to brain, transferrin and sucrose brain concentrations were >100-fold higher than systemic concentrations. Results of this study showed that enhanced distribution of large and small molecules can be obtained in the brain through maintaining convection. This in turn can result in achieving high drug concentrations in the brain as well (Bobo et al., 1994). A clinical trial has been conducted to study the safety and efficacy of the use of intratumoural convection-enhanced delivery (CED) of paclitaxel for the treatment of patients with recurrent malignant gliomas. CED of paclitaxel was associated with high (73%) antitumour response rates in patients included in this study (Lidar et al., 2004). Mardor and his group used magnetic resonance imaging (MRI) to assess convection efficiency and cytotoxic tissue response to different anticancer agents in a rat brain model. Using convection for direct delivery of drugs to brain based on delivering a continuous infusion via intracranial catheter is a novel drug delivery approach. Using this method to deliver different anticancer agents including taxol and carboplatin was assessed and showed efficient distribution in the brain. This method can be applied to other anticancer agents especially those with high molecular weights (Mardor et al., 2005).

The results of these studies support the usefulness of utilizing CFF as a tool to improve drug delivery to solid tumours. Utilizing the knowledge gained from the factors that limit drug penetration and drug delivery to solid tumours can help designing methods, experiments and techniques to study this problem. The following section will discuss these techniques.

1.7 Methods used to study drug penetration into solid tumours:

A wide range of *in vitro* and *in vivo* techniques have been used to examine drug penetration in solid tumours. These techniques include the use of multicellular spheroids (MCS), (MCLs) and animal's studies, details of which are outlined below.

1.7.1 *In vitro* techniques:

Multicellular spheroids: Multicellular spheroids (Figure 1-10a), are spherical aggregates of cells. MCS were first described by Sutherland's group in the 1970's and it provides one of the first 3 dimensional culture models which could be used to study drug resistance and tumour biology (Inch et al., 1970). Drug penetration studies employed MCSs as a reasonable model for solid tumours with similarities to solid tumours environment (Nederman and Twentyman, 1984). Similarities of MCSs to solid tumours environment are represented by the ability of MCSs to generate an ECM, presence of tight junctions between cells, gradients of cell proliferation, gradients of nutrient concentration, gene expression, and biological behaviour of cells (Durand,

1989; Nederman and Carlsson, 1984; Sutherland, 1988; Sutherland et al., 1979; West et al., 1980). Using fluorescent or radiolabeled drugs, studies have shown limited penetration of doxorubicin, vinblastine, paclitaxel and methotrexate into the deeper layers of spheroids (Minchinton and Tannock, 2006; Sutherland et al., 1979; West et al., 1980). Analysis of drug penetration into MCS is however restricted to those drugs that are naturally fluorescent or can be radiolabeled. The multi-cell layer model (Figure 1-10b) described below circumvents this limitation as a wide range of analytical techniques can be applied.

Multicell layers: The multicell layer model was initially described by Wilson and his colleagues (Cowan et al., 1996; Hicks et al., 2006) and it provides a quantitative method that permits direct assessment of drug penetration through cell layers (Tannock and Rotin, 1989). The apparatus is shown in (figure 1-10c) and tumour cells are grown on collagen coated micro porous Teflon membrane to form the MCL. The resulting MCLs have a symmetrical, planar structure. To examine penetration, a drug is added to one side of the MCL (donating chamber) and its appearance on the other side of the MCL (receiving reservoir) is measured as a function of time using an appropriate analytical method, (Figure 1-10d). MCL is similar to MCS in sharing several properties of solid tumours derived from the same cell type, including a similar ECM, and tight junctions between epithelial cells. Studies conducted using MCLs have shown poor penetration of many anticancer agents through them (Kyle et al., 2004; Kyle et al., 2007; Phillips et al., 1998; Primeau et al., 2005; Tunggal et al., 1999). Phillips and his team described and characterized a

modified version of the assay published by Cowan et al in 1996, (Cowan et al., 1996). This study also illustrated the application of this assay for evaluating the ability of bioreductive drugs such as EO9 and tirapazamine to penetrate multicell layers. Results of this study showed limited penetration of these drugs especially EO9 through the MCLs of DLD-1 which suggested that the failure of EO9 in the clinic was mainly due to combination of poor delivery and rapid in vivo elimination of the drug (Phillips et al., 1998). Tunggal and his team used the MCLs to quantify the penetration of four widely used anticancer drugs. The penetration of doxorubicin and mitoxantrone was limited and very slow compared to the penetration of methotrexate and 5-FU. MCLs have been shown to act as a substantial barrier to the effectiveness of these drugs (Tunggal et al., 1999). Tannock has also used MCLs to study the penetration of some anticancer drugs and suggested that the limited ability of anticancer drugs to reach tumour cells that are distant from blood vessels might be an important cause of clinical resistance of solid tumours to chemotherapy (Tannock et al., 2002). Using MCLs, different analytical techniques can be used such as high-performance liquid chromatography and mass spectrometry. The application of these techniques provides many advantages including the ability to differentiate between the parent compound and any metabolic products formed. This feature is not possible with spheroids (Minchinton and Tannock, 2006).

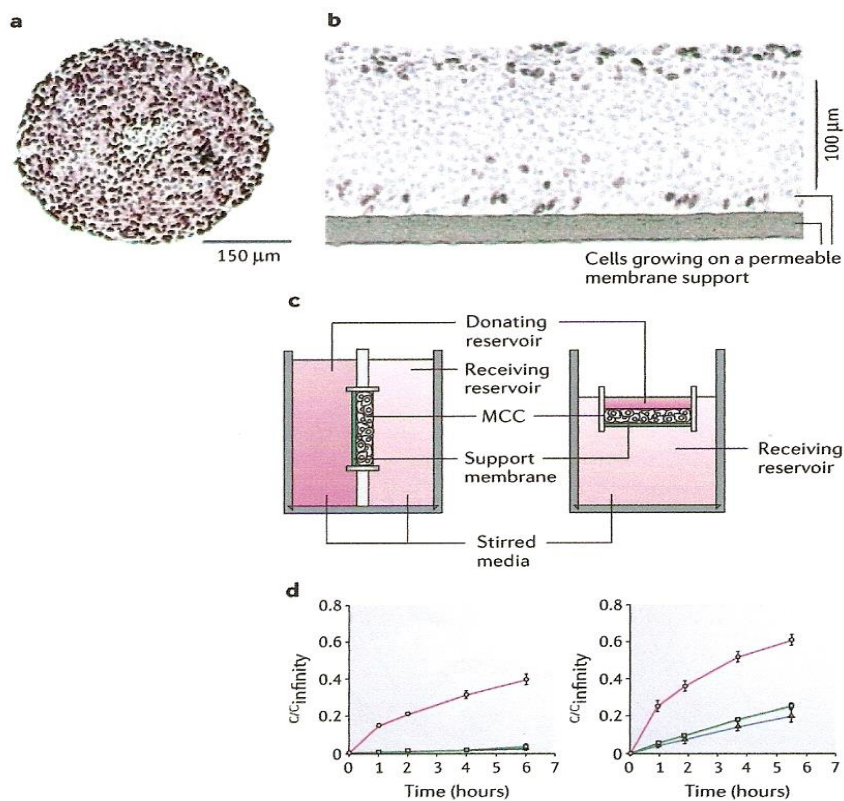


Figure 1-10: "Multicellular models used to study drug penetration. (a) Multicellular spheroids are grown in spinner culture to form spherical aggregates. (b) Multilayered cell cultures (MCCs) are grown on permeable support membranes; proliferating cells are located predominantly close to the upper and lower surfaces. (c) Studies of drug penetration are usually performed by separating two reservoirs with an MCC (left) or by floating an MCC on a medium with the drug of interest added to the small compartment above the MCC, and sampling from the lower receiving reservoir (right). (d) The penetration of a drug through an MCC (lower curves) is usually compared to penetration through the support membrane alone (upper curves), as shown for doxorubicin (left) and 5-fluorouracil (right)." (Minchinton and Tannock, 2006).

1.7.2 *In vivo* techniques:

Different *in vivo* methods can be used to study drug penetration into solid tumours. These include:

Window chambers: *In vivo* techniques can be performed in animals directly in a model called window chambers. In this technique, tumour is implanted under the skin of an experimental animal. The tumour is then covered with a translucent window. In this *in vivo* model, tumours are observed directly in the living animals prior to and after drug administration. Direct assessment of fluorescent drug penetration or distribution into tissue can be achieved using this technique (Chary and Jain, 1989; Dreher et al., 2006; Netti et al., 2000). This technique can also give information about the *in vivo* effect of an anticancer agent (Chary and Jain, 1989; Helmlinger et al., 1997).

Tumour sections: *In vivo* techniques can also be performed through using sections of tumours taken either from animal (Figure 1-11) or human (Figure 1-12) treated tissues. Using these sections, drug distribution in tumour can be studied using direct fluorescence or immunohistochemistry. Direct visualisation of fluorescent drugs like doxorubicin in a tumour microenvironment was studied using this technique (Henneberry and Aherne, 1992; Ozols et al., 1979). Drug distribution in tumours in relation to blood supply or hypoxia can also be studied using fluorescent-labelled antibodies (Lankelma et al., 1999; Primeau et al., 2005) as seen in figures 1-11 and 1-12.

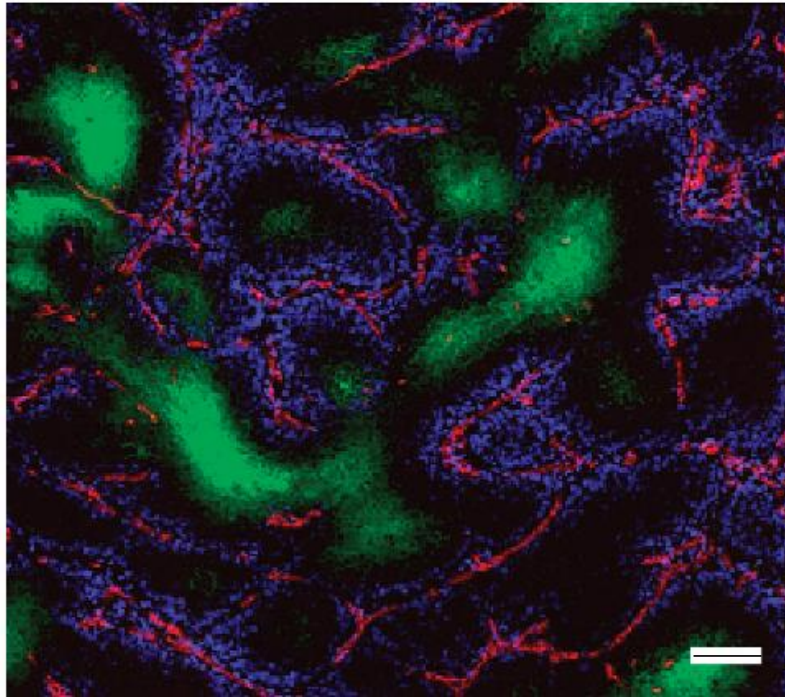


Figure 1-11: Doxorubicin distribution into sections of tumour tissue: Perivascular distribution of doxorubicin (blue) in relation to hypoxic regions (green) and blood vessel (red) in tissue sections of mouse mammary adenocarcinoma (16C). Bar, 100 μm . (Primeau et al., 2005).

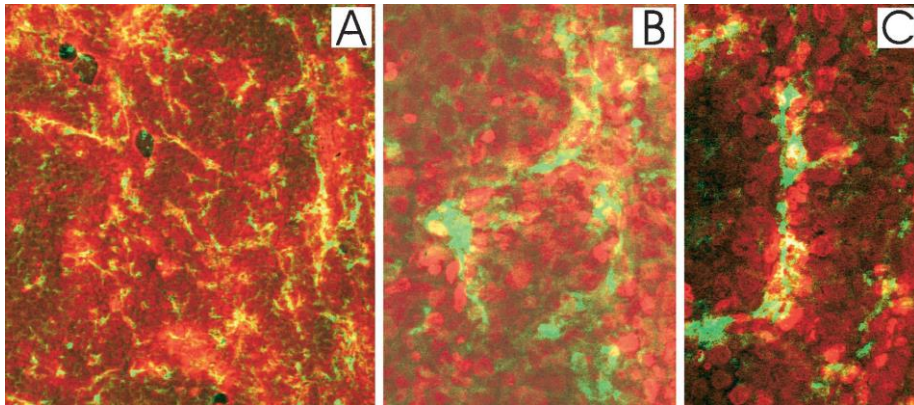


Figure 1-12: Doxorubicin distribution in human tissue: Doxorubicin distribution (*red*) at 2 h after doxorubicin injection of patient. Immunostaining vessels with an antibody to CD31 (*green*), both colours yields (*yellow*) when superimposed. Doxorubicin nuclear concentrations were highly observed near the microvessles. Magnifications: x10 (A); x40 (B and C). (Lankelma et al., 1999).

Non-invasive imaging techniques: The development of non-invasive imaging techniques such as magnetic resonance imaging (MRI) and positron-emission tomography (PET) for studying drug distribution in tissues of animals or humans are promising tools. The only problem facing these methods is the resolution which is not yet able to assess drug distribution in solid tumours. However, with the development of more advanced technology, these techniques might improve in the future and become useful tools for researchers who are interested in this field (Brindle, 2008).

There are advantages and disadvantages of using *in vivo* methods to study drug penetration. The advantage of using *in vivo* methods is that they are more realistic than *in vitro* methods as they represent the whole factors that affect drug distribution in tissues including drug metabolism which is not present in the *in vitro* techniques. On the other hand, the high cost, time consumption and the extensive use of animals are the most important disadvantages of *in vivo* techniques.

These *in vitro* and *in vivo* methods can be exploited to design experiments and models to study drug penetration and to develop strategies to improve drug delivery to solid tumours. These strategies are discussed in the following section.

1.8 Strategies used to improve drug penetration into solid tumours:

Understanding the barriers to drug delivery to solid tumours is central to the development of strategies that are designed to improve drug delivery to cancer cells. Several strategies have been developed and these include; manipulating tumour vasculature, reducing IFP, manipulation of tumour pH, modification of the ECM, modifying drug administration regimens, and modifying drug pharmacokinetics or physicochemical properties of compounds. These strategies with some examples are explained below:

1.8.1 Manipulating tumour vasculature:

Pre-treating solid tumours with anti-angiogenic therapy: Anti-angiogenic agents such as the monoclonal antibody bevacizumab that targets vascular endothelial growth factor (VEGF), seems to improve the effect of cancer chemotherapy mainly by normalizing the vascular architecture in tumours, improving blood flow and reducing the IFP (Jain, 2001, 2005; Tong et al., 2004). Experimental studies showed that combining anti-VEGF target drugs with other chemotherapeutic agents increased the responses of experimental tumours (Segers et al., 2006; Wildiers et al., 2003). Using bevacizumab in clinical trials for the treatment of patients with metastatic colorectal cancer (Arkenau et al., 2009; Hurwitz et al., 2004), non-small-cell lung cancer (Herbst et al., 2011; Herbst et al., 2007; Sandler et al., 2006) and malignant gliomas (de Groot and Yung, 2008), prolonged survival rates when combined with other chemotherapeutic agents have been recorded.

Use of vascular disrupting agents: A number of agents have been developed to directly target the vasculature of tumours with the aim of either cutting off the blood supply to the tumour or trapping drug inside the tumour by collapsing the vasculature when the drug concentration in the tumour is at its maximum (Curnis et al., 2002; Siemann et al., 2005). Drugs in this class include tumour necrosis factors, flavone acetic acid, dimethylxantheone acetic acid, and the tubulin binding agents like combretastatin-A4 disodium phosphate (Horsman and Siemann, 2006; Siemann, 2011). The effect of these agents on the tumour vasculature include elevation of vessels permeability, reducing tumour blood flow, reducing drug clearance from tumour and hence increasing drug accumulation at the tumour site. On the other hand, if vascular disrupting agents were given before chemotherapy they may cause reduction in blood flow which in turn can increase the IFP which leads to a decrease in drug delivery to the tumour (Horsman and Siemann, 2006). Some of the vascular disrupting agents are being or have been tested in clinical trials. The most important of them are the tubulin-depolymerizing vascular disrupting agent combretastatin A-4 phosphate CA4P (Fosbretabulin) and the flavonoid vascular disrupting agent ASA404 (Vadimezan) (Siemann, 2011). In a phase II clinical trial, ASA404 in combination with carboplatin and paclitaxel has given 5 month patient survival advantage when it was given to patients with non-small cell lung cancer (McKeage, 2011; McKeage et al., 2009). Combretastatin A-4 phosphate has been tested in phase II and III clinical trials for the treatment of anaplastic thyroid cancer and phase II clinical trial for the treatment of non-small cell lung cancer with promising results (Siemann, 2011;

Siemann et al., 2009). Other randomized phase II and phase III clinical trials using combretastatin and ASA404 combined with standard chemotherapy in advanced non-small cell lung cancer are currently on-going. The results of these clinical trials are expected to be reported shortly (McKeage, 2011). If successful, these agents could be used to develop strategies that may enhance the delivery of partner therapeutics.

Modulating muscle tone of the blood vessel: Using histamine or a selective endothelin receptor-A antagonist like Botulinium neurotoxin type-A which relax the blood vessel and increase tumour blood flow which in turn can reduce the IFP and improve drug delivery (Brunstein et al., 2006). Histamine showed synergistic antitumour effect when combined with melphalan as perfusion for the treatment of experimental rats with soft tissue sarcoma liver metastasis. The technique used in this experiment is called Melphalan-based isolated hepatic perfusion (M-IHP). The author concluded that the results of this experiment are encouraging and that phase I-II study to explore the efficacy in the clinic is worthwhile (Brunstein et al., 2007). Injecting botulinium neurotoxin type-A locally into mouse tumours increased tumour oxygenation and perfusion. The tumour has also shown improvement by responding to radiotherapy and chemotherapy. The significant increase in tumour oxygenation and perfusion is expected to be due to the botulinium neurotoxin relaxation of the tumour vessels. The results of this experiment can be applied in clinical trials to improve drug delivery and reduce chemotherapy resistance (Ansiaux et al., 2006; Ansiaux and Gallez, 2007). In another study, botulinium neurotoxin type-A has significantly increased the uptake of gemcitabine in

hepatomas implanted in mice. Compared with two other perfusion-enhancing vascular modifiers (BQ123 and thalidomide), botulinium neurotoxin type-A has significantly enhanced tumour growth inhibition when combined with gemcitabine in the same study (Cron et al., 2008). The results of this study and the previous study are promising for preclinical and clinical evaluation of botulinium neurotoxin type-A as a vascular modifier to enhance drug delivery to solid tumours.

1.8.2 Reducing interstitial fluid pressure (IFP):

Because of the higher IFP in tumours compared to normal tissues, the net convection flow in tumour interstitium is outward from the core of a tumour (Jang et al., 2003). Reducing IFP using one of the previous methods or through the use of one of the following methods can potentially improve drug delivery to the tumours via re-instating the normal convective fluid flow from the blood vessel into the interstitium.

Use of platelet derived growth factor (PDGF) inhibitors: PDGF mediates high IFP in tumours through stimulating cells contractility and through promoting interactions between the extracellular matrix molecules and the integrins of stromal fibroblasts (Heldin et al., 2004). For this reason, using a PDGF inhibitor such as imatinib might decrease IFP in tumours and hence enhances drug delivery (Pietras et al., 2002). PDGF antagonists have lowered tumour IFP, increased drug uptake and increased treatment efficiency in preclinical models. Imatinib through inhibiting PDGF and reducing tumour IFP increased the therapeutic index of the epothilone B microtubule stabilizing

agent EPO906 (Patupilon) through increasing EPO906 uptake into human anaplastic thyroid carcinomas implanted into mice (Pietras et al., 2003). Another study showed that the PDGF receptor beta (PDGFR- β) inhibitor CDP860 caused fluid accumulation and increased vascularized volume in patients with advanced ovarian or colorectal cancer. Although this clinical trial was stopped early because of the fluid accumulation noticed in most of the patients, however, its results suggested that inhibiting PDGFR- β might improve the delivery of anti-cancer agents (Jayson et al., 2005). The concept of adding a PDGF antagonist to reduce IFP and improve drug uptake and efficacy was applied in a clinical trial conducted by Starling and his group (Starling et al., 2011). This clinical trial aimed to define safe doses of gemcitabine plus oxaliplatin combined with imatinib in patients with advanced gemcitabine-refractory pancreatic cancer. Gemcitabine and oxaliplatin were safely and feasibly combined with imatinib given every other week.

Use of transforming growth factor β (TGF β) inhibitors: TGF β inhibitors are expected to decrease amount of extracellular matrix molecules and hence reduce IFP in tumours which in turn can enhance drug delivery (Lammerts et al., 2002). Lammerts and his colleagues reported that a decrease in tumour IFP was noticed in mice after 5-10 days of treatment with TGF β inhibitor. It was also observed in Lammerts study that using TGF β inhibitor leads to a reduction in the amount of collagen but not in hyaluronan content which suggests that the reduction of IFP in tumours was due to the inhibition of collagen synthesis (Jacobson et al., 2003). Inhibiting TGF β lowered IFP in KAT-4 experimental model for anaplastic thyroid carcinoma. Pre-treating KAT-

4 carcinomas with TGF β inhibitor increased cytotoxicity of doxorubicin against KAT-4 carcinoma cells (Salnikov et al., 2005). LY2109761 and 1D11 are TGF β inhibitors which were tested preclinically and showed the ability to reduce tumour burden and metastasis *in vivo* (Ganapathy et al., 2010; Melisi et al., 2008).

Use of tumour necrosis factor α (TNF α): TNF α is an inflammatory cytokine. It is expected to cause reduction in IFP due to its vasodilatory effect which is mainly mediated by the release of nitric oxide (NO) from endothelial cells or macrophages (Baudry and Vicaut, 1993). Use of TNF α in immunocompromized mice bearing human melanoma caused 64% decrease in tumour IFP and reduced the mean arterial pressure by 70% (Kristensen et al., 1996). Using isolated limb perfusion, melphalan concentrations in tumour tissues implanted in rats were six fold higher when combined with TNF α which indicates the synergistic anti-tumour effect between TNF α and melphalan (de Wilt et al., 2000). In humans, TNF α has enhanced the anti-tumour activity of chemotherapeutic agents when combined together through isolated limb perfusion for the treatment of patients with melanoma or sarcoma of the extremities (Grunhagen et al., 2006). Long term outcome of isolated limb perfusion with TNF α for patients with melanoma has proved long term local control in selected patients (Deroose et al., 2011).

Use of corticosteroids: Corticosteroids are expected to reduce IFP due to their anti-inflammatory action which can cause growth arrest and apoptosis induction as well as their ability to reduce stromal contents of the extracellular

matrix (ECM) (Li et al., 2004). Dexamethasone which is a corticosteroid has significantly reduced the IFP of human colon carcinoma xenograft implanted in mice (Kristjansen et al., 1993). This reduction in IFP was mainly due to a reduced microvascular permeability and vascular hydraulic conductivity in the tumours and due to decreased amounts of ECM contents. Dexamethasone has significantly reduced IFP, reduced the tumour growth and augmented the effect of 5-fluorouracil in rats bearing mammary tumours (Stuhr et al., 2006). The author reported that this reduction in IFP was mainly due to the anti-inflammatory effect of dexamethasone and due to inhibiting the production of ECM stromal contents.

Use of chemotherapy itself: The use of chemotherapy itself in a concept called low dose chemotherapy causes limited cell killing but in addition, it can reduce the tumour cell density, decompress blood vessel, decrease microvascular pressure and decrease the IFP (Jang et al., 2003). The use of low dose paclitaxel increased cells apoptosis and reduced the IFP which enhanced the delivery of paclitaxel in tumours implanted in mice (Griffon-Etienne et al., 1999). In another study, paclitaxel decreased IFP and improved oxygenation in breast cancer in patients treated with neoadjuvant chemotherapy (Taghian et al., 2005). Another study showed that treatment with imatinib in non-small-cell lung cancer (NSCLC) is associated with decrease of IFP and improved oxygenation in A549 human lung adenocarcinoma xenografts grown in mice (Vlahovic et al., 2006).

Use of vasodialating agents: Use of vasodialating agent like hydralazine can also reduce the IFP through decreasing tumour blood flow which in turn can reduce flow resistance and increase transcapillary pressure gradient (Zlotecki et al., 1995). Zlotecki (1995) and his group reported that hydralazine reduced IFP by 50% in mice bearing human colon adenocarcinoma xenograft. In another study, hydralazine has significantly reduced IFP by 31% and 14% from the initial value in two different solid tumour models implanted in mice (Podobnik et al., 2001). Other vasodilators such as bradykinin agonists, nicotinamide and prostaglandin E₁ (PGE₁) have also been reported to lower IFP and hence enhance drug uptake by tumours. In addition to its vasodialating effect, labradamil which is a bradykinin agonist can increase vascular permeability through increasing vasculature pore size and increasing vascular surface area which at the end reduces IFP and improves blood flow (Emerich et al., 2001a). Labradamil was reported to increase the tumour uptake of other chemotherapeutic agents such as carboplatin and doxorubicin in rats (Emerich et al., 2001b). A recent study reported that bradykinin agonists have improved the uptake of the MRI contrast Agent Gd-DTPA, into rodents bearing malignant brain tumours (Sarin et al., 2009).

Nicotinamide which is a water soluble vitamin lowers the mean arterial blood pressure which cause a decrease in the flow resistance in tumour which in turn reduce IFP and enhance drug uptake (Lee et al., 1992). Intraperitoneal injections of nicotinamide were found to reduce tumour IFP by about 40% in a study conducted by Lee and his group using mice bearing tumours. It is expected that lowering of IFP was due to lowering of the vascular resistance

as mentioned above and due to tumour ulceration which resulted in increasing tissue hydraulic conductivity (Lee et al., 1992). In another study, nicotinamide reduced IFP in a dose and time dependent manner when tested in mice bearing tumours (Peters et al., 1997). Prostaglandin E₁ (PGE₁) which is a proinflammatory factor has also been shown to reduce IFP through decreasing the contractility of stromal fibroblasts by decreasing fibroblasts-mediated collagen (Rubin et al., 2000). PGE₁ significantly reduced IFP and enhanced the anti-tumour efficacy of 5-FU in rats bearing colonic and mammary tumours (Salnikov et al., 2003).

1.8.3 Manipulation of tumour pH:

Low pH of extracellular environment is a characteristic of solid tumours (Kozin et al., 2001). Low pH can lead to a decrease in the ionization of weak acids and increase the ionization of weak bases. For this reason lower extracellular pH leads to increased activity and cellular uptake of weak acids and decreased activity and cellular uptake of weak bases as they will be sequestered in acidic pH (Tannock and Rotin, 1989; Vukovic and Tannock, 1997). This hypothesis was proved as the basic anticancer agents, e.g. doxorubicin and mitoxantrone were found to have difficulty in penetrating MCLs because they concentrate in perinuclear acidic endosomes. For this reason, addition of competing weak bases such as chloroquine, or the addition of a proton pump inhibitor such as omeprazole to convert the perinuclear endosomes pH from acidic to basic significantly helped those drugs to penetrate the MCLs (Lee and Tannock, 2006). The other effect of low pH is

that it can affect cellular uptake of some drugs which depend on active transport process such as methotrexate (Cowan and Tannock, 2001). Methotrexate is a weak acid. It is a well-known anticancer agent. It is actively transported into cells mainly through active transport mechanism depending on a transporter protein. This protein is inhibited at low pH. Using MCLs, this hypothesis was proved when the activity and cellular uptake of methotrexate were inhibited in acidic pH induced by adding folic acid (Cowan and Tannock, 2001). The explanation here was that low pH inhibited the energy dependent active transport process which in turn reduced cellular uptake of methotrexate. An *in vitro* preclinical study conducted to reduce the intracellular pH using cariporide and S3705 in order to enhance the pH-dependent cytotoxic effect of melphalan for human breast cancer cells. Lowering intracellular pH enhanced cell killing after multiple courses of melphalan. This study concluded that intracellular pH manipulation can influence the effect of chemotherapy (Wong et al., 2005). An *in vivo* study tested the effect of pH change -using glucose- on the efficacy of the weak acid chlorambucil and the weak base doxorubicin against lung carcinoma implanted in mice. A minor change in the intracellular-extracellular pH gradient by 0.2 units increased tumour growth delay induced by the weak acid chlorambucil by 2.3 folds compared to the weak base doxorubicin (Gerweck et al., 2006). This indicated that pH gradient difference between normal and tumour tissue may be exploited and targeted for the treatment of cancer through developing weak acid chemotherapeutic agents.

1.8.4 Remodelling the extracellular matrix (ECM):

Extracellular matrix (ECM) is known to limit drug penetration through either directly binding to the drugs or through its acidic pH as explained above. In addition, ECM has an adhesive effect. Tumour and stromal cells produce an ECM consisting of collagens, proteoglycans and other molecules that limit the transport of molecules. This adhesive effect can limit drug penetration into solid tumours (Netti et al., 2000).

Using *hyaluronidase*: Hyaluronidase which has anti-adhesive effect through breaking hyaluronic acid down has enabled drugs to permeate through the extracellular matrix component more freely (Heldin et al., 2004). Pre-treating multicellular tumour spheroids of squamous carcinoma with hyaluronidase enhanced doxorubicin penetration and cell killing (Kohno et al., 1994). Treating multicellular spheroids with *hyaluronidase* as an anti-adhesive agent allowed drugs such as cyclophosphamide to permeate the extracellular matrix more freely (Croix et al., 1996). In a pilot study, hyaluronidase improved the penetration of carboplatin and other standard chemotherapy used for the treatment of children with brain tumour (Pillwein et al., 1998). In a number of preclinical and clinical trials, adding hyaluronidase enhanced the efficacy of cytotoxic agents as it may decrease intratumoural pressure and loosen cell to cell contact which in turn enhances drug penetration (Baumgartner et al., 1998). Hyaluronidase has also improved the distribution and uptake of liposomal doxorubicin in human osteosarcoma xenografts implanted in mice (Eikenes et al., 2005). Although hyaluronidase enhanced penetration and

efficacy of some chemotherapeutic agents, however, this technique may not be applicable systemically. In addition it is expected that penetration might have been enhanced by mechanisms other than modulating the extracellular matrix (Croix et al., 1996).

Using *collagenase*: Collagen is expected to be a major determinant of resistance of drug transport in solid tumours as it hinders the transport of macromolecules. Tumours contain much denser collagen network which is thicker than that of normal tissue. In addition to this, tumours contain increased number of fibroblasts which are usually bound to the collagen fibres which create more tension between the fibres and this contributes towards increased IFP in tumours (Heldin et al., 2004). Reduction of collagen content in tumours using *collagenase* can be used as a method for enhancing drug delivery to solid tumours because it reduces IFP and loosen the interstitium of the solid tumour (Netti et al., 2000). Human osteosarcoma xenografts treated with *collagenase* improved the distribution of monoclonal antibodies (Eikenes et al., 2004). *Collagenase* also increased viral vectors transport in human melanoma xenografts (McKee et al., 2006). *Collagenase* has significantly increased nanoparticle penetration in collagen-treated multicellular spheroids (Goodman et al., 2007). In a recent study, ultrasound-guided administration of the collagen-2 selective *collagenase-2* improved liposomal doxorubicin accumulation and distribution in solid tumour xenografts. Intratumoural and intravenous administration of *collagenase-2* reduced IFP by 35 and 40% respectively compared to control (Zheng et al., 2011). Despite the results of this study and the previous studies which have shown the ability of

collagenase to enhance drug delivery to solid tumours but this strategy has not yet translated into clinical trials mainly because of the danger of affecting normal tissues and to avoid metastasis that can be created by the use of *collagenase* (Tredan et al., 2007). Developing types of *collagenases* that can selectively act only on the tumour collagen will make this strategy more attractive but this is challenging.

Using relaxin: The use of relaxin which is a hormone secreted by women during pregnancy has been shown to degrade the tumour ECM and to improve macromolecular diffusion in tumours (Brown et al., 2003). Relaxin is expected to inhibit collagen synthesis, increase collagen turnover and up-regulates the matrix metalloproteinases (Jain and Stylianopoulos, 2010; Seibold et al., 2000). Through these mechanisms relaxin enhanced the diffusion of IgG by twofold and increased the diffusion of dextran by threefold in human soft tissue sarcomas (Hsts26t) xenografts (Jain and Stylianopoulos, 2010; Perentes et al., 2009). More preclinical *in vivo* studies are required to prove the success of the use of relaxin as one of the strategies to improve drug delivery. These *in vivo* studies should of course show that relaxin has improved the delivery of some well-known anti-cancer agents such as doxorubicin.

1.8.5 Modifying drug administration technique:

The use of continuous infusion instead of bolus injections can maintain diffusion and convection for prolonged periods and achieve more uniform distribution in the tumour area compared to single bolus injection. The efficacy of 5-FU was better and its toxicity was less when administered as continuous

infusion compared to bolus injection in a multicentre study for patients with advanced colorectal cancer (de Gramont et al., 1997). Another study showed that weekly 24 hours infusion has enhanced 5-FU therapeutic index and reduced toxicity (O'Dwyer et al., 2001).

1.8.6 Modifying drug pharmacokinetics and nanoparticle delivery:

The use of liposomes or nanoparticle carriers can increase the half-life of the anticancer agent and enhance its passing through fenestrations in the tumour blood vessels (Jain and Stylianopoulos, 2010). In addition, coating the drug carrying liposomes with antibodies to specific tumour antigens can facilitate targeting malignant cells (Kontermann, 2006). Changes in the formulation of an existing anticancer agent like doxorubicin can help its penetration into solid tumours. Encapsulating doxorubicin into *liposomes* can alter the pharmacokinetics of the free drug and exploit tumour vessels permeability to liposomal profiles (Di Paolo, 2004; Vail et al., 2004). Another example of drug formulation change is the use of a nanoparticle formulation of paclitaxel bound to albumin. This modification might result in improving its ability to penetrate into solid tumours as it evades the delivery and adverse effect problems caused by the original hydrophobic formula because it is known that paclitaxel is a poorly water soluble drug. For this reason it is originally solubilised in a polyoxyethylated castor oil and ethanol formula. This formula causes hypersensitivity reactions and causes paclitaxel entrapment in plasma as micelles. Micelles alter the drug efficacy and affect its pharmacokinetics through decreasing its clearance and its volume of distribution. These

pharmacokinetic changes can also increase drug adverse effects. The pharmaceutical company (American BioScience, Santa Monica, CA) introduced a novel, solvent free, albumin bound, 130 nm particle form of paclitaxel. Albumin has the ability to bind to specific proteins in the tumour and hence transport paclitaxel to cancer cells. This formula has reduced adverse effects of paclitaxel as well (Nyman et al., 2005). Its mechanism exploits the enhanced permeability and retention effect (EPR) (Maeda, 2010b). Exploiting EPR effect has shown safety and improved delivery and efficacy of drugs such as doxorubicin and paclitaxel (Iyer et al., 2006; Maeda, 2010a; Torchilin, 2011).

1.9 Synopsis and objectives of the project:

Impaired drug delivery to solid tumours is a significant factor that limits curative potential. The effectiveness of cancer treatment depends on the delivery of the anticancer agent to all tumour cells located in different regions of the tumour because unaffected cells may act as clones that result in tumour re-growth and development of resistance (Hicks et al., 2003). Different drug penetration barriers exist in solid tumours and hence can cause chemotherapy resistance (Tredan et al., 2007). Drug penetration studies have demonstrated that a variety of anti-cancer drugs are indeed unable to penetrate fully into solid tumours, suggesting that an improved clinical response might be generated if the distribution of these drugs could be improved (Minchinton and Tannock, 2006). Elevated interstitial fluid pressure (IFP) in solid tumours is considered one of the barriers to drug penetration. High IFP is one of the characteristics of

solid tumours (Heldin et al., 2004). One of the consequences of IFP elevation in solid tumours is that it impedes the convective fluid flow (CFF) process through which drugs are transported to tumours (Heldin et al., 2004). This in turn can reduce drug uptake and resistance can then develop. Different strategies have been developed to study and to overcome barriers to drug transport in order to improve drug distribution to vascular and avascular regions of tumour. This requires the development of different *in vivo* and *in vitro* methods that can be used to study drug penetration. A variety of *in vitro* and *in vivo* techniques have been developed over the past couple of decades such that the concentration of therapeutic agents in tissues and tumours can now be measured (Minchinton and Tannock, 2006). However, Experimental models used to study IFP in solid tumours are mostly *in vivo* models. These models are expensive, time consuming and extensively using animals. The use of animal models also restricts the type of experiments that can be done. For example, it is difficult to systematically dissect individual pathways/mechanisms involved in maintaining high IFP due to the inherent complexity of the *in vivo* model. Developing an *in vitro* based assay to study the effect of IFP on drug penetration can overcome the disadvantages of using the *in vivo* models. In addition, it can be used to study the ability of several anticancer drugs to penetrate through tumours and can be utilized to develop strategies to overcome barriers and to improve drug penetration in order to reduce chemotherapy resistance.

The long term objective of this project is based on the hypothesis that understanding the pharmacological and biological factors that control drug

delivery to solid tumours especially those related to the tumour microenvironment such as IFP, can be exploited to develop methods and strategies to overcome limited drug penetration into solid tumours. Hence this will improve drug delivery in order to allow drugs to exert their therapeutic effect.

The specific objective of this project is to utilize the penetration model used by Phillips and his team (Phillips et al., 1998) to develop and evaluate novel models for assessing the impact of IFP on drug penetration. The traditional approach uses MCL systems where the fluid level in the upper and lower chambers is equal and the initial part of this thesis describes studies designed to optimise analytical techniques and characterise drug penetration rates when there is no pressure gradient across the MCL. By modifying the upper chamber to allow fluid levels to be raised above that of the bottom chamber, a pressure gradient will be established and this should drive convective fluid flow (CFF). This model will be characterised and its impact upon drug delivery/penetration determined.

2. MATERIALS AND METHODS:

2.1 Chemicals and reagents:

Doxorubicin was purchased from Sigma (Sigma Aldrich, Pool, UK). Epirubicin was purchased from Euroasiarnd (Euroasian Chemicals PVT.LTD, India). Imatinib and gefitinib were purchased from LC Laboratories (Woburn, MA, USA). For *in vitro* experiments, all drugs were dissolved in dimethyl sulphoxide (DMSO) (Sigma Aldrich) to provide stock solutions of 10mM which were subsequently aliquoted into 1.5 mL microcentrifuge tubes (Costar, USA) and stored at -20°C until required. Chemical structures and molecular weights of doxorubicin, imatinib and gefitinib are presented in appendix 1.

All chemicals used were of analytical grade and all solvents were HPLC grade unless otherwise stated. All reagents were purchased from Sigma Aldrich (Poole, Dorset, UK) unless otherwise stated.

2.2 Cell lines and cell culture conditions:

All cell lines were purchased from American Type Culture Collection (ATCC) or European Collection of Cell Culture (ECACC). A list of selected cell lines used in this study is presented in table 2-1. Cell lines were chosen based on their ability to form spheroids (Friedrich et al., 2007) and previous experience in this laboratory. Cells were routinely maintained at 37°C in a CO₂ enriched (5%) humidified atmosphere as monolayer cultures in T-75 flasks (Corning, NY, USA). Cells were grown in RPMI-1640 culture medium containing 25 mM

HEPES buffer and supplemented with 10% Foetal Bovine Serum (FBS), Sodium Pyruvate (1 mM) and L-Glutamine (2 mM). Cells were routinely passaged when they reached 70-80% confluent by trypsinisation. Cells were washed 3 times with 10 mL of Hanks balanced salt solution (HBSS) prior to the addition of 3 mL of Trypsin-EDTA (0.25% Trypsin-EDTA).

Table 2-1: List of used cancer cell lines and their tissue of origins

CELL LINES	ORIGIN	REFERENCE
DLD-1 (ATCC)	Human colorectal adenocarcinoma	(Dexter et al., 1979)
MCF7 (ATCC)	Human breast adenocarcinoma	(Soule et al., 1973)
SiHa (ATCC)	Human cervix carcinoma	(Friedl et al., 1970)
Panc-1 (ATCC)	Human Pancreatic adenocarcinoma	(Lieber et al., 1975)
Caski (ATCC)	Human cervix epidermoid carcinoma	(Pattillo et al., 1977)
A2780 (ECACC)	Human ovarian carcinoma	(Newman et al., 1988)
M14*	Human melanoma	(Mouches and Bove, 1983)
SK-MEL 23*	Human melanoma	(Pankovich and Jimbow, 1991)
HT29 (ATCC)	Human colorectal adenocarcinoma	(Fogh et al., 1977)
A549 (ATCC)	Human lung carcinoma	(Giard et al., 1973)
PC3 (ATCC)	Human prostate adenocarcinoma	(Kaighn et al., 1979)
786-0 (ATCC)	Human renal cell adenocarcinoma	(Williams et al., 1976)

* Obtained from the University of Leeds.

Following incubation at 37°C for 5 minutes or until cells became detached from the flask surface, 10 mL of complete media was added and the cell suspension was centrifuged (Heraeus megafuge 1.0, Thermo Electron Corporation) at room temperature for 5 minutes at 1000g. The supernatant

was discarded and the cell pellets were re-suspended in 10 mL of fresh RPMI medium. From the re-suspended cells, 2×10^5 cells were added to a new non-vented T-75 flask. Cells were discarded after 10 passages and replaced with fresh cultures obtained from liquid nitrogen stocks. All cell lines were proved to be free of mycoplasma by regular screening with mycoplasma detection kit (Roche, Mannheim, Germany). For cell counting, cells were trypsinized and re-suspended in fresh medium as described above. From the cells suspension, 10 μ L was then placed into a haemocytometer chamber. The haemocytometer contains 2 chambers, which are divided into 9 major squares. Each of these has a volume of 0.1 mm³ or 1×10^{-4} mL. Average cell counts were taken from a total of 10 grid counts using a low-power (10X) objective. The cell concentration was expressed as mean cell count $\times 10^4$ cells/mL.

2.3 Growth curves:

The growth characteristics of DLD-1 and MCF-7 cells were determined as these two cell lines formed the mainstay of experiments performed in this thesis. Their selection was based on previous studies which demonstrated that they readily formed multicell layers (Phillips et al., 1998). Cells were harvested as mentioned previously and the cell suspension was split into 8 T-25 flasks (Corning, NY, USA). On day 0, total number of cells in each flask was 1×10^5 cells/mL in a final volume of 10 mL per flask. Every day, cells were trypsinised and the total number of cells in each flask counted using a haemocytometer. Growth curves were constructed by plotting total cell number against time.

2.4 Growth characteristics of cells on transwell membranes:

2.4.1 Apparatus characteristics and MCLs formation:

The apparatus used for drug penetration assays is the transwell culture insert that has previously been used for multicell culture formation (Phillips et al., 1998). This apparatus (figure 2-1) consists of a transwell insert (TransWell-COL plastic insert, Corning Costar incorporated, NY, USA), containing a collagen-coated microporous polytetrafluoroethylene (PTFE) membrane (pore size 0.4 μm , diameter 6.5 mm, thickness 30 μm and surface area 0.33 cm^2), placed into one well of a 24 well plate. The micro porous membrane forms a barrier between the top and the bottom chamber and a surface upon which cells can be seeded to form MCLs. To initiate MCL formation, a total of 3×10^5 cells in no more than 200 μL of RPMI-1640 culture medium was added to the top chamber of the transwell. Transwells were then incubated at 37°C for 2 hours to allow cells to attach to the membrane before the addition of 2 mL of RPMI-1640 medium to the bottom chamber and flooding the top chamber with 1 mL of the same medium. Cells were incubated at 37°C in an atmosphere containing 95% air and 5% CO_2 for up to 7 days with medium being changed every other day in both the top and bottom chambers.

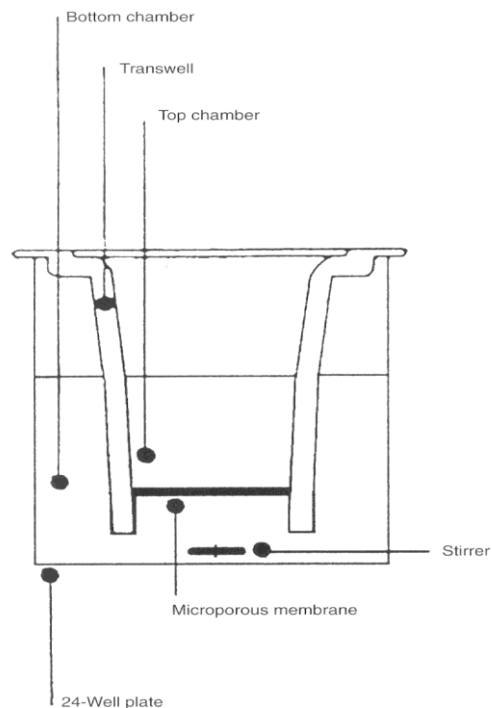


Figure 2-1: Schematic representation of the conventional drug penetration system which was considered model 1 (diffusion only $D \downarrow$) in this study. The transwell insert is placed into one well of a 24 well plate and cells (3×10^5 cells) are seeded into the top chamber to form MCL. Drug at selected concentrations is added to the top chamber and samples are withdrawn from the bottom chamber at different times for analysis. (Phillips et al., 1998).

2.4.2 Processing MCLs for thickness measurement:

2.4.2.1 Transwell fixation and membrane embedding:

At several time points, transwells were collected and fixed in order to measure the thicknesses of the MCLs. Transwells were fixed in Bouin's solution for one hour, then rinsed three times with 70% ethanol and stored at room temperature in 70% ethanol until required for measurement of the thickness of the multicell layer. The transwell was removed from ethanol and with a sharp

scalpel blade; the membrane was carefully detached from the plastic insert. The membrane was placed with labelled paper into a microsette processing embedding cassette with lid (Simport, Canada) and placed in an automatic tissue processor (Leica TP1020, Leica instruments GmbH, Germany). The following settings were used on the processor:

- 70% ethanol for 1 hour
- 80% ethanol for 30 minutes
- 95 % ethanol for 30 minutes
- 100% ethanol for 30 minutes (3 times, in 3 different tanks)
- HistoClear for 30 minutes (3 times, in 3 different tanks)
- Paraffin wax for 45 minutes
- Paraffin wax for 1 hour

Finally, each membrane was embedded into a labelled plastic mould (Disposable Embedding Molds, (Peel-A-Way), Polysciences, Inc., USA). The plastic mould was filled with fresh wax and the membrane was allowed to rest horizontally on the bottom of the mould and positioned at one edge to facilitate sectioning. It was then left to set on a refrigerated surface. Once set, wax blocks were kept at room temperature until required for sectioning.

2.4.2.2 Sectioning:

The wax block containing the membrane was incubated at 4-8°C for at least 30 minutes in order to increase the rigidity of the wax before sectioning. Wax blocks were then cut into sections using a Leica RM2155 microtome (Leica instruments GmbH, Germany). Sections (5 µm thick) were collected and

placed on APES (3-aminopropyltriethoxysilane) coated slides and stored at room temperature until required for Haematoxylin and Eosin staining. From each wax block, 3 sections were collected.

2.4.2.3 Haematoxylin and eosin staining:

Sections were de-waxed and re-hydrated according to the following schedule:

- Xylene for 5 minutes (twice, two different tanks)
- Xylene/ethanol 50:50 for 5 minutes
- Ethanol 100% for 5 minutes (Twice, 2 different tanks)
- Ethanol 90% for 5 minutes
- Ethanol 70% for 5 minutes

Slides were then stained in Harris haematoxylin for 10 minutes, washed with running tap water, then immersed in acidic alcohol (0.25% v/v conc. HCL in 70% ethanol) for 5 seconds. This step is performed to remove the excess haematoxylin from the cells leaving the nuclei strongly stained but not the cytoplasm. After that, slides were washed briefly in running tap water then stained in Scott's tap water substitute (3.5g sodium bicarbonate and 20g magnesium sulphate dissolved in 1000 mL H₂O) for 2 minutes. This solution is strongly alkaline and turns the section blue. Sections were counterstained in 1% (w/v) aqueous eosin for 1 minute then washed briefly in tap water and drained for 1 minute to let excess water run out. Sections were then dehydrated as follow:

- Ethanol 100% for 1 minute, then ethanol 100% in a different tank for 3 minutes.

- 50% xylene/ethanol for 3 minutes
- Xylene for 3 minutes
- Clean xylene for 5 minutes

Sections were then mounted using DPX medium (VWR international Ltd. Poole, England), a cover slip was added and left to dry at room temperature.

2.4.2.4 MCL thickness measurement:

The average thickness of the multicell layer was determined by taking 5 random measurements from each section under a 20X objective lens using a LEICA (DMRB, Germany) microscope connected to a camera (Leica MPS52, Q Imaging, Germany) and using AcQuis, (Annotating acquisition system (32 bit), from syncroscopy) software. The microscope was automatically calibrated for a 20X objective lens using the software contained within the AcQuis program.

2.4.3 Ability of cell lines to form MCLs:

The cell lines listed in table 2.1 were all evaluated to determine if they formed MCLs. In all cases, 3×10^5 cells were added to each transwell and the protocol described in 2.4.1 and 2.4.2 was followed. After 5 days of culture, transwells were fixed and processed as described above. Cell lines were judged to have formed MCLs based upon histological analysis of the cross sections (e.g. gaps in the MCL).

2.4.4 Collagen expression in the MCL using immunohistochemistry:

Collagen is an essential component of the extracellular matrix and digesting or modifying it is a potential strategy for altering IFP and therefore enhancing drug delivery. To determine whether MCL express collagen, preliminary immunohistochemical studies were performed according to the following protocols. DLD-1 MCL (Day-7) sections were used and DLD-1 tumour xenograft sections were used as positive control. The first step in the protocol was to de-wax and rehydrate the paraffin embedded sections as follow:

- Xylene - 10 mins x 2
- 50% xylene/ethanol – 5 mins
- Absolute ethanol – 5 mins x 2
- 90% ethanol – 5 mins
- 70% ethanol – 5 mins
- Distilled water – 5 mins

Rehydrated sections were placed in 1% H₂O₂ for 30 minutes to quench endogenous peroxidase. Sections were then washed in PBS for 10 minutes. Antigen retrieval was performed in citrate buffer at medium-high microwave for 20 minutes. Sections were allowed to cool down for 30 minutes then washed in PBS for 10 minutes. Sections were then covered for 20 minutes with normal goat blocking serum (IVD, Vector laboratories Inc. Burlingame, CA), diluted 15:1000 in PBS. Excess serum was shaken off then sections were covered for one hour with the primary antibody (Rabbit Polyclonal to Collagen IV, ab (6586), Abcam, PLC, UK), which was diluted 1:500 in PBS. Negative control

sections were covered with the blocking serum for the same length of time. Primary antibody was shaken off then sections were washed in PBS for 10 minutes. Sections were then covered for 30 minutes with the secondary antibody (Biotinylated Anti-Rabbit IgG made in goat, IVD, Vector laboratories Inc., Burlingame, CA) which was diluted 1:200 in PBS. Secondary antibody was washed off then sections were washed in PBS for 10 minutes prior to incubation with ABC reagent (Vectastain ABC Kit, Peroxidase standard PK 4000, Vector laboratories Ltd.) for 30 minutes. After 30 minutes incubation with ABC reagent, sections were washed in PBS for 10 minutes then incubated with DAB (DAB Peroxidase Substrate kit, Vector laboratories, CA) for 5 minutes. DAB was washed off then sections were washed in distilled water for 5 minutes. Sections were counterstained in Harris Haematoxylin solution for 20 seconds then washed in tap water. Sections were then placed in Scott's tap water for 2 minutes. This step was followed by dehydration using:

- 70% ethanol
- 90% ethanol
- Absolute ethanol X2
- 50% xylene/ethanol
- Xylene II

for 2 minutes each; then clean xylene for 5 minutes. At the end, sections were mounted in DPX, cover slips were added then slides were left to dry at room temperature. Immunohistochemical staining was evaluated under a 20X lens using a LEICA (DMRB, Germany) microscope connected to a camera (Leica

MPS52, Q Imaging, Germany) and using Acquits, (Annotating acquisition system (32 bit), from syncroscopy) software.

2.4.5 Testing the ability of the MCL to form a barrier using trypan blue:

To determine whether molecules can cross MCLs by moving in between cells (i.e. via intracellular spaces) rather than through cells, trypan blue was added to the top chamber and its appearance in the bottom chamber was measured spectrophotometrically. As trypan blue will not cross intact membranes, the only way it can reach the bottom chamber is via movement through intercellular spaces. In this experiment, 0.2% (w/v) of trypan blue was added to the top chamber in a volume of 100 μ L in PBS and the bottom chamber contained 600 μ L of PBS which was constantly stirred. Following 3 minutes incubation at 37°C, the transwell was removed and 500 μ L was collected from the bottom chamber and stored at 4°C until required for analysis. This experiment was performed in triplicate using DLD-1 MCL on day 1 of growth on the membrane and blank (cells-free) transwells. Samples collected were analysed using a spectrophotometer (Varian, CARY- 50 Bio, UV-Visible Spectrophotometer, Oxford, UK). For each sample and calibration standard, 50 μ L was added to 950 μ L of PBS to give a final volume of 1 mL. Calibration samples were 2X serial dilutions of 0.2% trypan blue. Samples and calibration standards were placed in disposable cuvettes (1.5 mL semi-micro Plastibrand, Germany) and absorbance was read at 590 nm.

2.5 Analysis of doxorubicin:

Before experiments designed to measure the ability of doxorubicin to penetrate MCLs were conducted, the following procedures were performed to establish robust experimental methodologies: 1) Establishment of a HPLC method to analyse doxorubicin and the internal standard; 2) Establishment of methods for extracting doxorubicin from cell culture media, analysis of extraction efficiencies and limit of detection of each technique; 3) Testing inter and intra-day experimental variations; 4) Drug stability studies in cell culture medium at 37 °C.

2.5.1 HPLC analysis of doxorubicin:

Sample analysis was performed using high performance liquid chromatography system (HPLC). A C18 HIRPB, Hichrom column, 250mm x 4.6mm i.d. (inner diameter), was used for separation. A Waters 2996 photodiode array and a Shimadzu RF-10 AXL Fluorescence detector at an excitation of 480 nm and an emission of 560 nm, with Masslynx 4.0 software (Micromass Ltd.) were used for spectral analysis of the peaks of interest. An isocratic separation was performed using 60% of mobile phase-A composed of 90% 5mM Ammonium formate buffer and 10% Acetonitrile, and 40% of mobile phase-B composed of 40% 5mM Ammonium formate buffer and 60% of Acetonitrile. Ammonium formate buffer was prepared by dissolving 0.315g of Ammonium formate in 1L of distilled water and its pH was adjusted to 3.55 using formic acid (VWR International Ltd, UK). The flow rate was set at 1.5 mL/min using a Waters 2795 (Alliance HT) separations module system. The

total running time of each sample was 10 minutes and the volume of injection was 10 μL unless otherwise stated. The structurally related epirubicin was used as an internal standard (Zheng et al., 2001).

2.5.2 Extraction techniques and extraction efficiency test:

As it was expected that a wide range of drug concentrations to be present from the penetration assays, different extraction techniques were used in order to analyse these concentrations and identify a suitable extraction method. A suitable extraction method is the one which is the most convenient and yet provides sufficient sensitivity. Therefore, the method chosen is dependent on the concentration of drug being investigated. In addition to these characteristics, the extraction technique used should be inexpensive and not time consuming. Extraction efficiency is measured by dividing the peak areas of extracted samples by the peak areas of non-extracted samples. Samples were extracted using three different extraction techniques as follows:

2.5.2.1 Doxorubicin extraction from tissue culture medium (TCM) using protein precipitation technique without evaporation:

These experiments were conducted using 500 nM doxorubicin. In this technique, 200 μL of acetonitrile was added to 100 μL of phenol red-free medium containing doxorubicin (500 nM) to give a final volume of 300 μL . The sample was then mixed for a few seconds then centrifuged at 10,000g for 5

minutes at 4°C. The supernatant was then carefully removed and 50 µL was injected into the (HPLC).

2.5.2.2 Doxorubicin extraction from tissue culture medium (TCM) using protein precipitation technique with evaporation and reconstitution:

In this technique, the same steps used in the previous method were used except that the supernatant was evaporated at room temperature using an EZ-2 Plus evaporator (Genevac Limited, Ipswich, UK). The sample was then reconstituted in 300 µL of mobile phase A. The reconstituted sample was then centrifuged for 2 minutes at 10,000g. Finally 50 µL was injected into the HPLC.

2.5.2.3 Doxorubicin extraction from tissue culture medium (TCM) using solid phase extraction (SPE):

In this technique, samples were extracted using Isolute (IST) C18 EC SPE 50 mg cartridges (Biotage, EU). Cartridges were placed on an AASP VAC-ELUT system (Analytichem International) and each cartridge was primed by adding 1 mL of methanol under vacuum. 1 mL of 0.02% formic acid was then added to the cartridge and passed through the cartridge very slowly. Samples (300 µL, composed of 200 µL of phenol red free medium added to 100 µL of doxorubicin (500 nM) prepared in the same medium) were added to each cartridge and passed through very slowly. The cartridge was then washed with 1 mL of 0.02 % formic acid solution and dried under vacuum (DA7C, Charles Austen pumps Ltd. Surrey, England). Finally, 1 mL of propan-2-ol (Fisher

Scientific, UK): methanol (3:1) solution was added and passed through each cartridge very slowly collecting samples in labelled tubes. The final eluent was evaporated at room temperature using EZ-2 Plus evaporation machine (Genevac Limited, Ipswich, UK) and the dry sample was reconstituted into 300 μL of mobile phase A, mixed, centrifuged for 2 minutes at 10,000g and transferred to HPLC vials. 50 μL was injected into the HPLC.

2.5.3 Extraction efficiencies, intra-day and injection reproducibilities:

Extraction efficiency of each extraction technique was calculated by dividing the peak areas of the extracted samples by the peak areas of non-extracted standards. The extraction efficiency (EE) was calculated as follows:

$$\%EE = \frac{\text{Mean peak area of doxorubicin extracted samples}}{\text{Mean peak area of doxorubicin non extracted standards}} \times 100$$

The extraction efficiency was calculated based on 6 readings injected from 6 independent samples and 6 readings injected from the same vial. The results of those injections were also used to test intra-day and injection reproducibilities by using the (coefficient of variation [CV]). Intra-day reproducibility is used to check the human sampling error and it is tested by injecting 6 injections from 6 independent vials having the same concentration and prepared in the same way on different occasions whereas injection reproducibilities are used to check the reproducibility of the HPLC by injecting 6 samples from the same vial that contain a specific concentration of drug. Intra-day and injection reproducibility variations (coefficient of variation [CV])

are calculated based on the mean peak areas and the standard deviation of the injected samples using the following equation:

$$C.V = \frac{\text{Standard deviation (SD) of doxorubicin mean peak area}}{\text{Mean peak area of doxorubicin}} \times 100$$

2.5.4 Calibration curves and limit of detection:

Calibration curves were prepared on the same day of each experiment using the same stock of doxorubicin for both calibration curve and experimental samples. All standard concentration used were prepared using a stock solution of doxorubicin at 10 mM in DMSO which was diluted in complete phenol red-free RPMI-1640 medium or mobile phase to give 100 μ M. This was further diluted to prepare the required concentrations of standards in tissue culture medium or mobile phase as required. Because of the different extraction techniques used and variations in experimental protocols during optimisation phases of the project, the concentration range for calibration curve standards varied to cover the expected minimum and maximum concentrations. The linear regression analysis of the ratios of peak area of the drug versus internal standard was plotted against concentration. In all cases, the calibration curves used were linear. The equation used for calculating the unknown concentration was the linear regression equation as follow:

$$y = y^{\circ} + ax$$

$$x = \frac{y - y^{\circ}}{a}$$

where:

x : is the unknown concentration

y : is the relative ratio (Doxorubicin peak area/Internal Standard Peak area)
X1000

y° : is the y-intercept, and

α : is the slope.

The limit of detection for doxorubicin using HPLC was calculated using signal to noise (S/N) ratios (>5) and exploiting the results of these calibration curves.

2.5.5 Doxorubicin stability at 37°C:

Doxorubicin stability under the experimental conditions used, i.e. tissue culture medium at 37°C for 30 minutes or 1 hour, was determined according to the following procedure. Three different doxorubicin (1 μ M) standards in complete phenol red-free RPMI-1640 medium were prepared and placed in three different eppendorf tubes, each containing 1 mL of drug solution. 100 μ L aliquots were taken from each tube and labelled as time point 0. The remaining solution (900 μ L) was then transferred to three different wells of a 24 well plate and incubated at 37°C. At various time intervals (15, 30, 60 and 120 minutes), 100 μ L samples were collected from each well and placed into an eppendorf tube. Acetonitrile (200 μ L containing 500 nM epirubicin) was added immediately to each sample, mixed for few seconds and centrifuged for 5 minutes at 10,000g at 4°C (Heraeus Labofuge 400R, Kendro Laboratory

Products, Germany). The supernatant was removed carefully, transferred into short thread vial (9 mm PP, Kinesis Inc., Malta, USA) and injected directly into the HPLC system (50 μ L injection volume).

2.6 Analysis of imatinib and gefitinib:

2.6.1 HPLC, LC/MS, and LC/MS/MS analysis of imatinib and gefitinib:

For imatinib and gefitinib, HPLC, LC/MS and LC/MS/MS were used for analysis depending on the expected concentration of each experiment. In case of analysis using HPLC, isocratic separation was performed using 55% of mobile phase-A (MPA) which consisted of 90% distilled water and 10% methanol and 45% of mobile phase-B (MPB) which composed of 10% distilled water and 90% methanol. Formic acid (0.1%) was used to adjust the pH in both mobile phases to 3.5. The column used was a C₁₈ HIRPB, Hichrom column, 250mm x 4.6mm i.d. (inner diameter) and compounds were detected at 265 and 343 nm for imatinib and gefitinib respectively using a Waters 2996 photodiode array detector. The flow rate was set at 1.2 mL/min using a Waters 2795 (Alliance HT) separations module system. The total running time of each sample was 10 minutes and the volume of injection was 50 μ L. HPLC was used for analysing samples that were expected to contain high concentrations of drug.

For analysis using LC/MS, the same column mentioned above was used for separation. A Waters 2996 photodiode array and a Micromass ZMD single quadruple mass spectrometer (Micromass, Manchester UK) with Masslynx software were used for spectral analysis and mass analysis of the peaks of

interest. An isocratic separation method was performed using 50% of mobile phase-A (MPA) which composed of 90% distilled water and 10% methanol and 50% of mobile phase-B (MPB) which composed of 10% distilled water and 90% methanol. Formic acid (0.1%) was used to adjust the pH in both mobile phases to 3.5. The MS Parameters were optimised to: desolvation gas flow 506 lit/hr, cone gas flow 35 lit/hr, capillary 3.5 kV, sample cone 45 V, extraction cone 5 V, RF lens 0.20 V, source block temperature 100°C and desolvation temperature 150 °C. Drugs were detected as singularly charged ions using selected ion recording (SIR). The flow rate was set at 1 mL/min using a Waters 2695 separations module system. The total running time of each sample was 10 minutes and the volume of injection was 30 µL.

LC/MS/MS settings were as follows: An ACQUITY UPLC® BEH C18 1.7 µm column was used for separation. A Waters Acquity photodiode array and a Waters Quattro Premier XE triple quadrupole mass spectrometer, with Mass Lynx 4.1 software were used for spectral analysis of the peaks of interest. An isocratic separation method was performed using 65% of mobile phase A (MPA) which composed of 90% distilled water and 10% methanol and 35% of mobile phase B (MPB) which composed of 10% distilled water and 90% methanol. The MS/MS parameters were optimized to: Ionization mode ES+, Capillary (KV) 3.75, Cone (V) 40, Extractor (V) 4, RF Lens (V) 1.0, Source temperature (°C) 130, Desolvation temperature (°C) 250, Cone Gas Flow (L/Hr) 50, Desolvation Gas Flow (L/Hr) 697, Collision 30, Multiplier (V) 650, Syringe Pump Flow (µL/min) 20, Pressure (mbar) 8.79e-3, Collision Gas Flow (mL/min) 0.35. Drugs were detected as singularly charged ion using selected

ion recordings (SIR) or monitoring fragmentations using multiple reaction monitoring (MRM). The flow rate was set at 0.35 mL/min using a Waters Acquity UPLC (Ultra High Pressure Liquid Chromatography) module. The total running time of each sample was 4 minutes and the volume of injection was 10 μ L. In all cases, gefitinib was used as internal standard for imatinib which in turn was also used as an internal standard for gefitinib.

2.6.2 Extraction of imatinib and gefitinib from TCM:

Unless otherwise stated, all samples created containing imatinib and gefitinib were extracted from TCM using protein precipitation without evaporation by adding 300 μ L of methanol to 100 μ L of imatinib or gefitinib in phenol red free medium. Samples were vortexed for few seconds centrifuged at 10,000g for 5 minutes at 4°C. Supernatant was then carefully removed and 50 μ L was injected into the (HPLC) and LC/MS and 10 μ L was injected into LC/MS/MS. This extraction technique was selected for all three analytical techniques described above except in the case of low gefitinib concentrations which were extracted using SPE as explained earlier (section 2.5.2.3).

2.6.3 Calibration curves and limits of detection:

As in the case of doxorubicin, calibration curves were prepared based on the expected concentrations of analysed drug depending on the penetration assay method used. Different calibration curve standards were used ranging from 10 nM to 100 μ M. The same method used for calculating the unknown concentrations of doxorubicin was applied for imatinib and gefitinib. The limit of detection for imatinib and gefitinib using LC/MS/MS, LC/MS and HPLC

respectively were calculated using signal to noise (S/N) ratios (> 5) and exploiting the results of these calibration curves.

2.6.4 Stability test of imatinib and gefitinib at 37°C:

The stability of imatinib and gefitinib at 37°C in cell culture medium was determined according to the following procedure. Three different (1 μ M) preparations of each drug were made in complete phenol red-free RPMI-1640 medium and 100 μ L aliquots were taken from each tube and labelled as time point 0. The remaining solution of each tube (900 μ L each) was placed at 37°C and 100 μ L sample was collected from each tube and placed into an eppendorf tube at 15, 30, 60 and 120 minute intervals. Methanol (300 μ L containing 500 nM internal standard either imatinib or gefitinib) was added immediately to each sample, mixed for few seconds and centrifuged for 5 minutes at 10,000g at 4°C. Supernatant was removed carefully, transferred into short thread vials (9 mm PP, 0.3mL, Kinesis Inc., Malta, USA) and injected directly into the HPLC system (50 μ L injection volume).

2.7 Drug penetration assays using model-1:

Following validating the analytical procedures, drug penetration assays were performed using the conventional drug penetration system which was considered model-1, diffusion only (D \downarrow), described in section 2.4. To examine drug penetration, an anticancer agent can be added to the top chamber and the concentration that migrates to the bottom chamber can be measured as a function of time using an appropriate analytical method. Drug penetration assays were performed using two strategies. The first, termed variable

concentration gradient (VCG) is where a defined concentration is added to the top chamber and is not replenished during the experiment. In this case, the concentration in the top chamber will decrease whilst the concentration in the bottom chamber increases until equilibrium is established. The second, termed 'constant concentration gradient' (CCG) is where the concentration of drug in the top chamber is maintained at a constant concentration by replacing the top chamber with fresh media containing drug every time a sample is taken. In this case, the concentration in the top chamber remains approximately constant. Details of these two different assays are explained below.

2.7.1 Drug penetration assays using variable concentration gradient (VCG) technique:

Drug penetration assays were carried out after 1, 3, 5 and 7 days of growth of DLD-1 and/or MCF-7 cells on the membrane considering seeding day as day 0. When required, medium was removed from the top chamber of the transwell and replaced with 100 μL of phenol red-free RPMI-1640 medium supplemented with 10% foetal bovine serum, 1 mM Sodium Pyruvate, 2 mM L-glutamine and contained working drug concentration at 100, 50 or 25 μM . The transwell was then inserted into one well of a 24-well plate containing 600 μL of phenol red-free medium and incubated at 37°C with the bottom chamber being constantly stirred. At two minutes interval for the first 10 minutes and five minutes intervals thereafter for the next 50 minutes, 10 μL of medium was removed from the bottom chamber and added to a micro centrifuge tube containing 290 μL of phenol red free media containing 0.5 μM epirubicin (as an internal standard). Samples were then mixed and stored at -80°C until

required for HPLC analysis. At each time point, 10 μL of fresh medium was added to the bottom chamber to maintain the volume at 600 μL . At the end of the experiment, transwells were fixed in Bouin's solution for one hour then rinsed 3 times with 70% ethanol and stored at room temperature in 70% ethanol until required for histological analysis of multicell layer thickness as described earlier. All experiments including blank (cell-free) transwells were repeated independently three times.

2.7.2 Calculating drug penetration rates using variable concentration gradient (VCG) technique:

To calculate the penetration rates using penetration assay with VCG-technique, concentration values of the first 6 sampling points were converted into amounts and expressed as (nmoles). Penetration rate was calculated based on fitting a linear regression to the first 6 sampling points on the curve which represents the initial linear component of the amount versus time curve using the linear regression equation. The slope of the linear regression equation was considered the penetration rate. Penetration rates were expressed as nmoles/minute.

2.7.3 Drug penetration assays using constant concentration gradient (CCG) technique:

In this technique, drug was added to the top chamber in a volume of 100 μL (concentrations varied depending on the drug and the specific experiment) and the bottom chamber contained 600 μL of complete phenol red free media which was constantly stirred as before. At various time intervals, the contents

of the top chamber were removed and replaced with 100 μL of media containing fresh drug at the original concentration. At the same time, the transwell was removed and transferred to a new well of the 24 well plates that contained 600 μL of complete phenol red free media. In this way, the concentration gradient between the top and bottom chambers remained constant. From the bottom chamber, 500 μL was collected and added to a micro centrifuge tube, mixed and stored at -80°C until required for analysis. This procedure was repeated every 5 minutes for 30 minutes. This experiment was performed in triplicate using blank (cell-free) transwells and cell seeded transwells (i.e. MCLs) with 3 different working concentrations (25, 50 and 100 μM). To analyse samples created using this method, the 500 μL sample which was removed from the bottom chamber was added to 100 μL of phenol red-free medium containing 500 nM of the internal standard to give a final volume of 600 μL . Samples were then extracted using solid phase extraction following the same steps as explained in section 2.5.2.3.

2.7.4 Calculating drug penetration rates using constant concentration gradient (CCG) technique:

Using penetration assay with CCG-technique, cumulative drug concentration values which were plotted versus time and expressed as μM were converted into amounts and expressed as (nmoles). The penetration rate was calculated based on fitting a linear regression to the plotted curve which represents the drug amounts (nmoles) versus time (min.). The slope of the linear regression equation was considered the penetration rate and expressed as (nmoles/min).

2.8 Impact of hydrostatic pressure (HP), on convective fluid flow (CFF) and drug penetration using models 2 and 3:

As described in the introduction, tumours have high IFP which affects drug delivery and distribution through solid tumour tissue. To assess the impact of IFP on drug penetration, the drug penetration apparatus was modified. Modifications to the penetration assays apparatus were conducted and three models were generated. The first is the one described previously where there is no difference in the height of medium between the top and bottom chamber of the transwell apparatus. There is therefore no pressure gradient across the membrane and in this case, it is equivalent to an *in vivo* situation where $HP = IFP$ i.e. no convective fluid flow (CFF). In this model, drug penetration to the bottom chamber will occur mainly by diffusion. This model was named 'diffusion only' and denoted (**D** ↓). The second system is where the fluid height in the top chamber is much greater than that in the bottom chamber. In this case, a pressure gradient is established across the membrane and this drives CFF. This model is equivalent to a situation *in vivo* where the HP is greater than IFP. This model was named 'convection plus diffusion' and denoted (**C**↓**D**↓). In the third model, the fluid height in the bottom chamber is raised above that of the top chamber. The pressure gradient and CFF is therefore reversed compared to model 2 and is equivalent to an *in vivo* situation where HP is less than the IFP. This model was named 'diffusion opposing convection' and denoted (**D**↓ **C**↑). In all three models, the arrows denote the direction of either diffusion (**D**) or convection (**C**). Full details of the second and third model are provided below.

2.8.1 Model 2, convection plus diffusion (C↓D↓):

The apparatus used in this model is presented in figure 2-2. Briefly, a graduated tube was inserted into the top chamber and this can be filled with media to different heights. The variable height enables different pressure gradients to be applied but typically, 13 mL of media containing working drug concentrations was used. This creates a physiologically relevant hydrostatic pressure equivalent to 28 mmHg across the transwell membrane. In the bottom chamber, 200 μ L of Phenol Red Free tissue culture medium was placed. Samples (100 μ L) were collected from the bottom chamber every 5 minutes over a 30 minutes run time. Collected samples (100 μ L) were added to 100 μ L of internal standard (50 μ M) and stored at -80°C until required for analysis. The medium in the top chamber was removed and replaced with 13 mL of fresh medium containing the same working concentration i.e. the concentration at the top chamber was maintained constant. The same method was followed for blank samples where blank transwells (no cells) were used. Convective flow (CFF) was measured by weighing the bottom chamber every 5 minutes and the rate of convective fluid flow was determined from linear regression analysis of weight of fluid in the bottom chamber plotted against time. Samples created from this method were extracted using SPE cartridges as described previously in case of doxorubicin. Imatinib and gefitinib were extracted using protein precipitation without evaporation. Samples were reconstituted in mobile phase and finally 10 μ L in case of doxorubicin or 50 μ L in case of imatinib and gefitinib were injected into HPLC. Penetration rates

using this model were calculated following the same method used in case of CCG technique.

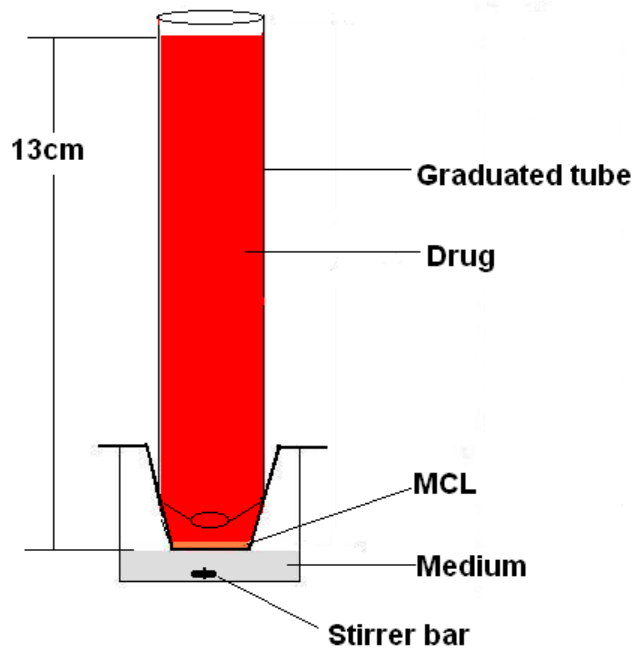


Figure 2-2: Schematic representation of model 2 (convection plus diffusion $C \downarrow D \downarrow$): A graduated tube was inserted into the transwell insert which was placed in a 24 well plate. Drug at selected concentrations is added to the top chamber (coloured in red to indicate where the drug is added) and samples are withdrawn from the bottom chamber at different times for analysis. Drug volume at the top chamber exerts a physiologically relevant pressure on the bottom chamber equivalent to 28 mmHg. Convection is measured by weighing the bottom chamber pre and post each time point.

2.8.1.1 Calculating hydrostatic pressure in model 2:

As described previously, volume of medium at the top chamber of model 2 creates a physiologically relevant hydrostatic pressure of 28 mmHg which is similar to that found in some solid tumours. This was calculated based on the following: Pressure = Force / Area

The force in the system is applied by the weight of the medium placed at the top chamber. Force is calculated by multiplying the mass by the gravity, i.e. Force = weight of medium in the top chamber

$$= \text{Mass} * \text{gravity} (9.8 \text{ m /s}^2)$$

As 1 Kg = 9.8 Newton, then 13 gm or 13 mL of medium at the top chamber equals $(13 * 9.8) / 1000 = 0.1274$ Newton.

The area of the transwell = 0.33 cm^2 which equals $3.32 \times 10^{-5} \text{ m}^2$

Pressure is measured by Pascal value which is calculated by dividing the mass expressed as Newton by the area² expressed as m²: i.e. Pascal = N / m²

In the model those two values were calculated, therefore,

$$\text{Pressure in Pascal} = 0.1274 / 3.32 \times 10^{-5} = 3840.36 \text{ Pascal}$$

Pascal can be converted into mmHg as follow:

$$1 \text{ Atmospheric pressure} = 101000 \text{ Pascal} = 1010 \text{ mbar} = 760 \text{ mmHg}$$

$$\text{Based on this, } 3840.36 \text{ Pascal} = 38.4 \text{ mbar} = 28.8 \text{ mmHg}$$

2.8.1.2 Influence of MCL thickness and hydrostatic pressure (HP) on CFF in model 2:

The influence of the MCLs thicknesses and the influence of different hydrostatic pressure (ΔP) on CFF were assessed using several thicknesses of DLD-1 MCLs. By varying the volume of media in the top chamber, the effect of pressure on CFF could be determined. CFF versus MCL thickness was assessed on days 1-7 of growth of DLD-1 and/or MCF-7 on the membrane using (C↓D↓) penetration assay model. This experiment was conducted as described previously (see 2.8.1) and was performed in triplicate. CFF was measured by weighing the bottom chamber pre and post each time point. Weight differences were considered equivalent to volumes assuming medium density equals 1. Volumes were converted into μL s and CFF vs. thickness was plotted as $\mu\text{L}/\text{min}$ vs. MCL thickness (μm).

CFF vs. (ΔP) was also assessed using DLD-1 and MCF-7 MCLs on day one of growth on the membrane and utilizing the (C↓D↓) penetration assay model. This experiment was performed in triplicate using 5 different volumes of medium in the top chamber. Volumes used were 1, 4, 7, 10 and 13 mLs. Each one of these volumes created a different hydrostatic pressure at the top chamber and hence created different CFF. Hydrostatic pressures created by 1, 4, 7, 10 and 13 mL of medium were 2.15, 8.61, 15.07, 21.53 and 28.8 mmHg respectively. Each volume was allowed to convect through one day old MCL of DLD-1 over 5 minutes and convection to the bottom chamber was calculated by weighing the bottom chamber pre and post each time point. Weight differences were converted into volumes considering medium density

equals 1 as explained above and CFF ($\mu\text{L}/\text{min}$) was plotted versus volume (mL).

2.8.2 Model 3, diffusion opposing convection ($D\downarrow C\uparrow$):

Drug penetration and the convective flow from the bottom to the top chamber in this model was tested using the modified penetration system presented in figure 2-3. In this model, 100 μL of media containing drug at a working concentration was added to the top chamber and 20 mL of phenol red free tissue culture medium placed in the bottom chamber. Samples (900 μL) were collected from the bottom chamber every 5 minutes over 30 minutes. Top and bottom chambers were replaced with fresh drug and fresh medium respectively to maintain constant concentration and pressure gradient in the system every 5 minutes. The orientation of the transwell in this apparatus was inversed compared to the previous models such that the pressure gradient did not detach the MCL from the membrane. Collected samples for analysis were added to 100 μL of internal standard (500 nM), extracted using SPE, evaporated as explained above, reconstituted in 50 μL mobile phase and finally 10 μL was injected into HPLC in the case of doxorubicin or LC/MS/MS in the case of imatinib and gefitinib.

Convective flow was measured by observing the tissue culture medium which was able to convect into the graduated tube every minute or by weighing the bottom chamber pre and post penetration. Penetration rates using this model were calculated following the same method described in section 2.7.4.

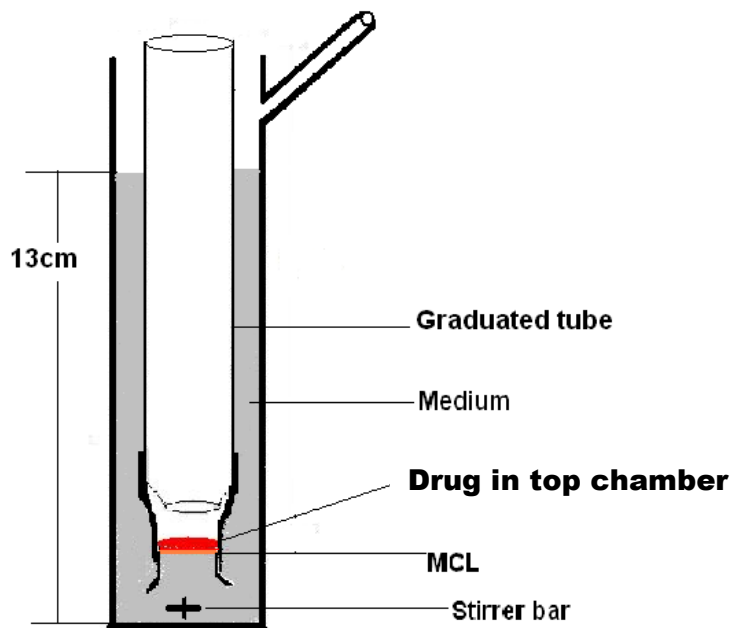


Figure 2-3: Schematic representation of model 3 (diffusion opposing convection $D\downarrow C\uparrow$): The graduated tube and the insert in model-2 were immersed into a cylindrical tube containing medium. Drug (100 μL) at selected concentrations is added to the top chamber and samples are withdrawn from the bottom chamber at different times for analysis. Medium volume at the bottom chamber creates a reverse physiologically relevant pressure on the top chamber. Convection is measured by weighing the bottom chamber pre and post each time point.

2.8.3 Modified model 3, diffusion opposing convection ($D\uparrow C\downarrow$):

A modified version of the previous model was also evaluated. It is similar to model 2 in construction but in this case, drug is added to the bottom chamber and the concentration of drug appearing in the top chamber is measured. By increasing the volume in the top chamber to produce a pressure gradient, the forces of diffusion and convection are in opposition (Figure 2-4). Samples (900 μL) were collected from the top chamber every 5 minutes over 30 minutes. Top and bottom chambers were replaced with fresh medium and fresh drug

respectively to maintain constant concentration and pressure gradients in the system every 5 minutes. Collected samples for analysis were added to 100 μL of internal standard (500 nM), extracted using SPE, evaporated as explained above, reconstituted in 50 μL mobile phase and finally 10 μL was injected into HPLC. This model was tested using doxorubicin only. Convective flow was measured by weighing the bottom chamber pre and post penetration. Penetration rates using this model were calculated following the same method described in section 2.7.4.

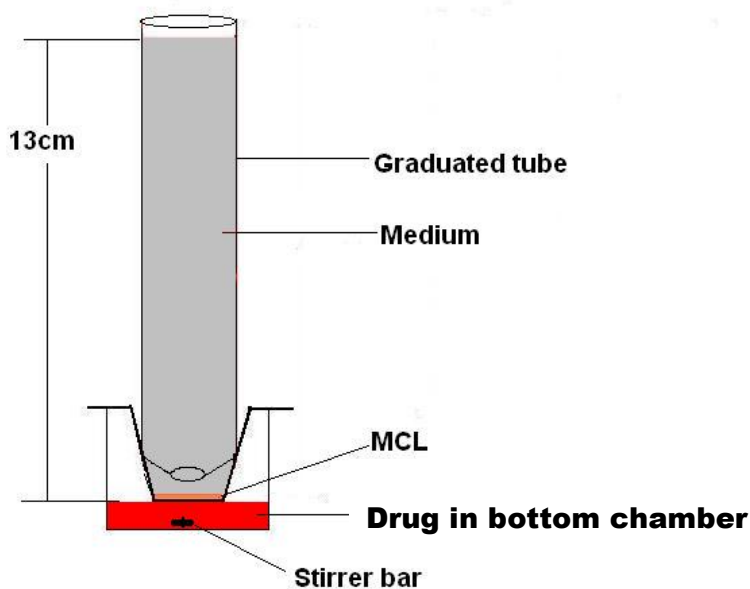


Figure 2-4: Schematic representation of modified model 3 (diffusion opposing convection $D\uparrow C\downarrow$): This system resembles model 2. The difference here is that the drug (200 μL) at selected concentrations is added to the bottom chamber and samples are withdrawn from the top chamber at different times for analysis. The graduated tube at the top chamber is filled with medium which creates a physiologically relevant hydrostatic pressure equivalent to 28 mmHg that opposes the direction of diffusion. Convection is measured by weighing the bottom chamber pre and post each time point.

2.9 Penetration assay detailed methodology for all models and drugs:

The three different penetration assay systems were tested and evaluated using doxorubicin, imatinib and gefitinib at 100 μM each on one day old DLD-1 MCLs. A wide variety of extraction and analytical techniques were employed as described previously, full details of which can be found in summary form in appendix 2.

2.10 Influence of penetration assays convection versus exposure time on cell survival:

Each of these experiments generated concentrations versus time curves and to assess the effect of different exposures on cell kill, chemosensitivity studies were conducted. *In vitro* chemosensitivity of DLD-1 cells to the cumulative concentrations of doxorubicin, imatinib and gefitinib retrieved from the three different penetration systems (Table 2-2) was determined using the 3-(4,5-dimethylthiazole-2-yl)-2,5-diphenyltetrazolium bromide assay (MTT assay) explained elsewhere (Mosmann, 1983). This experiment was conducted in triplicate by seeding DLD-1 in 96 well plates at density of 2×10^4 cells per well in a final volume of 100 μL in complete RPMI-1640 medium. After 24 hours of incubation at 37°C and 5% CO_2 , medium was removed, then cells were exposed to 100 μL of various concentrations of drug (Table 2-2) for 30 minutes. After 30 minutes exposure, wells were washed with 200 μL of Hanks Balanced Salt Solution (HBSS) followed by adding 200 μL of medium to each

well. Cells were then incubated for 5 days at 37°C and 5% CO₂. On the fifth day, 20 µL of a 5 mg/mL solution of MTT were added to each well then cells were incubated at 37°C and 5% CO₂. After incubation for 4 hours, medium and MTT were removed and replaced with 150 µL of DMSO and absorbance was determined at 540 nm using multiskan Ex (Thermo electron corporation). Survival was calculated as the true absorbance of treated lanes divided by the true absorbance of control lanes and expressed as a percentage.

Table 2-2: Doxorubicin, imatinib and gefitinib cumulative concentrations retrieved from the three different penetration models and used to assess the influence of those concentrations versus time on DLD-1 cells survival rates using MTT assay.

	C↓D↓	D↓	D↓C↑
Drug	Conc (µM)		
Doxorubicin	112	2.8	0.03
Imatinib	68.21	2.73	0.08
Gefitinib	61.34	5.16	0.03

3. RESULTS

3.1 Growth curves in monolayer setting:

The growth characteristic of DLD-1 and MCF-7 cells cultured as monolayers is presented in figure 3-1. In DLD-1 cells, an initial lag period of 24 hours was observed before cells entered exponential growth. After 4 to 5 days in culture, cells entered plateau phase and cell numbers remained constant until the end of the experiment. No significant lag phase was observed in MCF-7 cells and these cells entered plateau phase between 5 and 6 days of culture.

3.2 Growth characteristics of cell lines on the transwell's membrane and MCL thickness measurements:

3.2.1 Growth characteristics and thicknesses of DLD-1 and MCF-7 MCLs:

Growth characteristics and thicknesses of DLD-1 and MCF-7 MCLs are presented in figures 3-2 and 3-3. The average thickness of DLD-1 and MCF-7 on day one of growth on the transwell microporous membrane was 12.9 ± 3.01 μm and 12.2 ± 1.02 μm respectively. Coverage of the entire membrane was generally very good with only occasional gaps in the cell layer being visible under phase contrast microscopy. If gaps in the monolayer were observed, these transwells were discarded. The thickness of the MCL increased as a function of time and on day 7, thickness of the MCLs were 69.40 ± 7.40 and 61.28 ± 4.54 μm for DLD-1 and MCF7 cells respectively.

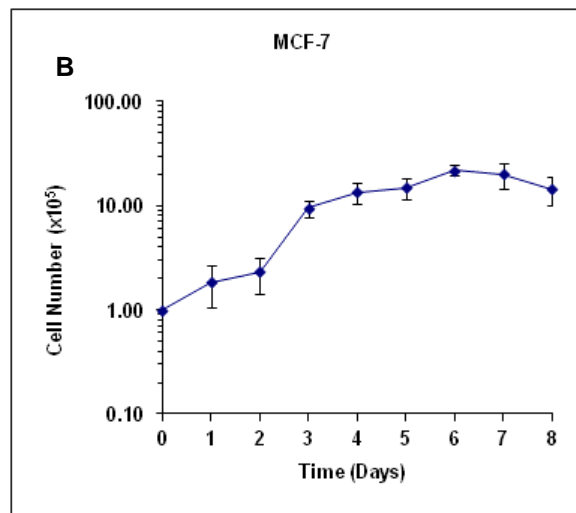
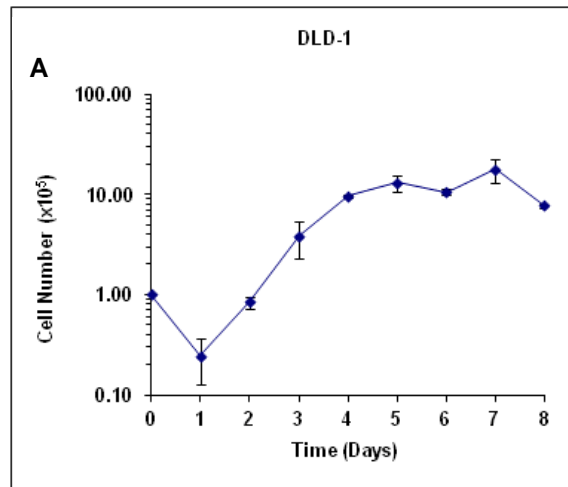


Figure 3-1: Growth curves of DLD-1(A) and MCF-7 (B). T-25 flasks were seeded with 1×10^5 cells and cultured in 10 mL complete growth medium for 8 days. Cells were trypsinised and counted using a haemocytometer. Each data point represents the mean \pm SD for 3 independent experiments.

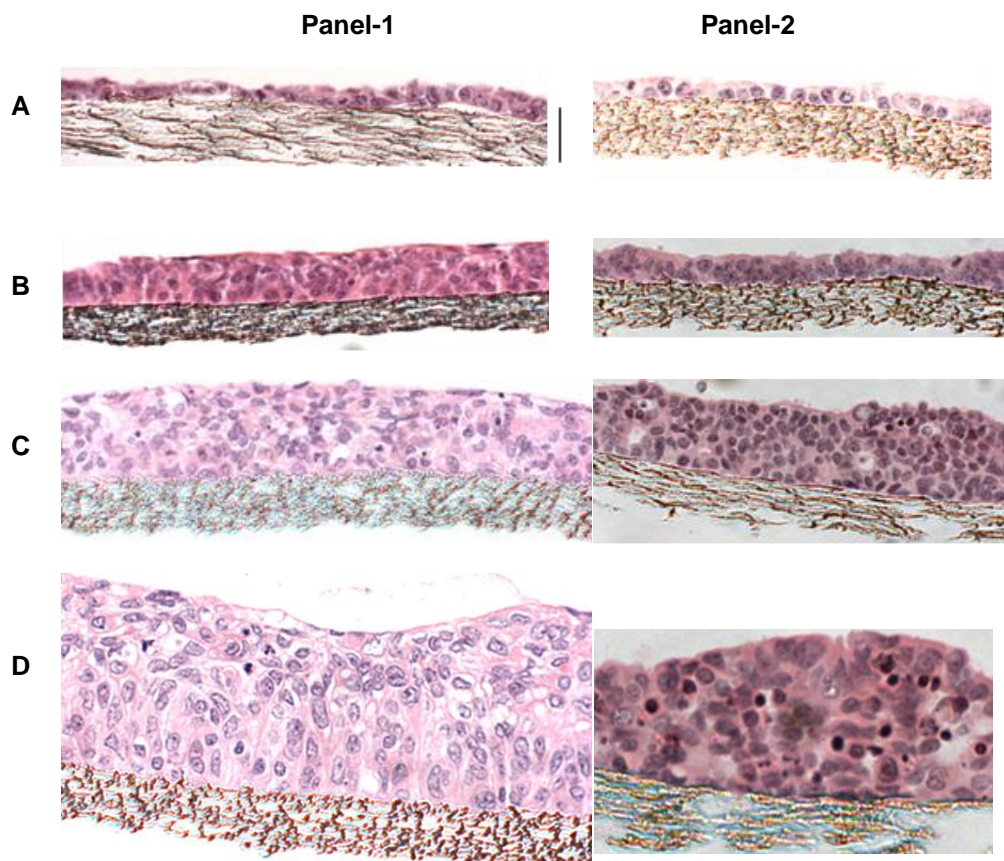


Figure 3-2: Histological sections through MCLs of DLD-1 (panel-1) and MCF-7 (Panel-2), on days 1(A), 3(B), 5(C) and 7(D) of growth on the transwell membrane. Bar = 30 μ m.

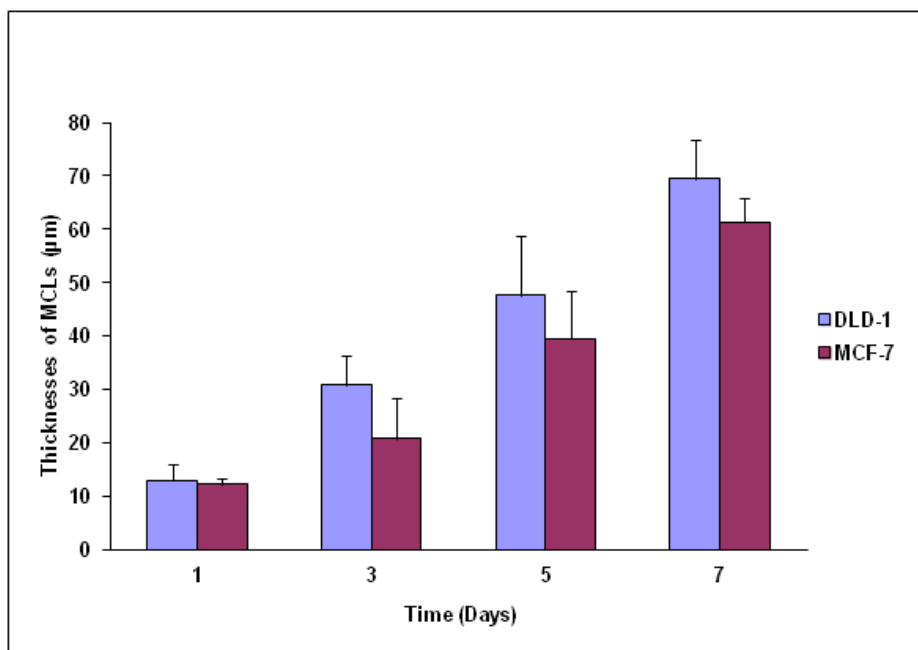


Figure 3-3: Thicknesses of DLD-1 and MCF-7 MCLs. Each point represents the mean thickness \pm SD for 15 measurements on a total of three histological sections of three separate experiments.

3.2.2 The ability of a panel of cell lines to form MCLs:

Based upon previous studies, DLD-1 and MCF7 cells were known to form MCL's. The ability of other cell lines to form MCLs was determined and the results are presented in figures 3-4 and 3-5. The cell lines included SiHa, Panc-1, Caski, A-2780, M14, SK-MEL 23, HT-29, A549, PC3 and 786-0. These cell lines were processed in the same way as DLD-1 and MCF-7. They were all seeded at a density of 3×10^5 cells on the transwell membrane and allowed to grow for 5 days at 37°C and 5% CO₂. Panc-1, SK-MEL 23, A-2780, M14, SiHa and Caski cell lines formed MCLs with thicknesses ranging from 20 – 120 µm. However, A-549, 7860, HT-29 and PC3 formed thin MCLs with thickness ranging from 8 – 13 µm. Although SiHa and Caski formed a thin

MCL, the MCLs formed were uniform and tightly attached to the membrane with no gaps or holes. Panc-1 and SK-MEL 23 formed thicker MCLs compared to DLD-1 and MCF-7. The average thickness of DLD-1 and MCF-7 MCL on the 5th day of growth on the membrane was $47.6 \pm 11.26 \mu\text{m}$ and $39.55 \pm 8.81 \mu\text{m}$ respectively. However, the MCL formed by Panc-1 and SK-MEL was

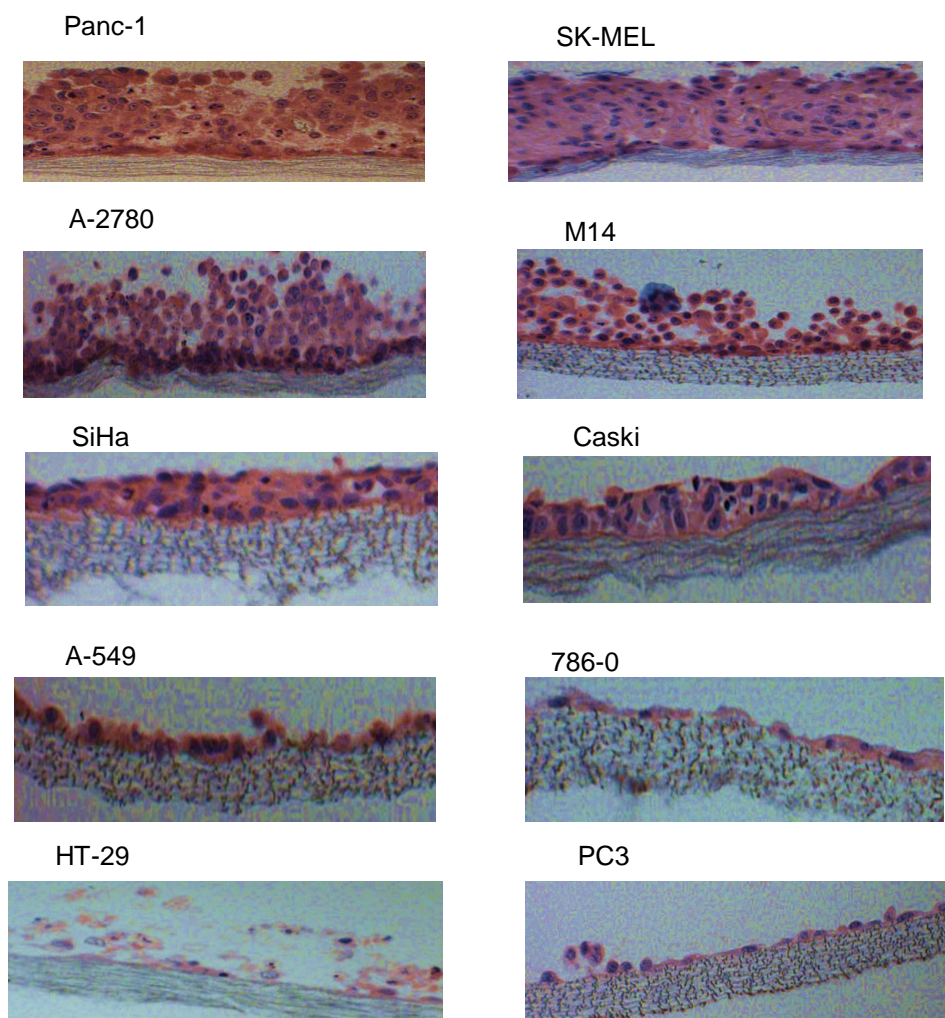


Figure 3-4: Histological sections through Panc-1, SK-MEL 23, A-2780, M14, SiHa, Caski, A-549, 786-0, HT-29 and PC3 MCLs on day 5 of growth on the transwell membrane.

three times thicker than that of DLD-1 and MCF-7 on the same day of growth. MCLs formed by A-549, 7860, HT-29 and PC3 were thin and there were gaps between the cells, particularly for HT-29 and PC3 cell lines.

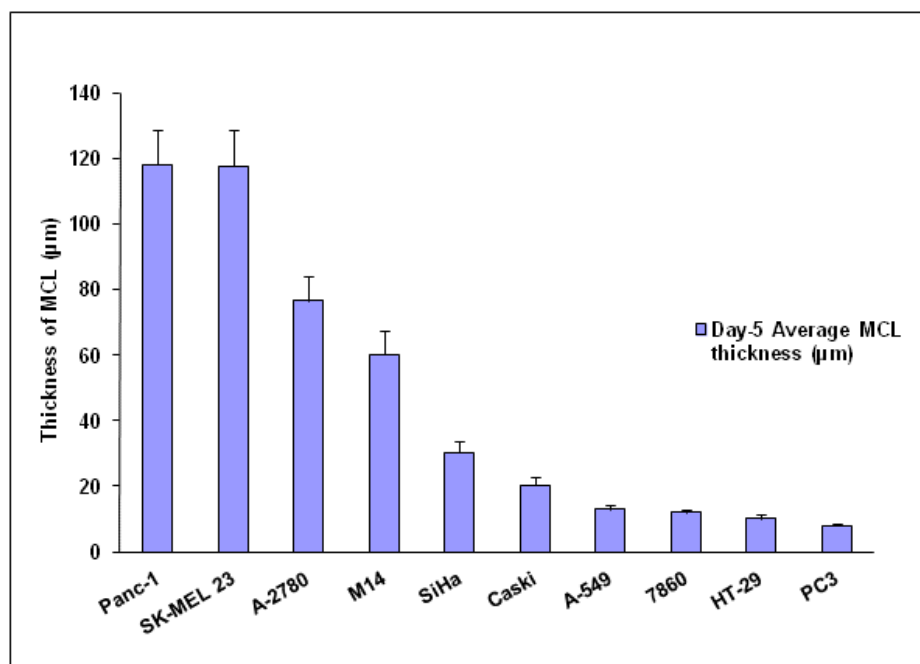


Figure 3-5: MCL thicknesses of Panc-1, SK-MEL 23, A-2780, M14, SiHa, Caski, A-549, 7860, HT-29 and PC3 after 5 days of growth on the transwell membrane. Results represent mean \pm SD of 15 readings from 3 different sections of 3 different replicates.

3.2.3 Testing the ability of the MCL to form a homogenous barrier using trypan blue:

In order to determine whether drugs cross the MCL by penetrating through cells or via gaps between cells, the ability of trypan blue (which is excluded from cells with intact membranes) to cross DLD-1 MCLs was determined. Trypan blue was allowed to penetrate through DLD-1 MCL (Day-1) and through blank membrane (no cells) over 3 minutes at 37°C. Concentrations of

penetrating trypan blue to the bottom chamber were measured spectrophotometrically based on calibration curve standards (figure 3-6).

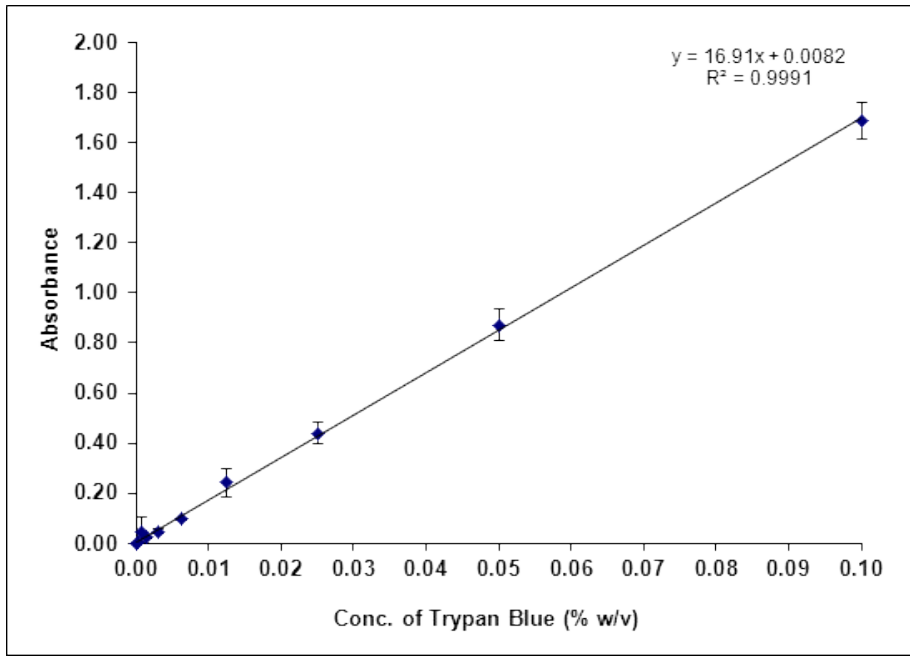


Figure 3-6: Calibration curves used to calculate penetrating trypan blue concentrations. Results represent mean \pm SD for three independent replicates.

Penetrating trypan blue was calculated as concentration (% w/v) as in figure 3-7. The significant difference in penetrating trypan blue through blank membrane compared to DLD-1 MCL can be clearly noticed where 0.0019 % (w/v) was measured in the bottom chamber in case of blank membrane compared with 0.0002 % (w/v) in case of DLD-1 MCL. These results show that trypan blue penetration through blank membrane was 10 times higher than that penetrated through DLD-1 MCL which indicates that trypan blue

penetrated the MCL through gaps between the cells and that the MCL had the ability to limit trypan blue penetration to the bottom chamber.

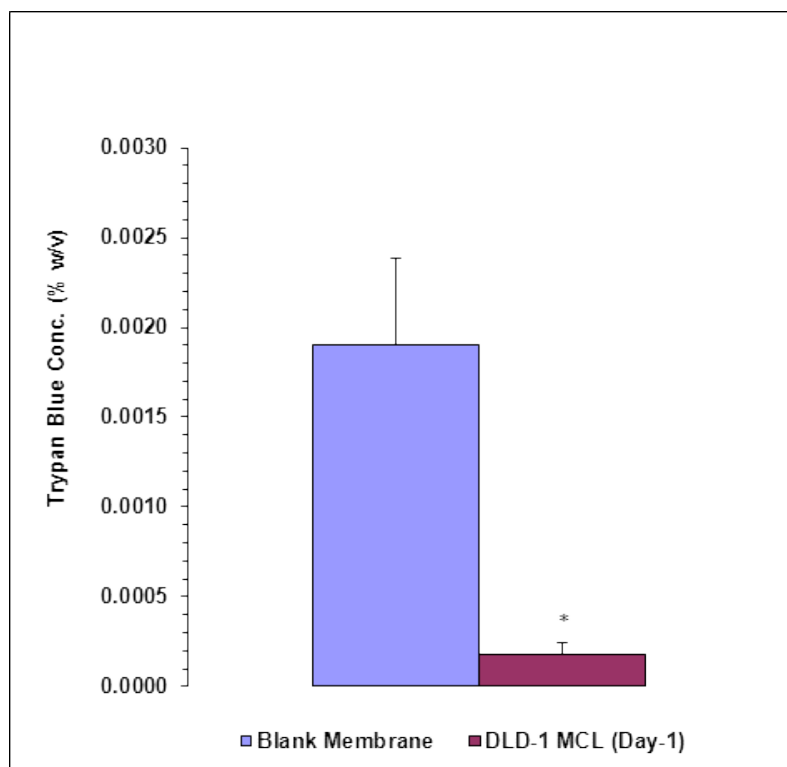


Figure 3-7: Concentrations (% w/v) of penetrating trypan blue through blank membrane and through DLD-1 MCL. Results represent mean \pm SD of three different replicates. (*) $P < 0.05$.

3.3 Analysis of doxorubicin:

3.3.1 HPLC analysis of doxorubicin:

Figure 3-8 shows the retention time and peak areas of doxorubicin and the internal standard epirubicin. Doxorubicin elutes first followed by epirubicin with one minute interval between them. The representative chromatograms presented in figure 3-8 were obtained using doxorubicin alone (A), doxorubicin and epirubicin mixed together (B) and epirubicin alone (C).

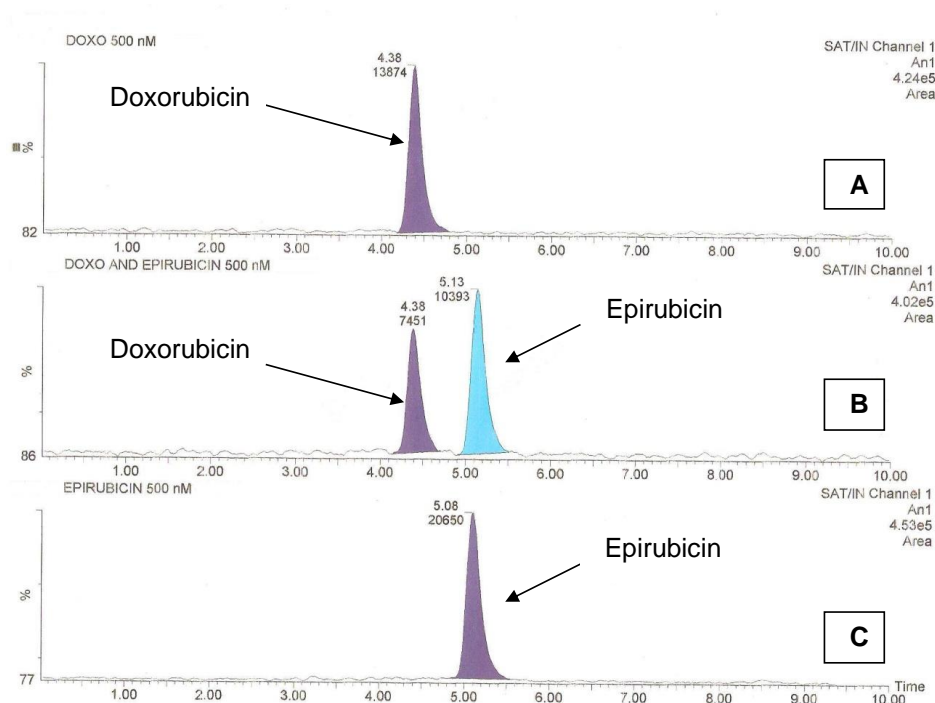


Figure 3-8: HPLC Chromatogram showing peak areas and retention times of doxorubicin and epirubicin. The concentrations of doxorubicin and epirubicin were 500 nM

3.3.2 Calibration curves, limits of detection, extraction efficiencies, intra-day variations and injection reproducibility:

Quantification of doxorubicin in tissue culture medium or in mobile phase was performed based on standard calibration curves prepared daily by linear regression of the ratio of drug to internal standard peak area versus concentration. The calibration curves used for the determination of doxorubicin in tissue culture medium were linear over the concentration range of 10 nM to 100 μ M. Correlation coefficient (r^2) values ranged between 0.991 and 0.995.

Figure 3-9 represents an example for one of the calibration curves which were used to determine doxorubicin. This calibration was used to analyse samples retrieved from the third penetration model (diffusion opposing convection $D \downarrow C \uparrow$), which usually permeates very low drug concentrations. Using calibration curves, the lower reproducible limit of quantification (LLOQ) for doxorubicin using HPLC was 10 nM.

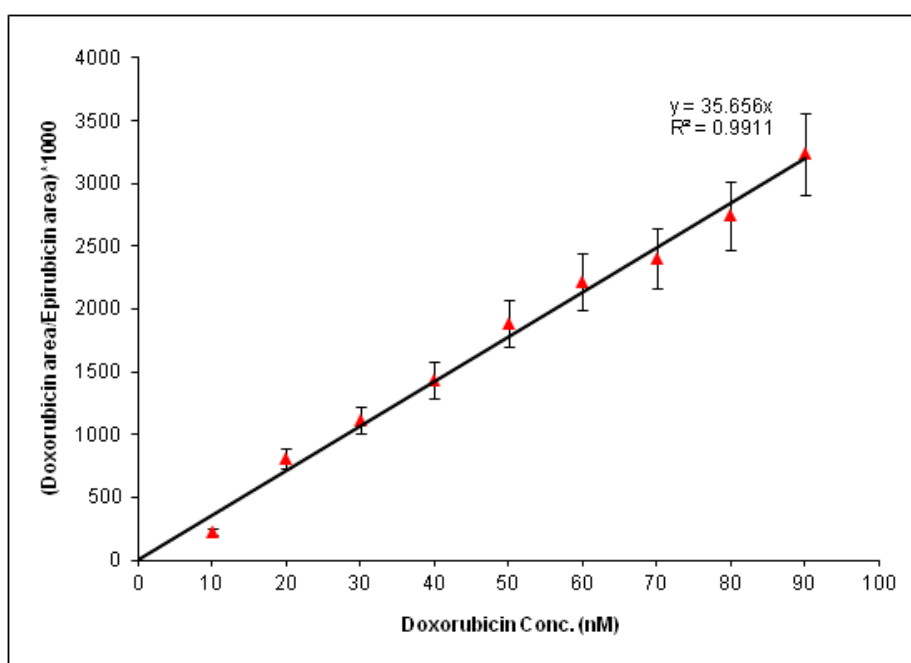


Figure 3-9: Calibration curve standards used to analyse samples created using model 3 (diffusion opposing convection $D \downarrow C \uparrow$). Results represent mean \pm SD of 3 replicates.

Limits of detection, extraction efficiencies of extraction techniques obtained for doxorubicin and experimental variations due to human sampling error or due to machine error during analysis (% precision) are all summarized in table 3-1. Different extraction techniques were used to extract doxorubicin from tissue culture medium details of which were described previously. Solid phase

extraction (SPE) had an extraction efficiency of 55% and 10 nM limit of detection. Protein precipitation without evaporation and protein precipitation with further evaporation had extraction efficiencies of 77% and 51% respectively and limits of detection of 50 nM and 20 nM respectively. Although solid phase extraction had an extraction efficiency of 55%, however, it was considered to be the best method of extraction because of its selectivity compared to other methods and due to its better limit of detection. Intra-day variations and injection reproducibility and precision were calculated by injecting 6 quality control injections from 6 independent vials or from the same vial containing doxorubicin (500 nM) respectively. Precision was calculated using the coefficient of variation equation which was described in section (2.5.3). Precision values obtained using the three different extraction techniques were less than 15%.

Table 3-1: Extraction efficiencies, limits of detection, intra-day variations and injection reproducibility (precision) of each extraction technique using HPLC.

Comparison/Method	Non extracted	Solid Phase Extraction	Protein precipitation without evaporation	Protein precipitation with evaporation and reconstitution
%Extraction efficiency (mean \pm SD)	n/a*	55.2 \pm 9.7	77.3 \pm 7	51.3 \pm 3.8
Limit of detection (nM)	5 nM	10 nM	50 nM	20 nM
Experimental precision (%),(n=6)	3.55	8.59	6.75	4.25
Injection precision (%),(n=6)	0.314	0.092	0.25	0.25

* = Not applicable.

3.3.3 Doxorubicin stability at 37°C:

Drug penetration assays are conducted at 37°C over a time period of 30 minutes to 1 hour. As a control experiment, the stability of doxorubicin under experimental conditions (phenol red free complete medium at 37°C) is presented in figure 3-10. Doxorubicin 1 μM was extracted using protein precipitation without evaporation and analysed by HPLC. The results demonstrate that doxorubicin is stable under these experimental conditions for at least 2 hours.

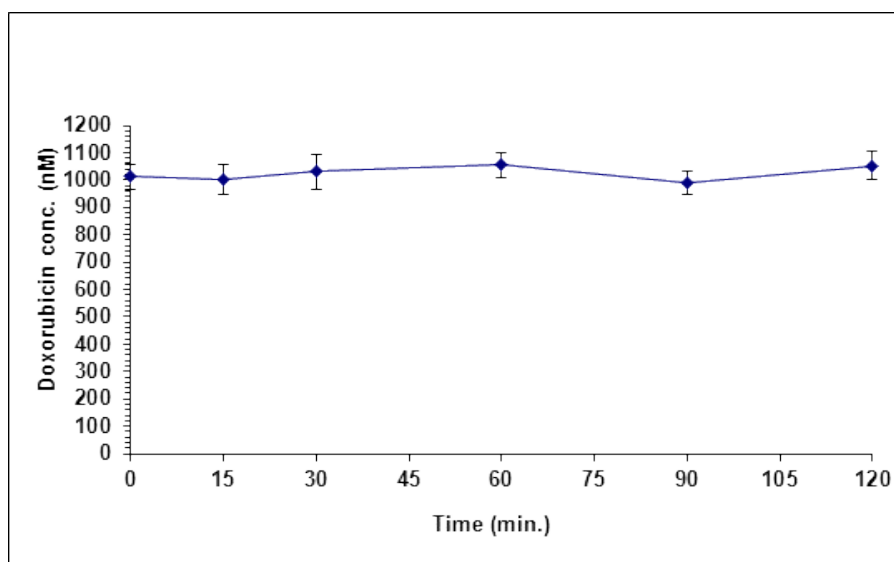


Figure 3-10: Doxorubicin (1 μM in tissue culture medium) stability test at 37°C over 2 hours. Results represent mean \pm SD for three different replicates.

3.4 Analysis of imatinib and gefitinib:

3.4.1 HPLC, LC/MS and LC/MS/MS analysis of imatinib and gefitinib:

HPLC, LC/MS and LC/MS/MS were used to analyse imatinib and gefitinib. LC/MS/MS was reserved for samples which were expected to contain very low

concentrations i.e. those produced by the third model (diffusion opposing convection $D \downarrow C \uparrow$), LC/MS was used to analyse samples created from diffusion only model ($D \downarrow$) and HPLC was used to analyse samples which were expected to contain high concentrations of drug i.e. those produced by the second model (convection plus diffusion $C \downarrow D \downarrow$). Figures 3-11 – 3-14 represent the chromatographic traces of imatinib and gefitinib using HPLC, LC/MS and LC/MS/MS. Panel (A) of figure 3-11 shows the absorbance spectrum for imatinib and section (B) on the same figure represent the absorbance spectrum for gefitinib obtained using reverse-phase liquid chromatography. They were scanned across the wavelength range between 200 and 400 nm. Imatinib absorbance peaks occur at 265 nm while gefitinib absorbance peaks occur at 252 nm and 343 nm. Panel (C) on the same figure represents HPLC chromatographic traces for gefitinib (10 μ M) and imatinib (10 μ M) separated using the HPLC analysis conditions described in section (2.6). Samples were extracted using simple protein precipitation with methanol. It is noticed from the chromatogram that gefitinib eluted at 4.30 minute while imatinib eluted at 7.55 minute. Figure 3-12 represents LC/MS chromatographic traces for imatinib (10 μ M). Reverse-phase liquid chromatography with MS was used for the separation of imatinib. Panel (A) on the figure represents the diode array detection of imatinib at a wavelength of 265 nm and a retention time of 5.94 minutes. Panel (B) represents an MS trace supporting correct identification of imatinib in MS detector. In this trace, total ion chromatogram (TIC) scanning of singularly charged ion $[ES^+]$ with retention time at 5.90 minutes. Panel (C) represents selected ion recording (SIR) of imatinib in specific $[ES^+]$ mass to

charge ratio (m/z) of 494 with retention time at 5.91 minutes. Finally, panel (D) on figure 3-12 represents spectral characteristics of imatinib at m/z of 494.11. Gefitinib (10 μM) LC/MS chromatogram traces on the other hand are presented on figure 3-13. Gefitinib was also separated using reverse-phase liquid chromatography with MS. Panel (A) on the figure represents the diode array detection of gefitinib at a wavelength of 343 nm and a retention time of 3.16 minutes. Panel (B) represents an MS trace supporting correct identification of gefitinib in MS detector. In this trace, scanning of a singularly charged ion [ES⁺] is presented with retention time at 3.28 minutes. Panel (C) represents selected ion recording (SIR) of gefitinib in specific [ES⁺] mass to charge ratio (m/z) of 446.85 with retention time at 3.24 minutes. Finally, panel (D) on the same figure represents spectral characteristics of gefitinib at m/z of 446.85. LC/MS/MS chromatograms of imatinib and gefitinib are presented in figure 3-14 which shows the chromatographic traces of imatinib 100 nM alone as seen on panel (A), gefitinib 500 nM alone panel (B) and both imatinib 100 nM and gefitinib 500 nM together as on panel (C). As seen on panel (C), total ion chromatogram (TIC) scanning of singularly charged ion [ES⁺] with gefitinib eluted at minute 1.58 and imatinib eluted at minute 2.48. Total running time was 4 minutes with flow rate of 0.35 mL/min and an injection volume of 10 μL .

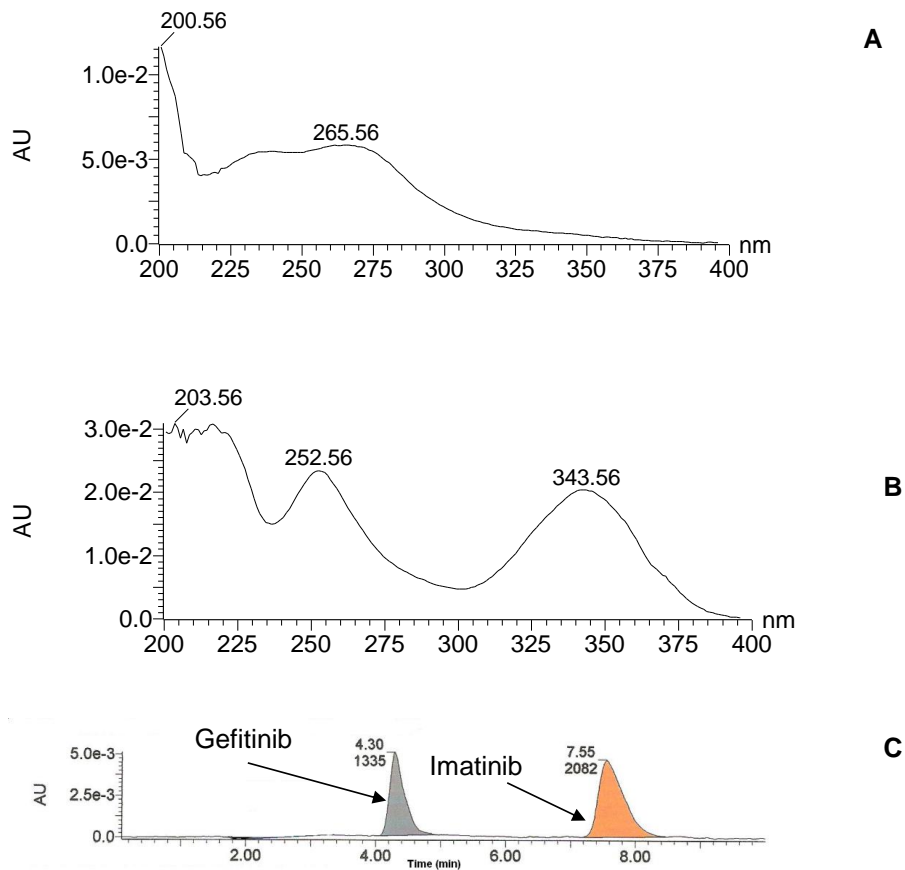


Figure 3-11: Detection of imatinib and gefitinib at (10 μ M) using HPLC. Reverse-phase liquid chromatography was used for the separation of imatinib and gefitinib. Absorbance spectrum (range 200-400 nm) for imatinib (A) and gefitinib (B). Absorbance peaks occur at 265 nm for imatinib and at 252 nm and 343 nm for gefitinib. (C) Chromatograms of imatinib and gefitinib using diode array detection (DAD) at wavelength of 343 nm and retention times of 4.3 and 7.55 minutes for imatinib and gefitinib respectively.

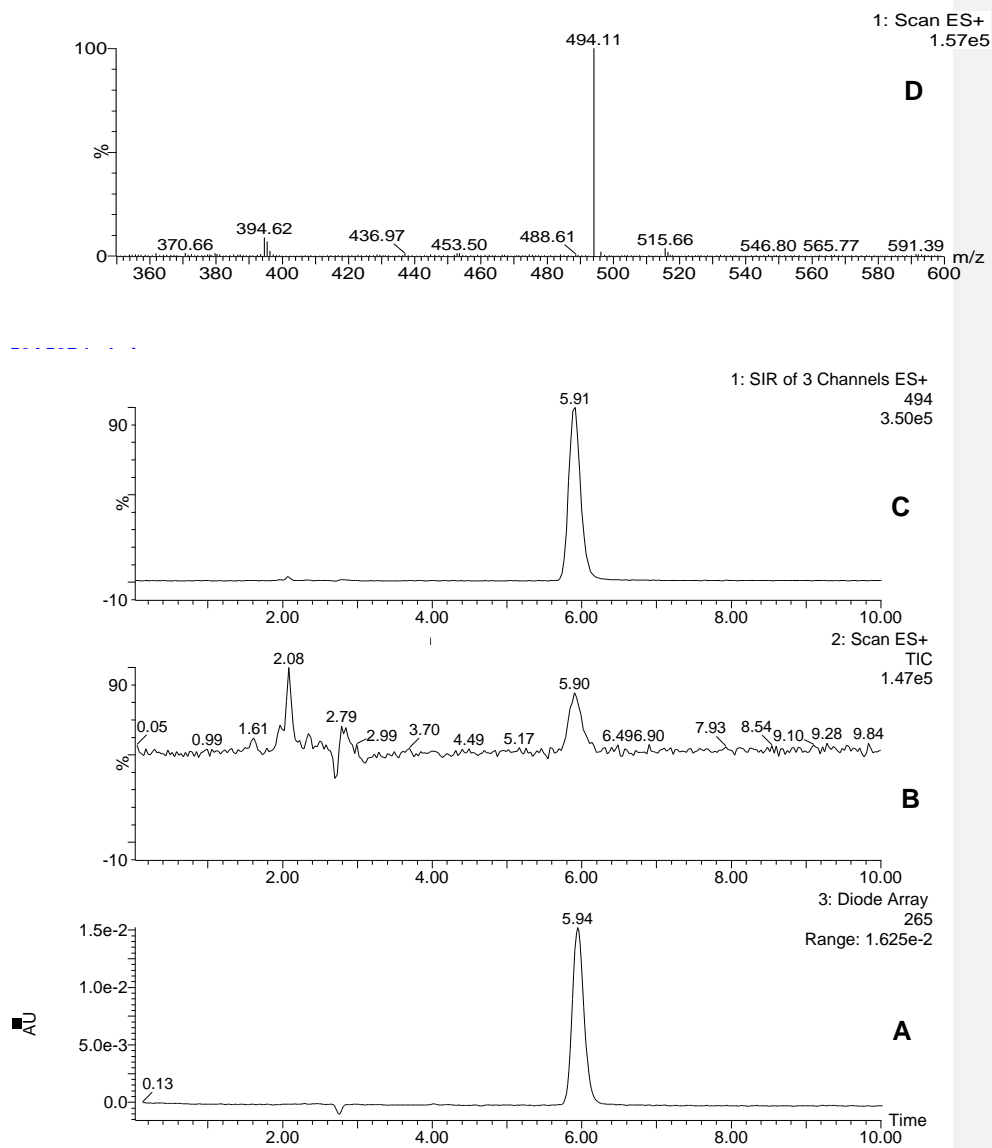


Figure 3-12: Detection of (10 μ M) imatinib using LC/MS. Reverse-phase liquid chromatography was used for the separation of imatinib. **(A)** DAD trace representing peak and retention time at 5.94 minutes. **(B)** MS trace supporting correct identification of imatinib in MS detector. Total ion chromatogram (TIC) scanning of singularly charged ion [ES+] with retention time at 5.90 minutes. **(C)** Selected ion recording (SIR) of imatinib in specific [ES+] m/z of 494 with retention time at 5.91 minutes. **(D)** Spectral characteristics of imatinib at m/z of 494.11.

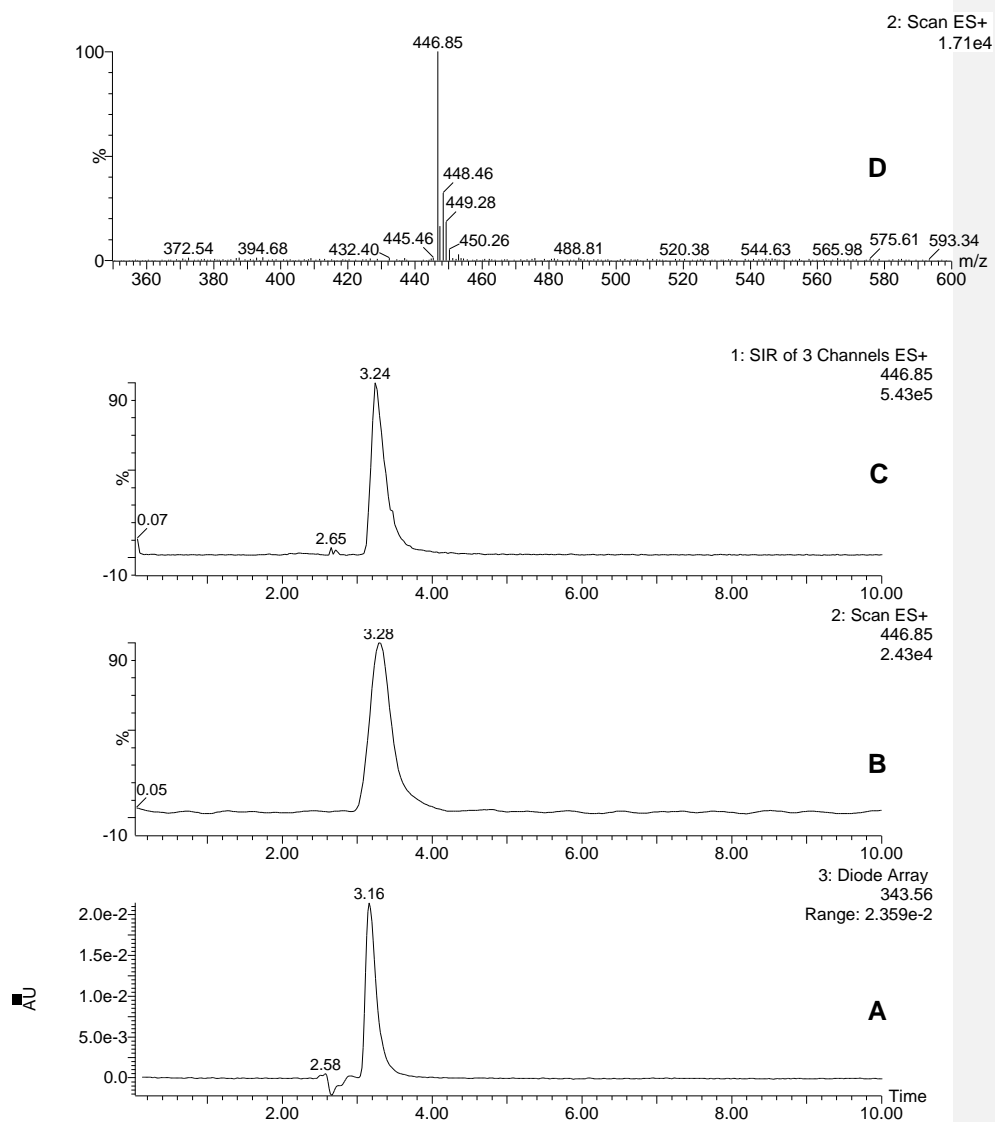


Figure 3-13: Detection of (10 μ M) gefitinib using LC/MS. Reverse-phase liquid chromatography was used for the separation of gefitinib. **(A)** DAD trace representing peak and retention time at 3.16 minutes. **(B)** MS trace supporting correct identification of gefitinib in MS detector. Trace represents scanning of singularly charged ion [ES⁺] with retention time at 3.28 minutes. **(C)** Selected ion recording (SIR) of gefitinib in specific [ES⁺] m/z of 446.85 with retention time at 3.24 minutes. **(D)** Spectral characteristics of gefitinib at m/z of 446.85.

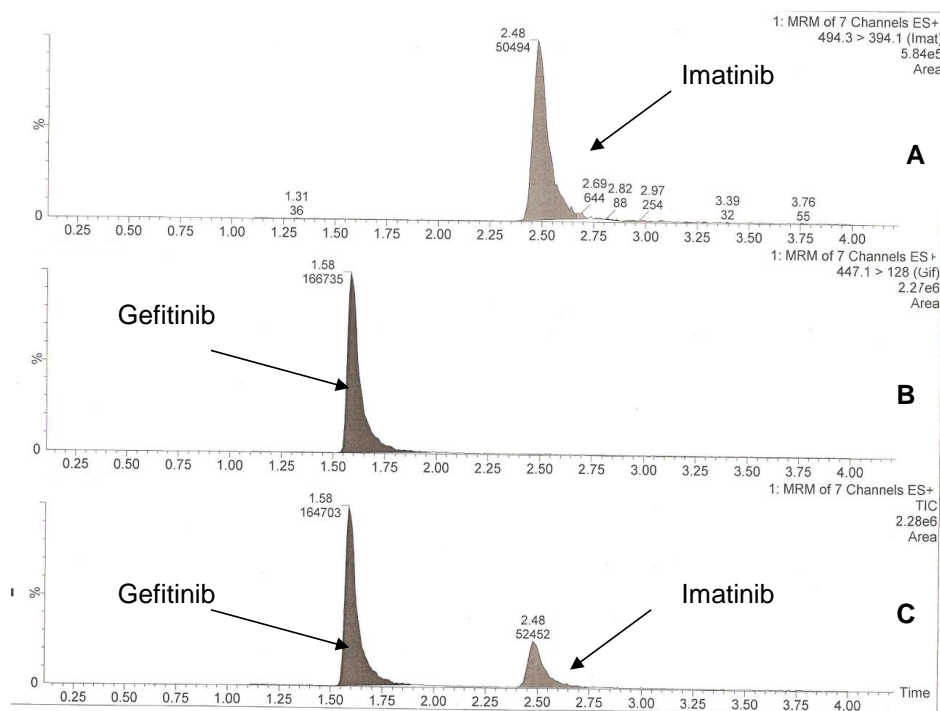


Figure 3-14: Chromatographic traces of imatinib 100 nM (A) and gefitinib 500 nM (B) using LC/MS/MS. Panel (C) represents total ion chromatogram (TIC) and peak areas of both drugs together. Gefitinib eluted at minute 1.58 and imatinib eluted at minute 2.48.

3.4.2 Calibration curves and limits of detection:

As in case of doxorubicin, imatinib and gefitinib quantification in tissue culture medium or in mobile phase was performed based on standard calibration curves. Quantification was performed by linear regression of the ratio of drug to internal standard peak area versus concentration of at least ten concentration standards (in triplicate). The calibration curves used for the determination of imatinib and gefitinib in tissue culture medium were linear over the concentration range of 10 nM to 100 μ M depending on the penetration model

used with the correlation coefficient (r^2) values ranging between 0.96 and 0.99. Calibration curve standards were selected depending on the penetration model used as each model operates over different ranges of drug concentrations. A series of calibration curves were generated, the details of which varied depending upon the specific experiment performed (appendix 2). Figures 3-15 and 3-16 represent typical examples of calibration curves used to quantify imatinib and gefitinib concentrations respectively. These calibration curves were used to analyse samples retrieved from the third penetration model (diffusion opposing convection $D \downarrow C \uparrow$), which usually permeates very low drug concentrations. Using calibration curves, the lower reproducible limit of quantification (LLOQ) for imatinib and gefitinib using LC/MS/MS was 1 nM. However, 100 nM and 1 μ M were detected and quantified using LC/MS and HPLC respectively.

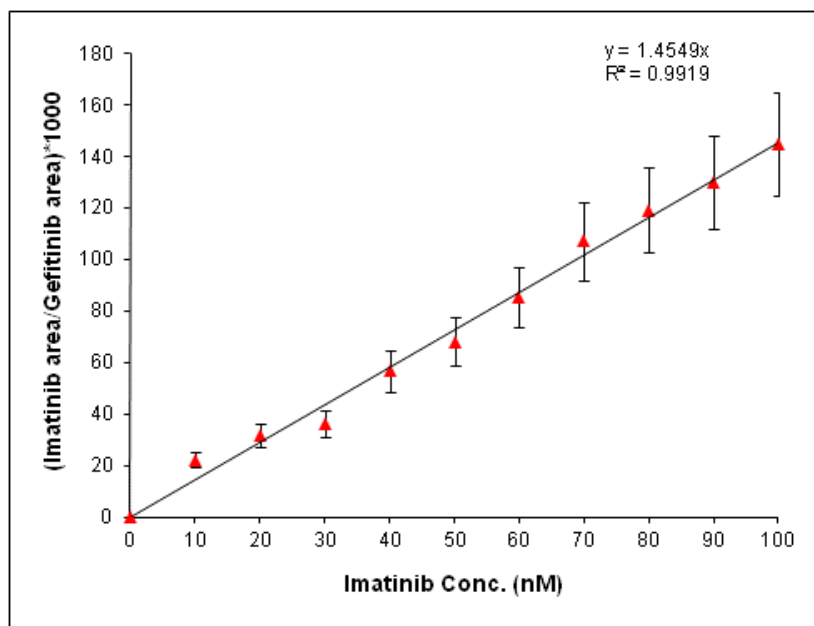


Figure 3-15: Imatinib calibration curve standards used to analyse samples created using model 3 (diffusion opposing convection $D \downarrow C \uparrow$). Results represent mean \pm SD of 3 replicates.

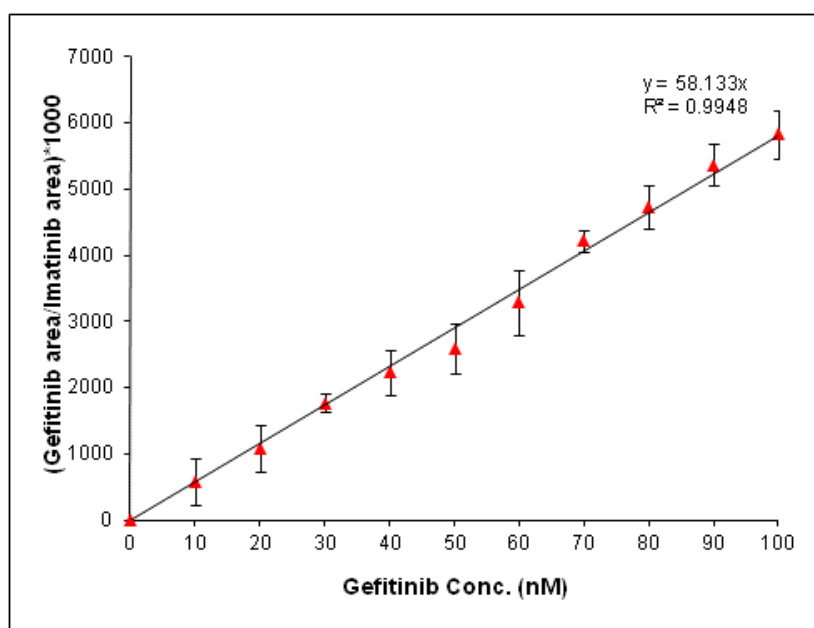


Figure 3-16: Gefitinib calibration curve standards used to analyse samples created using model 3 ($D \downarrow C \uparrow$). Results represent mean \pm SD of 3 replicates.

3.4.3 Stability of imatinib and gefitinib at 37°C:

The stability of imatinib and gefitinib in phenol red free complete medium at 37°C are presented in figure 3-17. Imatinib and gefitinib 1 μ M each were extracted using protein precipitation without evaporation and analysed by HPLC. The results demonstrate that they were both stable under these experimental conditions for at least 2 hours.

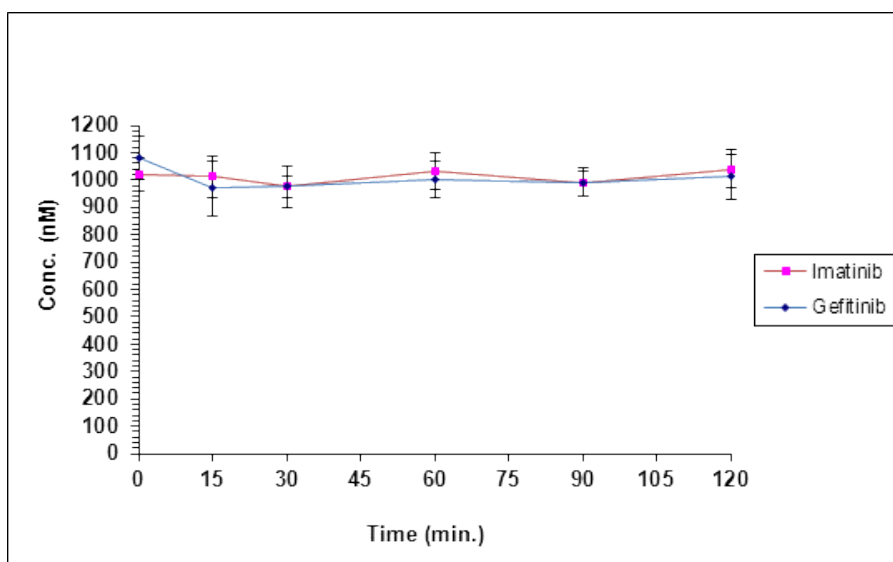


Figure 3-17: Stability of imatinib and gefitinib 1 μ M each in tissue culture medium at 37°C over 2 hours. Results represent mean \pm SD for three different replicates.

3.5 Drug penetration assays using model-1:

3.5.1 Drug penetration assay using variable concentration gradient (VCG) technique:

The penetration of doxorubicin through blank transwells (no cells seeded) is presented in figure 3-18. In the absence of cells, doxorubicin at an initial concentration of 100 μM penetrated the membrane and reached a maximum concentration in the bottom chamber of $9.26 \pm 2.21 \mu\text{M}$ after 45 minutes. Doxorubicin at 50 μM and 25 μM penetrated the membrane and reached concentrations of 4.41 ± 0.82 and $2.16 \pm 0.26 \mu\text{M}$ respectively after 45 minutes. It was clearly noticed that the penetration curves plotted using VCG-technique showed considerable variation as indicated by “spiking” in the curves (Figure 3-18). In addition, the expected theoretical steady state (14 μM in case of using 100 μM at the top chamber) was not achieved.

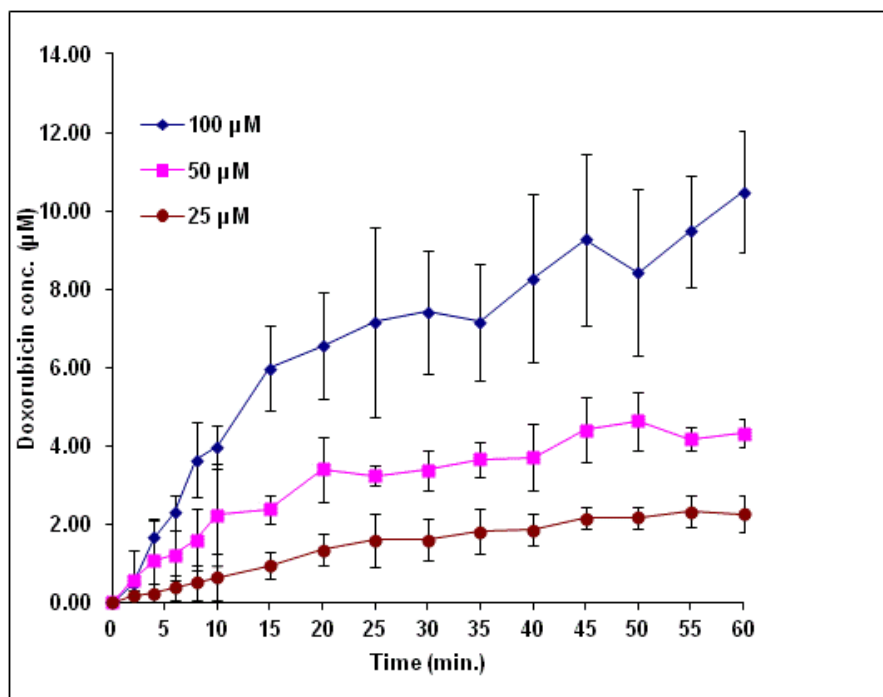


Figure 3-18: Penetration of doxorubicin 100, 50 and 25 µM through non hydrated blank (no cells seeded) membranes using VCG-technique. Results represent mean ± SD for 3 independent experiments.

Inadequate hydration of the membranes could be a cause of this spiking and for this reason; penetration assay was performed using a hydrated transwell where the transwell was incubated in medium at 37°C for 24 hours prior to conducting the penetration assay. Penetration assay was conducted using doxorubicin at 100 µM only. The results are presented in (figure 3-19). Transwell hydration did not improve the variation observed and curve spiking still occurred.

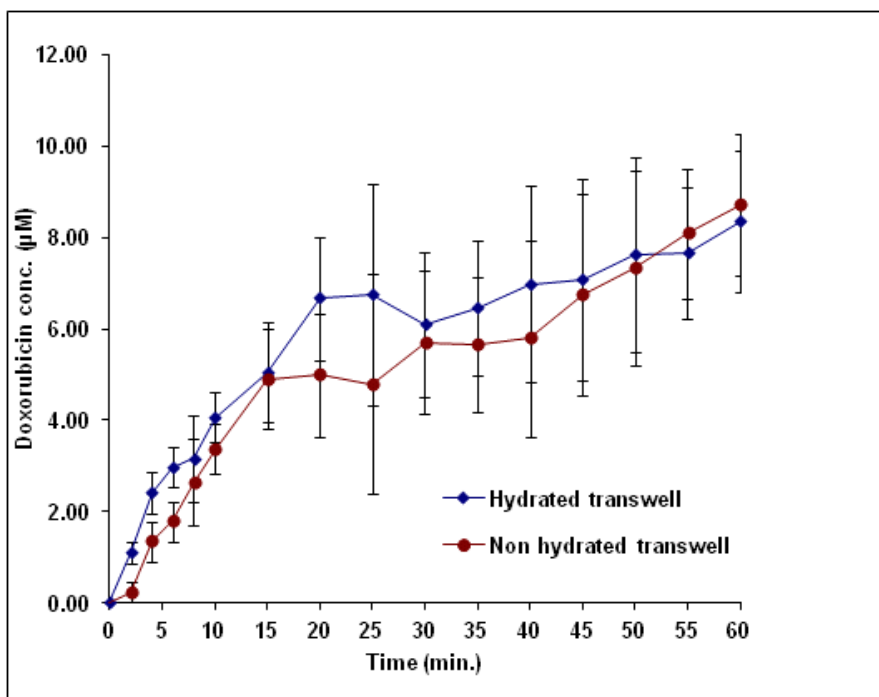


Figure 3-19: Penetration of doxorubicin 100 µM through hydrated and non-hydrated blank (no cells seeded) membranes using VCG-technique. Results represent mean ± SD for 3 independent experiments.

The next potential source of error explored was the collagen which coats the membrane. It was expected that collagen may bind to doxorubicin and hence influences its penetration through the membrane. An experiment was conducted using a trypsinized transwell. To remove collagen, transwell membrane was trypsinized with 0.5 mL of trypsin for 5 minutes then rinsed 3 times with HBSS solution prior to conducting the penetration assay. Penetration assay was conducted using doxorubicin at 100 µM. Although the resultant plotted curve came smoother and penetration rate was faster after trypsinization however, variation was still observed and curve spiking still occurred as shown on Figure 3-20.

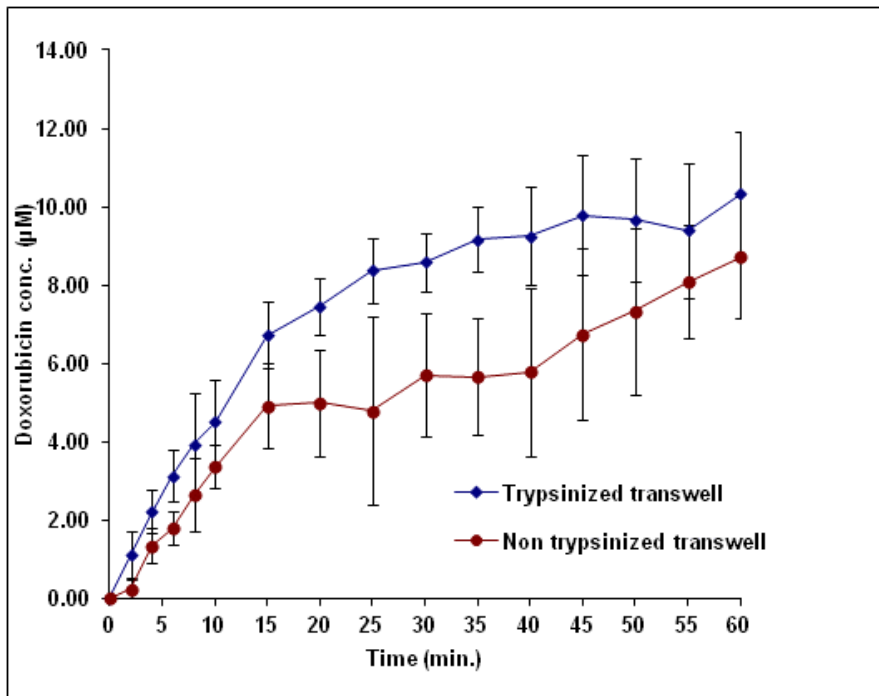


Figure 3-20: Penetration of doxorubicin 100 µM through a trypsinized and non-trypsinized blank (no cells seeded) membrane using VCG-technique.

The result of this experiment indicates that spiking and inherent variations in the plotted curves might not be due to the presence of collagen in the transwell. Although the variations and “spikes” noticed in the plotted curves using VCG technique through control transwells, penetration of doxorubicin through DLD-1 multicell layers was performed and it is presented in figure 3-21. Penetration of doxorubicin through DLD-1 MCLs was performed using doxorubicin at 100, 50 and 25 µM on days 1, 3, 5 and 7 of growth of cells on the membrane. In the presence of cells, doxorubicin at 100 µM penetrated the multicell layer on the first day of growth on the membrane and reached a maximum concentration of approximately 3.79 ± 1.77 µM after 45 minutes.

Using 50 and 25 μM in the top chamber, doxorubicin reached concentrations of 1.41 ± 0.60 and 0.75 ± 0.46 μM respectively after 45 mins of incubation. The rate of penetration through a MCL of 14.3 ± 2 μm is therefore concentration dependent. Doxorubicin penetration on days 3 and 5 of growth on the membrane showed that as the thickness of the MCL increased, the rate of doxorubicin penetration decreased. The inherent variations and spikes in the curves were still present as occurred with the control samples. Figure 3-21 represent mean \pm SD of doxorubicin 100, 50 and 25 μM penetration through blank transwells (no cells seeded) and through the multi cell layers on days 1, 3 and 5 of growth on the membrane. Day 7 samples were not analysed because of the clear limited penetration noticed on day 5. Using penetration assay with VCG-technique, penetration rates were calculated based on fitting a linear regression to the first 6 sampling points on the curve which represents the initial penetration rate. The slope of the linear regression equation was considered the penetration rate. Concentration values were converted into amounts and the rate was expressed as nmoles/minute. Tables 3-2 to 3-4, and figures, 3-22 and 3-23 show the penetration rates through DLD-1 MCLs (days 1-5) and through blank membrane. Rates of doxorubicin penetration were inversely proportional to the thickness of multicell layer with penetration rate of 0.0622 ± 0.006 nmol/min on day 1 (thickness 14.3 ± 2 μm), 0.0288 ± 0.007 nmol/min on day 3 (thickness 21.9 ± 2.7 μm) and 0.005 ± 0.002 nmol/min on day 5 where the thickness of the multicell layer was (37.3 ± 4.5 μm), for doxorubicin at 100 μM . Penetration rates of doxorubicin 50 and 25 μM using VCG are presented in tables 3-3 and 3-4. They show clear limited

penetration especially for doxorubicin at 25 μM on days 3 and 5 of growth on the membrane. Throughout all these experiments, considerable variation in data points was observed and ‘spiking’ of curves occurred frequently. Because of this, an alternative approach was employed where the concentration of drug in the top chamber was maintained at a constant value (the constant concentration gradient or CCG technique).

Table 3-2: Penetration rates of doxorubicin 100 μM , through blank (no cells seeded) and through DLD-1 MCLs on days 1, 3 and 5 of growth on the membrane using VCG-technique.

	Doxorubicin 100 μM			
	Penetration rate (nmoles/min)			
	Blank membrane (no cells)	MCL (Day-1)	MCL (Day-3)	MCL (Day-5)
Average Penetration rates (nmoles/min)	0.2425	0.0622	0.0288	0.005
SD	0.015	0.006	0.007	0.002

Table 3-3: Penetration rates of doxorubicin 50 μM , through blank (no cells seeded) and through DLD-1 MCL on days 1, 3 and 5 of growth on the membrane using VCG-technique.

	Doxorubicin 50 μM			
	Penetration rate (nmoles/min)			
	Blank membrane (no cells)	MCL (Day-1)	MCL (Day-3)	MCL (Day-5)
Average Penetration rates (nmoles/min)	0.1125	0.0118	0.0073	0.004
SD	0.015	0.006	0.0007	0.002

Table 3-4: Penetration rates of doxorubicin 25 μM , through blank (no cells seeded) and through DLD-1 MCL on days 1, 3 and 5 of growth on the membrane using VCG-technique.

	Doxorubicin 25 μM			
	Penetration rate (nmoles/min)			
	Blank membrane (no cells)	MCL (Day-1)	MCL (Day-3)	MCL (Day-5)
Average Penetration rates (nmoles/min)	0.0633	0.0081	BLD*	BLD
SD	0.015	0.006	BLD	BLD

*BLD = Below the limit of detection.

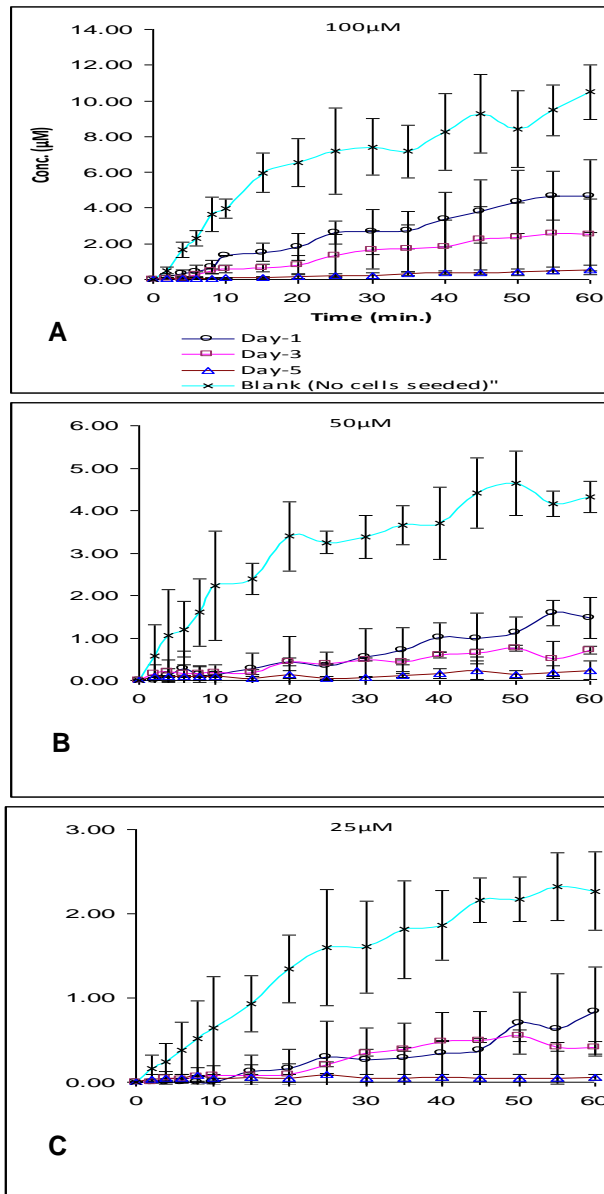


Figure 3-21: Penetration of doxorubicin 100 (A), 50 (B) and 25 µM (C) through blank (no cells seeded) and through DLD-1 MCL on days 1, 3 and 5 of growth on the membrane using VCG-technique. Legends in (A) represent (B) and (C).

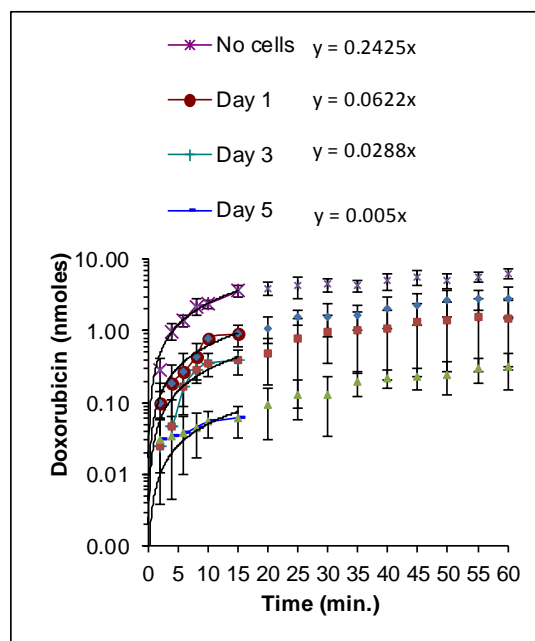


Figure 3-22 (A): Penetrating amounts of doxorubicin (100 μ M), through blank (no cells seeded) and through DLD-1 MCL on days 1, 3 and 5 of growth on the membrane using VCG-technique. Penetration rates were calculated from linear regression of the first 6 time points. Results represent mean \pm SD of three independent replicates.

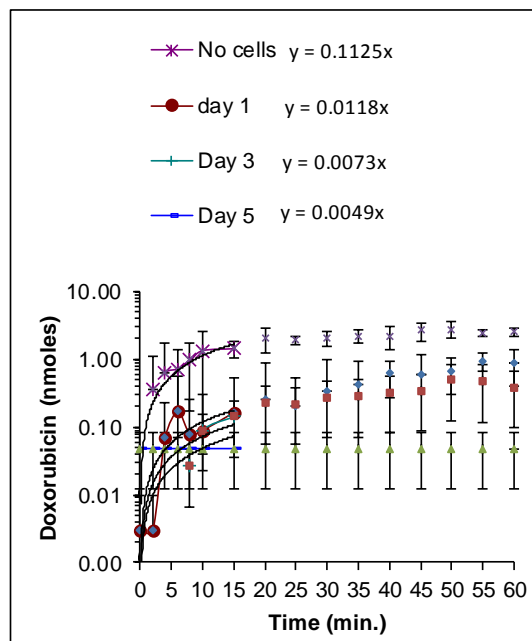


Figure 3-22 (B): Penetrating amounts of doxorubicin (50 μM), through blank (no cells seeded) and through DLD-1 MCL on days 1, 3 and 5 of growth on the membrane using VCG-technique. Penetration rates were calculated from linear regression of the first 6 time points. Results represent mean \pm SD of three independent replicates.

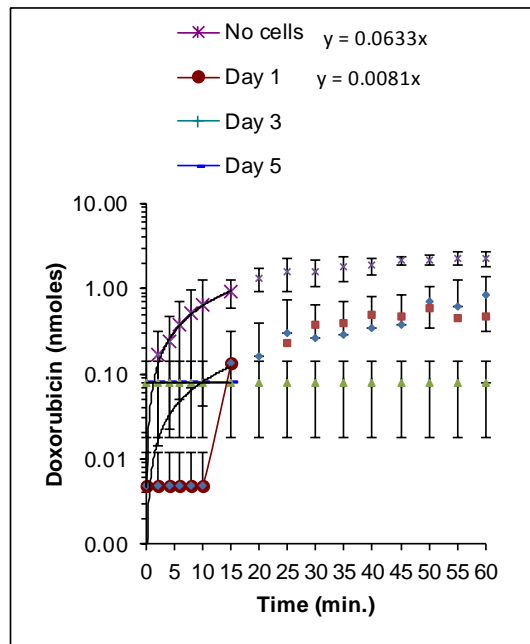


Figure 3-22 (C): Penetrating amounts of doxorubicin (25 μM), through blank (no cells seeded) and through DLD-1 MCL on days 1, 3 and 5 of growth on the membrane using VCG-technique. Penetration rates were calculated from linear regression of the first 6 time points. Results represent mean ± SD of three independent replicates.

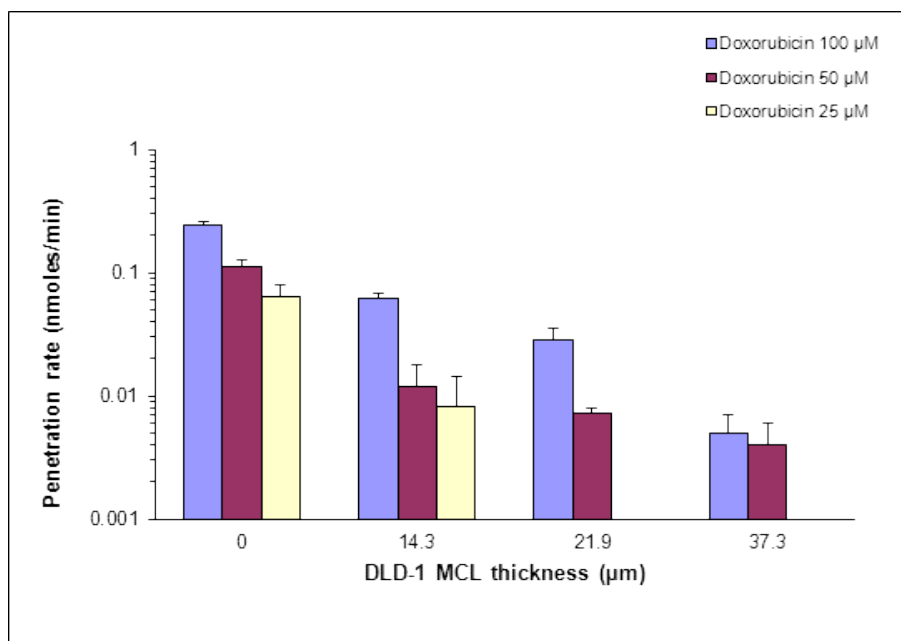


Figure 3-23: Penetration rates of doxorubicin 100, 50 and 25 µM, through blank (no cells seeded) and through DLD-1 MCLs on days 1, 3 and 5 of growth on the membrane using VCG-technique.

3.5.2 Drug penetration assay using constant concentration gradient (CCG) technique:

Using CCG-technique, doxorubicin penetration through blank membranes (figure 3-24), DLD1 (figure 3-25) and MCF7 MCLs (figure 3.26) was performed. With the CCG technique, data output was linear and the graphs did not show the significant 'spiking' noticed with the VCG technique. In addition, penetration rates were easy to calculate and finally, results were reproducible. The next step was to calculate the penetration rates using this technique to be compared with the results of the previous technique.

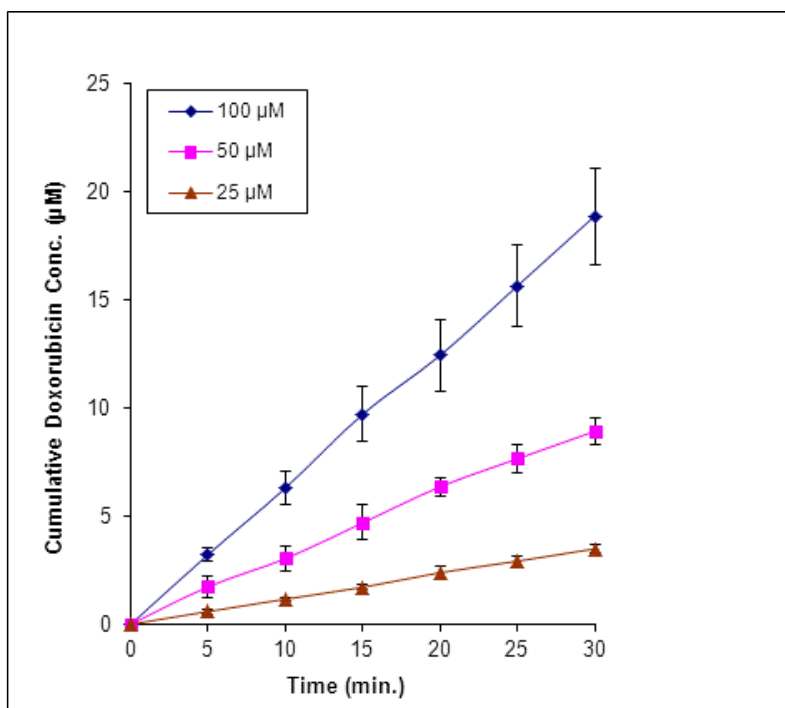


Figure 3-24: Penetration of doxorubicin 100, 50 and 25 µM through blank (no cells seeded) membranes using CCG-technique. Results represent mean \pm SD for 3 independent experiments.

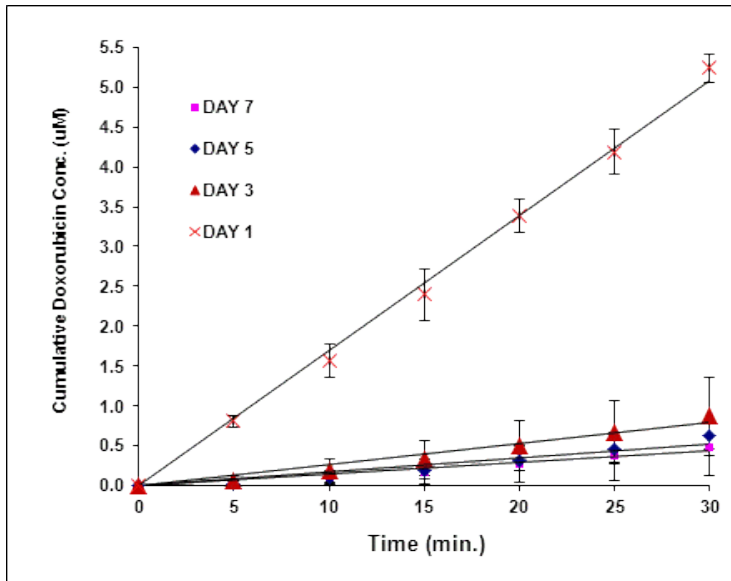


Figure 3-25: Penetration of doxorubicin 100 µM through DLD-1 MCLs on days 1, 3, 5 and 7 of growth on the membrane using CCG-technique. Results represent mean ± SD for 3 independent experiments.

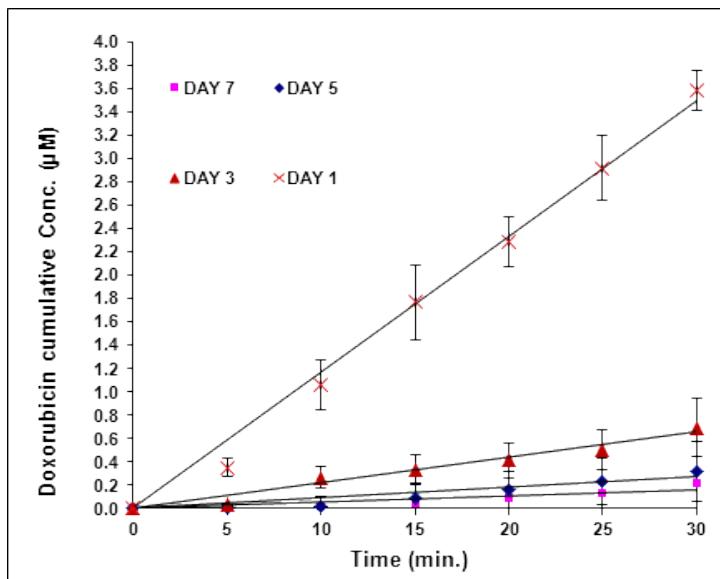


Figure 3-26: Penetration of doxorubicin 100 µM through MCF-7 MCLs on days 1, 3, 5 and 7 of growth on the membrane using CCG-technique. Results represent mean ± SD for 3 independent experiments.

Penetration rates were determined by linear regression analysis as described previously. Penetration rates of doxorubicin through blank membranes, DLD-1 and MCF-7 MCLs is presented in figures 3-27 to 3-29 and summarized in tables 3-5 to 3-10. The penetration rates were proportional to doxorubicin concentration, where 100 μM showed a penetration rate of 0.3774 ± 0.0122 nmol/min, 50 μM showed a penetration rate of 0.1834 ± 0.0249 nmol/min and 25 μM showed a penetration rate of 0.0699 ± 0.006 nmol/min through blank membranes. Penetration rates were also inversely proportional to the MCL thicknesses. Doxorubicin at 100 μM showed penetration rates of 0.1016 ± 0.0095 , 0.0160 ± 0.0079 , 0.0107 ± 0.0041 and 0.0087 ± 0.0027 nmoles/min on days 1, 3, 5 and 7 respectively through DLD-1 MCLs. Penetration rates obtained using this technique, were more reliable because of the linearity of the data obtained compared to VCG technique. Figures 3-30 and 3-31 summarize the penetration rates of doxorubicin 100, 50 and 25 μM through DLD-1 and MCF-7 MCLs respectively on days 1, 3, 5 and 7 of cells growth on the membrane.

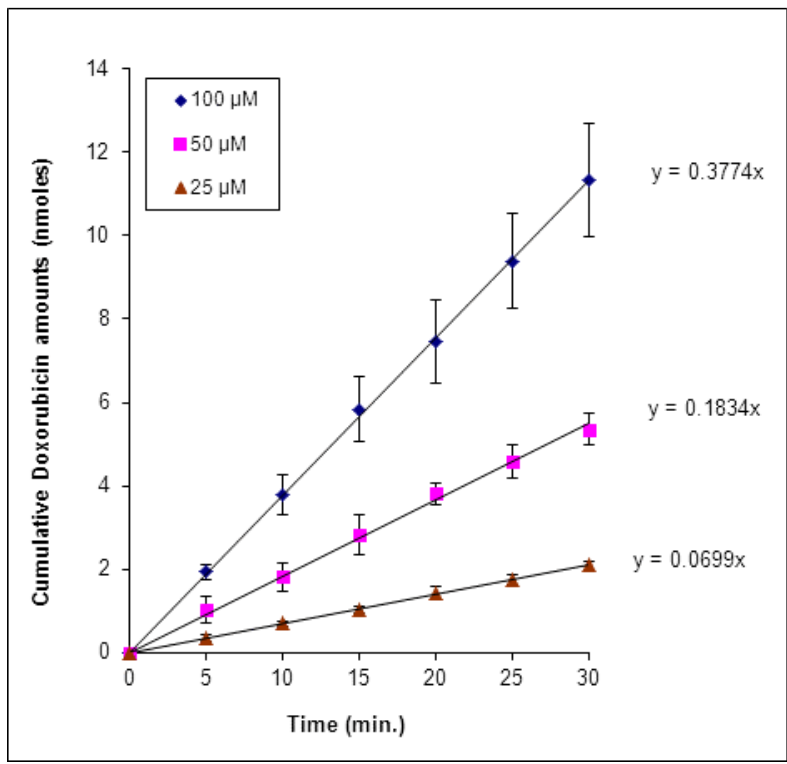


Figure 3-27: Cumulative penetrating amounts of doxorubicin 100, 50 and 25 μM through blank membrane using CCG-technique. Results represent mean ± SD for 3 independent experiments.

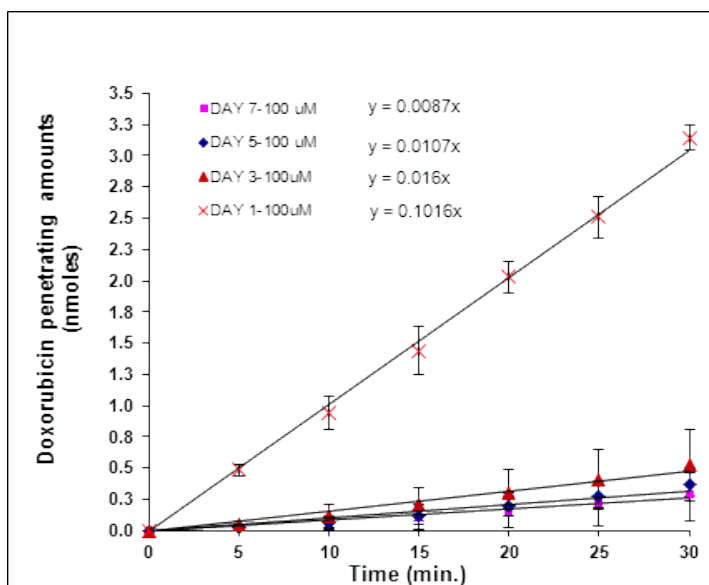


Figure 3-28: Cumulative penetrating amounts of doxorubicin 100 μM through DLD-1 MCLs on days 1,3,5 and 7 of growth on the membrane using CCG-technique. Penetration rates were calculated from the linear regression of the time points on the curve. Results represent mean ± SD for 3 independent experiments.

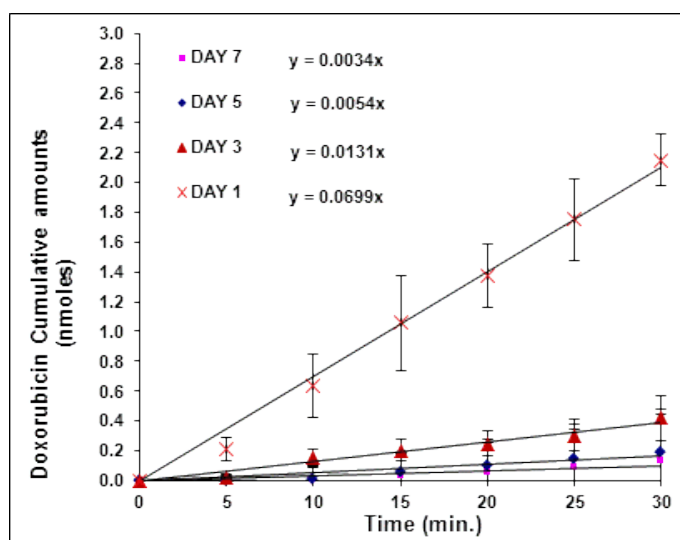


Figure 3-29: Cumulative penetrating amounts of doxorubicin 100 μM through MCF-7 MCLs on days 1,3,5 and 7 of growth on the membrane using CCG-technique. Penetration rates were calculated from the linear regression of the time points on the curve. Results represent mean ± SD for 3 independent experiments.

Table 3-5: Penetration rates of doxorubicin 100 μM , through blank (no cells seeded) and through DLD-1 MCL on days 1, 3, 5 and 7 of growth on the membrane using CCG-technique.

	Doxorubicin 100 μM				
	Penetration rate (nmoles/min)				
	Blank membrane (no cells)	MCL (Day-1)	MCL (Day-3)	MCL (Day-5)	MCL (Day-7)
Average Penetration rates (nmoles/min)	0.3774	0.1016	0.0160	0.0107	0.0087
SD	0.0122	0.0095	0.0079	0.0041	0.0027

Table 3-6: Penetration rates of doxorubicin 50 μM , through blank (no cells seeded) and through DLD-1 MCL on days 1, 3 and 5 of growth on the membrane using CCG-technique.

	Doxorubicin 50 μM				
	Penetration rate (nmoles/min)				
	Blank membrane (no cells)	MCL (Day-1)	MCL (Day-3)	MCL (Day-5)	MCL (Day-7)
Average Penetration rates (nmoles/min)	0.1834	0.0223	0.0096	0.0062	0.0042
SD	0.0249	0.0071	0.0019	0.0016	0.0016

Table 3-7: Penetration rates of doxorubicin 25 μM , through blank (no cells seeded) and through DLD-1 MCL on days 1, 3 and 5 of growth on the membrane using CCG-technique.

	Doxorubicin 25 μM				
	Penetration rate (nmoles/min)				
	Blank membrane (no cells)	MCL (Day-1)	MCL (Day-3)	MCL (Day-5)	MCL (Day-7)
Average Penetration rates (nmoles/min)	0.0699	0.0171	0.0052	0.0036	0.0012
SD	0.0060	0.0049	0.0014	0.0013	0.0007

Table 3-8: Penetration rates of doxorubicin 100 μM , through blank (no cells seeded) and through MCF-7 MCL on days 1, 3 and 5 of growth on the membrane using CCG-technique.

	Doxorubicin 100 μM				
	Penetration rate (nmoles/min)				
	Blank membrane (no cells)	MCL (Day-1)	MCL (Day-3)	MCL (Day-5)	MCL (Day-7)
Average Penetration rates (nmoles/min)	0.3774	0.0699	0.0131	0.0054	0.0034
SD	0.0122	0.0105	0.0012	0.0008	0.0007

Table 3-9: Penetration rates of doxorubicin 50 μM , through blank (no cells seeded) and through MCF-7 MCL on days 1, 3 and 5 of growth on the membrane using CCG-technique.

	Doxorubicin 50 μM				
	Penetration rate (nmoles/min)				
	Blank membrane (no cells)	MCL (Day-1)	MCL (Day-3)	MCL (Day-5)	MCL (Day-7)
Average Penetration rates (nmoles/min)	0.1834	0.0351	0.0098	0.0069	0.0042
SD	0.0249	0.0065	0.0015	0.0005	0.0006

Table 3-10: Penetration rates of doxorubicin 25 μM , through blank (no cells seeded) and through MCF-7 MCL on days 1, 3 and 5 of growth on the membrane using CCG-technique.

	Doxorubicin 25 μM				
	Penetration rate (nmoles/min)				
	Blank membrane (no cells)	MCL (Day-1)	MCL (Day-3)	MCL (Day-5)	MCL (Day-7)
Average Penetration rates (nmoles/min)	0.0699	0.0198	0.0086	0.0024	0.0009
SD	0.0060	0.0019	0.0008	0.0003	0.00009

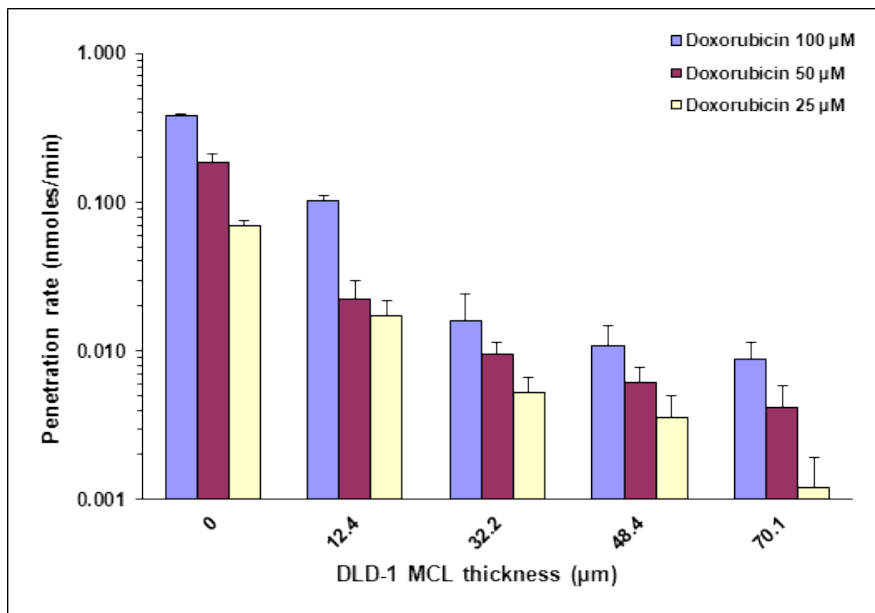


Figure 3-30: Penetration rates of doxorubicin 100, 50 and 25 μM, through blank (no cells seeded) and through DLD-1 MCL on days 1, 3, 5 and 7 of growth on the membrane using CCG-technique. Results represent mean ± SD for 3 independent experiments.

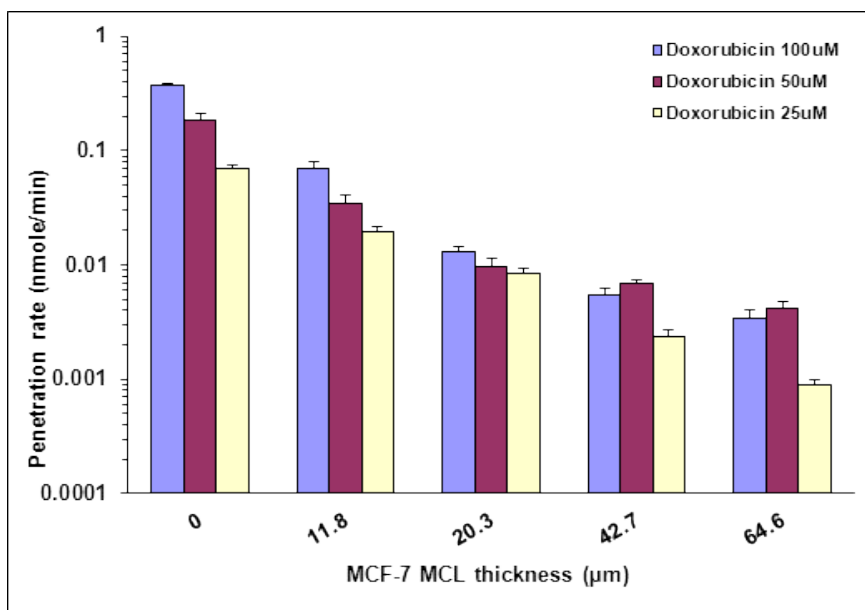


Figure 3-31: Penetration rates of doxorubicin 100, 50 and 25 μM, through blank (no cells seeded) and through MCF-7 MCL on days 1, 3, 5 and 7 of growth on the membrane using CCG-technique. Results represent mean ± SD for 3 independent experiments.

3.6 Drug penetration assays using models 2 and 3:

Model-1 (diffusion only $D\downarrow$) was used at the beginning of this project for validating the sampling, analysis, extraction efficiencies, drugs stability and inter and intra-day experimental and injection variations. Details of those results were presented in the previous sections. As there is no hydrostatic pressure difference in this model, drugs penetrate through it by diffusion. After the introduction of models 2 and 3, penetration assays through model 1 were used as control to evaluate the effect of HP change on CFF and penetration rates. Penetration assays using doxorubicin, imatinib and gefitinib 100 μM each were conducted using these models. Details of these drugs penetration through models 2 and 3 compared to model 1 will be presented in the following sections.

3.6.1 Model 2: Convection plus diffusion ($C\downarrow D\downarrow$) penetration assay:

The transwell chamber was modified by inserting a 10 mL pipette into the top chamber and securing it in place with superglue. The fluid level in the top chamber was raised above the level in the bottom chamber and the rate of transfer of fluid (i.e. convective fluid flow) from the top to bottom chamber determined. The results are presented in Figure 3-32. Using 13 mL of medium in the top chamber, a physiologically relevant pressure of 28 mmHg is generated and a convective flow rate of 18 $\mu\text{L}/\text{minute}$ was obtained. Convection was proportional to the volume of medium at the top chamber as noticed in figure 3-32.

Similar experiment was performed using 13 mL of medium at the top chamber against different DLD-1 MCL thicknesses as presented in figure 3-33 which

shows the convection versus thickness measured using convection plus diffusion penetration assay model. CFF calculated on day 1 was 21 $\mu\text{L}/\text{minute}$ which is mainly similar to the reading of the above experiment however, CFF was significantly reduced to 7 $\mu\text{L}/\text{minute}$ on the second day with a DLD-1 MCL thickness of 25.1 μm . CFF dramatically reduced to 1 $\mu\text{L}/\text{minute}$ on the third day where the MCL thickness was 31 μm . Four days old DLD-1 MCL with thickness of 41 μm was mainly able to stop convection completely.

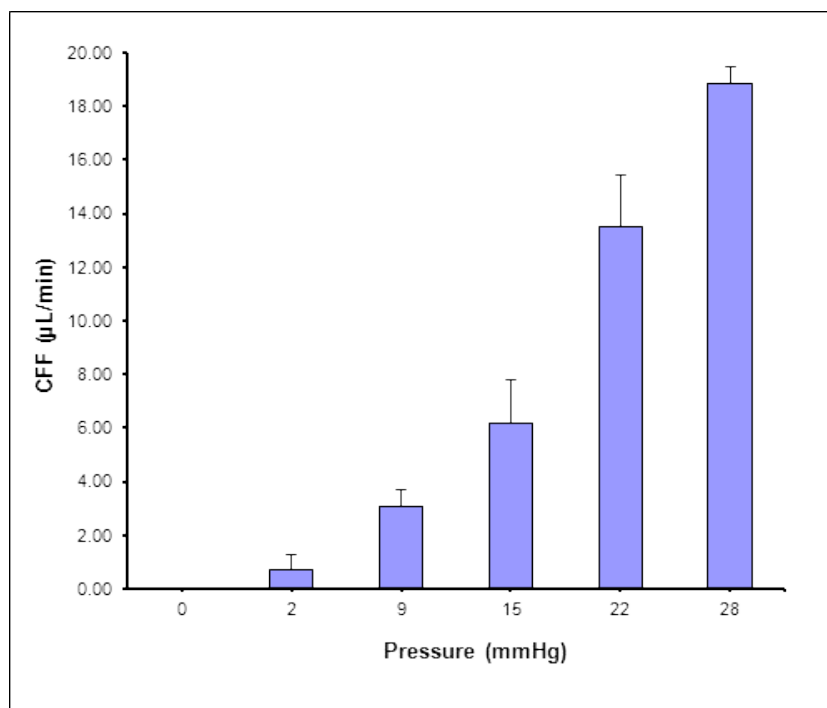


Figure 3-32: Convective fluid flow (CFF) through 12.21 \pm 3.2 μm thick DLD-1 MCL. CFF was measured using convection plus diffusion penetration assay model (C \downarrow D \downarrow) against different volumes of medium at the top chambers creating different pressure gradients (ΔP). Results represent mean \pm SD for 3 independent experiments.

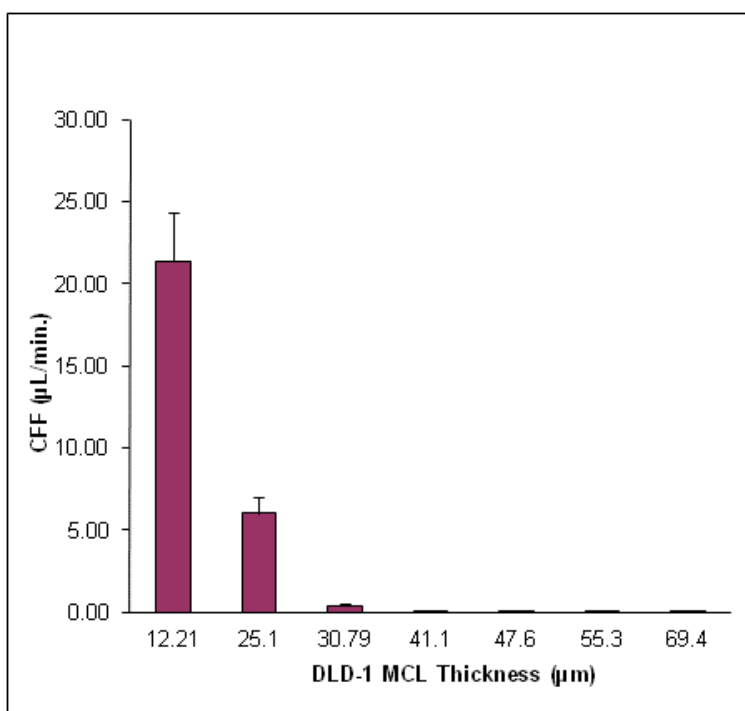


Figure 3-33: Convective fluid flow (CFF) through several thicknesses of DLD-1 MCL measured using convection plus diffusion penetration assay model (C↓D↓). Results represent mean ± SD for 3 independent experiments.

Figure 3-34 shows doxorubicin 100 µM penetration through DLD-1 MCLs using model 2 where drug penetration is driven by both convection and diffusion forces together (C↓D↓). Experiments were conducted using a physiologically relevant hydrostatic pressure applied to the top chamber of the penetration assay experimental system. A significant difference is clearly noticed in the cumulative concentrations which penetrate to the bottom chamber every 5 minutes compared to the previous technique (Model 1, diffusion only D↓) in which there is no hydrostatic pressure difference and hence no CFF.

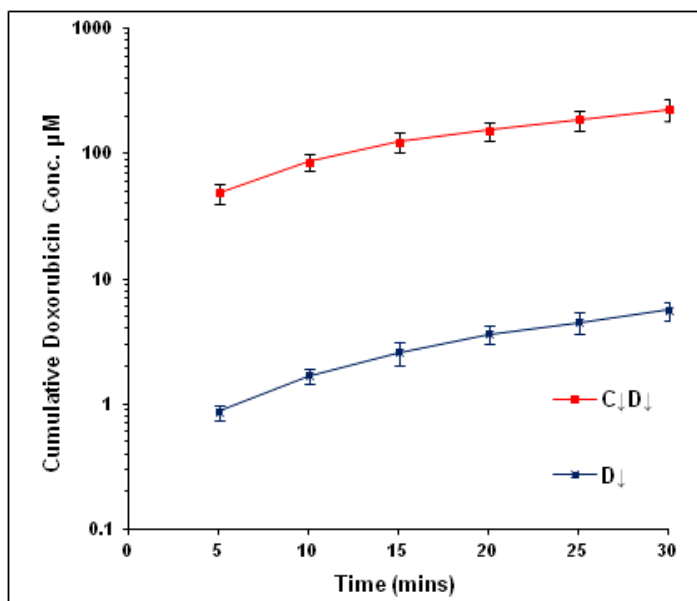


Figure 3-34: Penetration of doxorubicin (100 µM) through DLD-1 MCL (Day-1) using model 2 (C↓D↓) compared to model 1 (D↓). Results represent mean ± SD for 3 independent experiments.

3.6.2 Model 3, diffusion opposing convection (D↓C↑):

In this assay, the direction of CFF is reversed so that diffusion and CFF are opposing each other. The results of drug penetration through this model compared to model 1 are presented in Figure 3-35. Using doxorubicin at 100 µM and a 1 day DLD-1 MCL, drug penetration was significantly reduced compared to the same experiment conducted where CFF was zero.

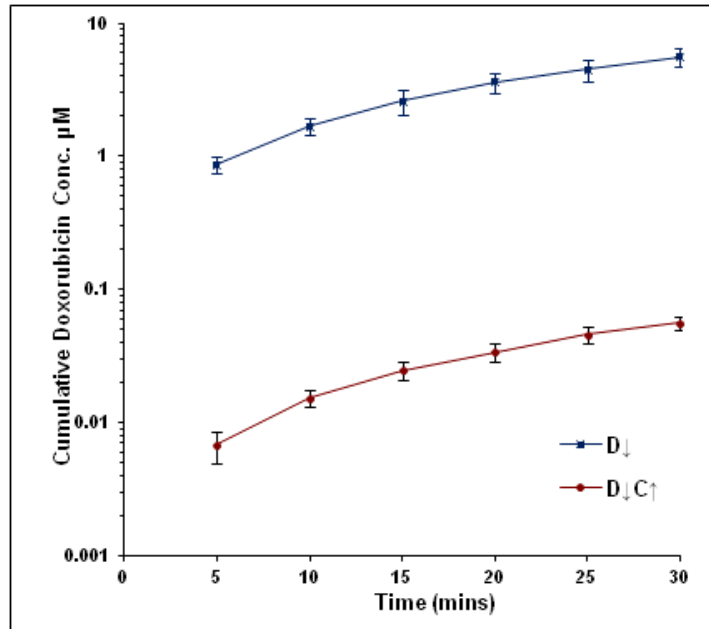


Figure 3-35: Doxorubicin 100 µM penetration through DLD-1 MCL (Day-1) using model 3 (D↓C↑) compared to model 1 (D↓). Reverse convection from the bottom chamber has significantly reduced drug penetration. Results represent mean ± SD for 3 independent experiments.

This model was further modified as will be explained in the following section.

3.6.3 Modified model 3, diffusion opposing convection (D↑C↓):

In order to reduce variations in CFF, reduce materials and time consumed by model 3, it was further modified by adding the drug to the bottom chamber and measuring that diffusing to the top chamber i.e. (D↑ C↓) as presented in figure 2-4. As in model 2, 13 mL of medium is placed at the top chamber to exert a physiologically relevant hydrostatic pressure from the top to the bottom

chamber. Using this model, CFF from top to bottom chamber was 26.7 ± 3.9 $\mu\text{L}/\text{min}$. Doxorubicin penetrated from the bottom chamber to the top chamber at rates of 0.08 ± 0.02 nmoles/min as presented in figure 3-36. The penetration rate with this model was also significantly lower compared to the diffusion only model as presented in figures 3-37 and 3-38.

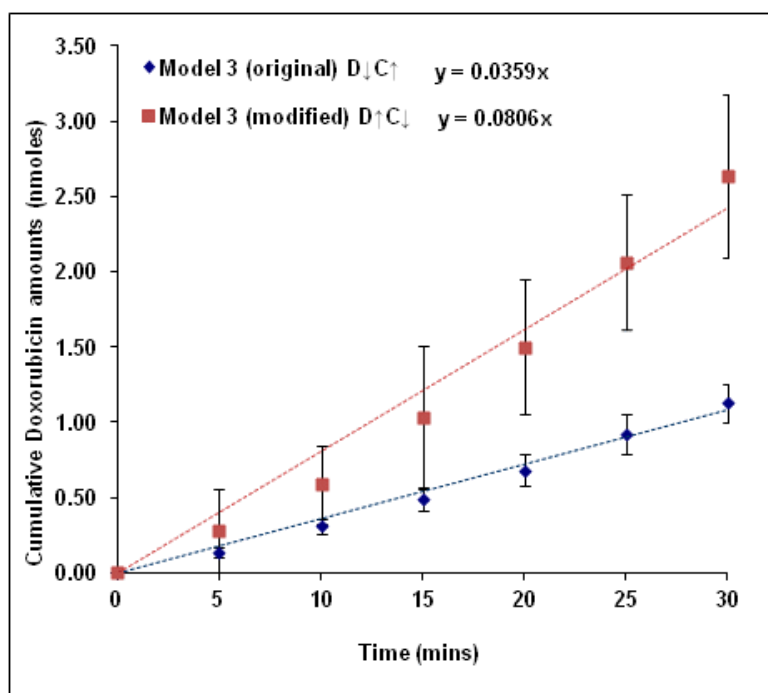


Figure 3-36: Cumulative amounts of doxorubicin 100 μM through DLD-1 MCL (day 1) using original (D↓C↑) and modified model 3 (D↑C↓). Slopes of the linear regressions were used for calculating penetration rates. Results represent mean \pm SD for at least 3 independent experiments.

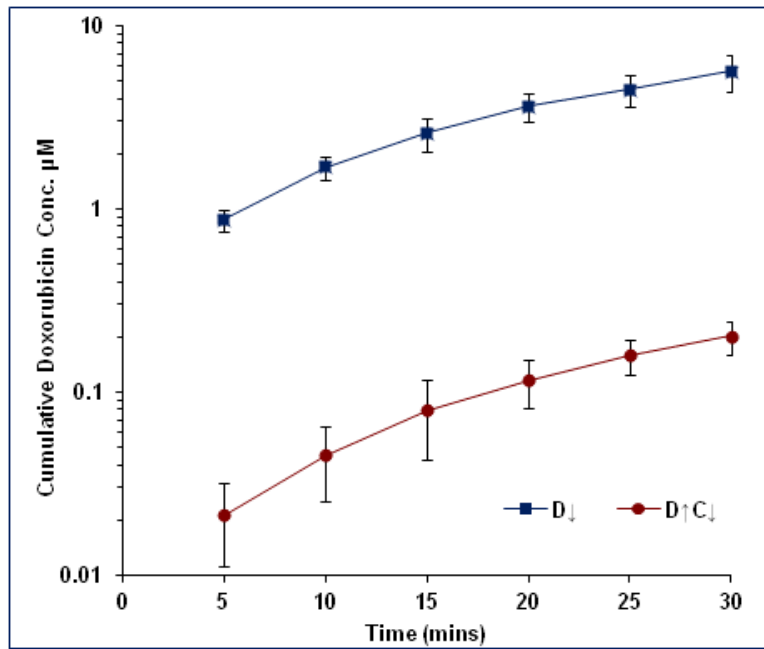


Figure 3-37: Doxorubicin 100 μM penetration through DLD-1 MCL (Day-1) using modified model 3 (D \uparrow C \downarrow) compared to model 1 (D \downarrow). Reverse convection from the top chamber has significantly reduced drug penetration. Results represent mean \pm SD for 3 independent experiments.

The penetration rates of doxorubicin were also significantly lowered compared to other models as presented on figure 3-38.

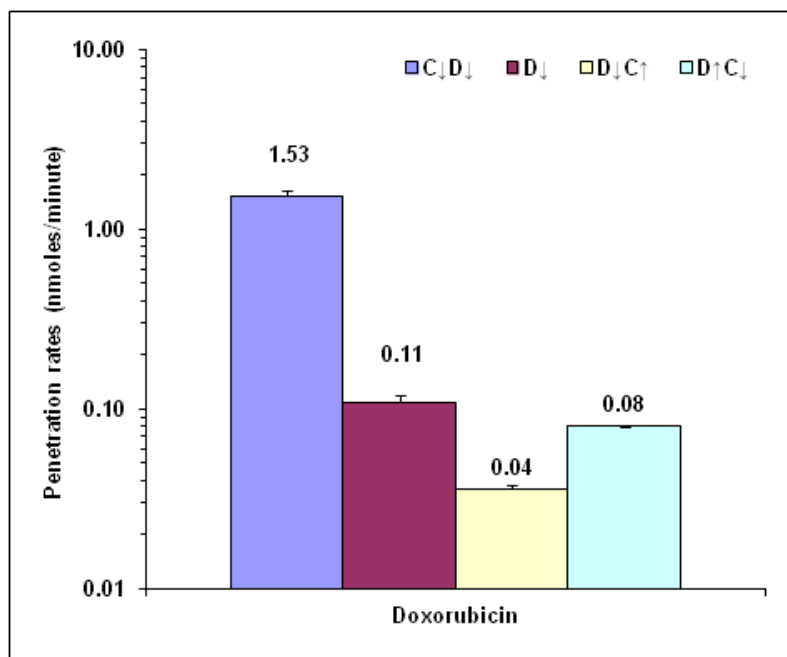


Figure 3-38: Doxorubicin 100 μ M penetration rates through DLD-1 MCL (Day-1) using modified model 3 (D \uparrow C \downarrow) compared to other models. Results represent mean \pm SD for 3 independent experiments.

Penetration models 1, 2 and 3 were validated using doxorubicin, imatinib and gefitinib where convection and penetration rates were calculated as will be presented in the following section.

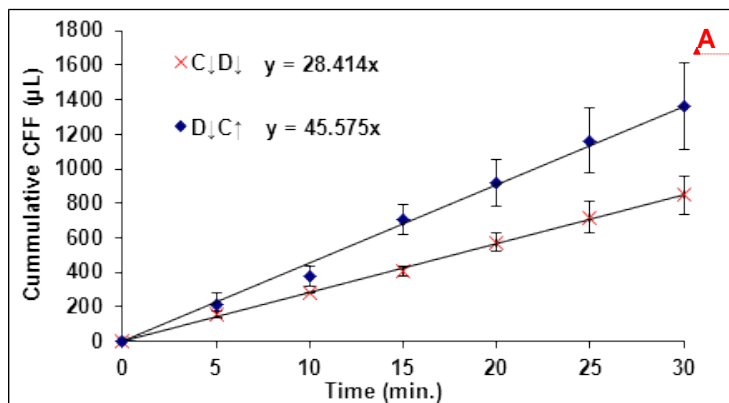
3.7 Impact of CFF on drug penetration through MCLs using doxorubicin, imatinib and gefitinib:

The three different penetration assay models were validated and evaluated using doxorubicin, imatinib and gefitinib. All drugs (100 μM) were tested for their ability to penetrate one day old DLD-1 MCLs using the three different penetration assay models in triplicate. Using penetration assay models 2 (convection plus diffusion $C\downarrow D\downarrow$) and 3 (diffusion opposing convection $D\downarrow C\uparrow$), both convection and penetration rates were calculated and compared to the first model (diffusion only $D\downarrow$) where no CFF exists. Convective fluid flow in case of ($C\downarrow D\downarrow$) and ($D\downarrow C\uparrow$) penetration models where doxorubicin, imatinib and gefitinib were used are presented in figures 3-39 and 3-40 and in table 3-11. It is clear from the results that calculated CFF was similar in both models with the ($D\downarrow C\uparrow$) penetration model giving marginally higher readings than the ($C\downarrow D\downarrow$) model. Using doxorubicin, CFF result through ($C\downarrow D\downarrow$) model was $28.4 \pm 2.97 \mu\text{L}/\text{min}$ compared to $45.57 \pm 6.94 \mu\text{L}/\text{min}$ in case of ($D\downarrow C\uparrow$) model. Using imatinib, CFF result through ($C\downarrow D\downarrow$) model was $21.08 \pm 9.48 \mu\text{L}/\text{min}$ compared to $60.23 \pm 11.89 \mu\text{L}/\text{min}$ in case of ($D\downarrow C\uparrow$) model and finally using gefitinib , CFF result through ($C\downarrow D\downarrow$) model was $24.04 \pm 5.49 \mu\text{L}/\text{min}$ compared to $44.90 \pm 1.65 \mu\text{L}/\text{min}$ in case of ($D\downarrow C\uparrow$) model. Within each model, these differences in convection however were not statistically significant at $P < 0.05$.

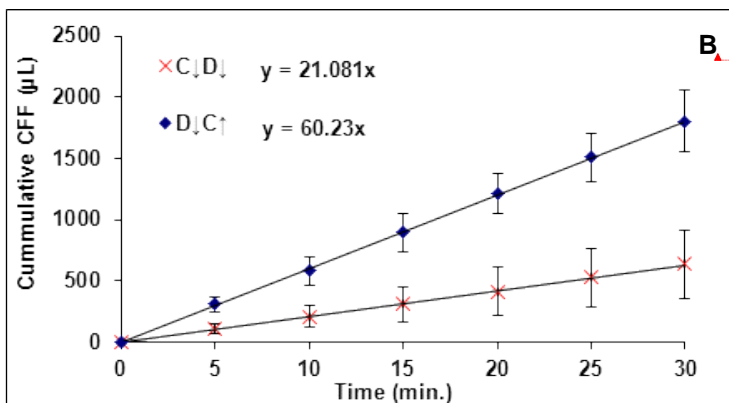
With regards to drug penetration rates, the penetration of doxorubicin, imatinib and gefitinib at 100 μM , are presented in figures 3-41 to 3-45 and in table 3-

12. Cumulative concentrations (figures 3-41, 3-42 and 3-43 for doxorubicin, imatinib and gefitinib respectively) were converted into amounts and expressed as (nmoles) as presented in figure 3-44. Slope of the linear regression of each experiment was considered the penetration rate. Penetration rate for doxorubicin (100 μ M) was 1.53 ± 0.17 nmoles/minute in case of (C \downarrow D \downarrow). This rate dramatically reduced to 0.11 ± 0.04 nmoles/minute and 0.04 ± 0.00 nmoles/minute in case of D \downarrow and D \downarrow C \uparrow models respectively. Penetration rate for imatinib 100 μ M was 0.90 ± 0.24 nmoles/minute in case of (C \downarrow D \downarrow). This rate significantly reduced to 0.10 ± 0.04 nmoles/minute and 0.04 ± 0.00 nmoles/minute in case of D \downarrow and D \downarrow C \uparrow models respectively. Lastly, penetration rate for gefitinib 100 μ M was 0.78 ± 0.17 nmoles/minute in case of (C \downarrow D \downarrow). This rate has been significantly reduced to 0.19 ± 0.04 nmoles/minute and 0.03 ± 0.01 nmoles/minute in case of D \downarrow and D \downarrow C \uparrow models respectively as presented in table 3-12 and figure 3-45.

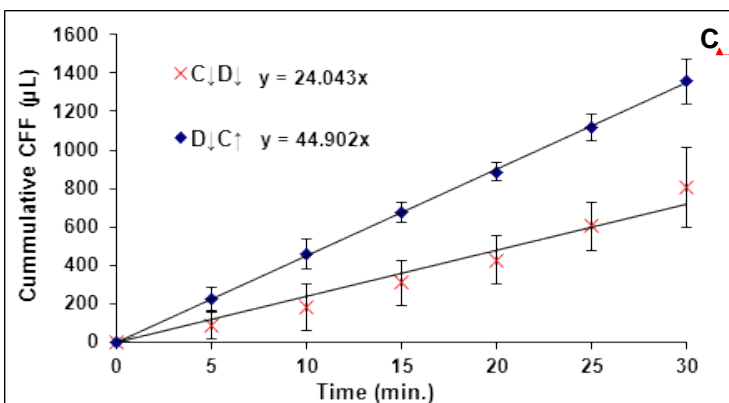
In case of model 2 (C \downarrow D \downarrow), doxorubicin, imatinib and gefitinib penetration rates have significantly increased by 42, 26 and 13 folds respectively compared to model 1 (D \downarrow) penetration rates. Furthermore, when diffusion was opposed by convection as in case of model 3 (D \downarrow C \uparrow), penetration rates of doxorubicin, imatinib and gefitinib were dramatically reduced respectively by 100, 81 and 195 folds compared to their penetration through model 1 (D \downarrow). These results show the significant impact CFF has on drug penetration.



Formatted: Font: (Default) Arial, Bold



Formatted: Font: (Default) Arial, Bold



Formatted: Font: (Default) Arial, Bold

Figure 3-39 (a): Cumulative CFF calculated for doxorubicin (A), imatinib (B) and gefitinib (C) penetration through DLD-1 MCL (day-1) using C↓D↓ and D↓C↑ penetration models. Slopes of the linear regressions were used for calculating CFF rates. Results represent mean ± SD for at least 3 independent experiments.

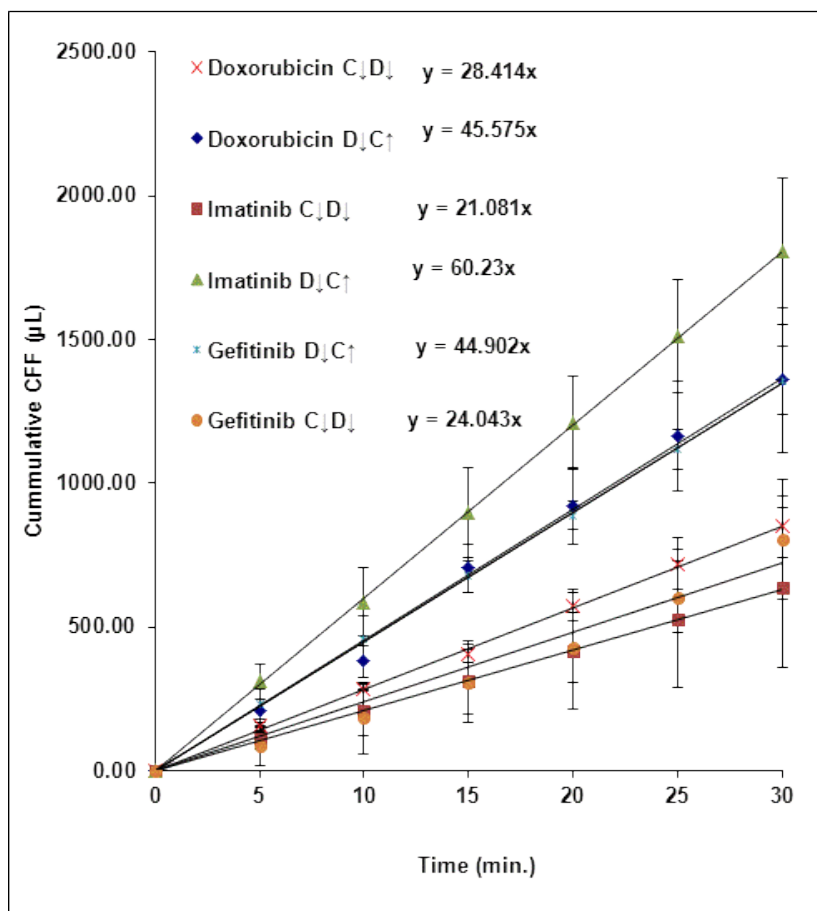


Figure 3-39(b): Cumulative CFF calculated for doxorubicin, imatinib and gefitinib penetration through DLD-1 MCL (day-1) using C↓D↓ and D↓C↑ penetration models. Slopes of the linear regressions were used for calculating CFF rates. Results represent mean \pm SD for at least 3 independent experiments.

Table 3-11: Convective fluid flow (CFF) calculated for doxorubicin, imatinib and gefitinib 100 μ M penetration through DLD-1 MCL using the three different penetration models. Results represent mean \pm SD for at least 3 independent experiments.

CFF (μ L/min)	C \downarrow D \downarrow		D \downarrow		D \downarrow C \uparrow	
	Average	SD	Average	SD	Average	SD
Control	20.10	1.75	0.00	0.00	40.44	3.00
Doxorubicin	28.41	2.97	0.00	0.00	45.57	6.94
Imatinib	21.08	9.48	0.00	0.00	60.23	11.89
Gefitinib	24.04	5.49	0.00	0.00	44.90	1.65

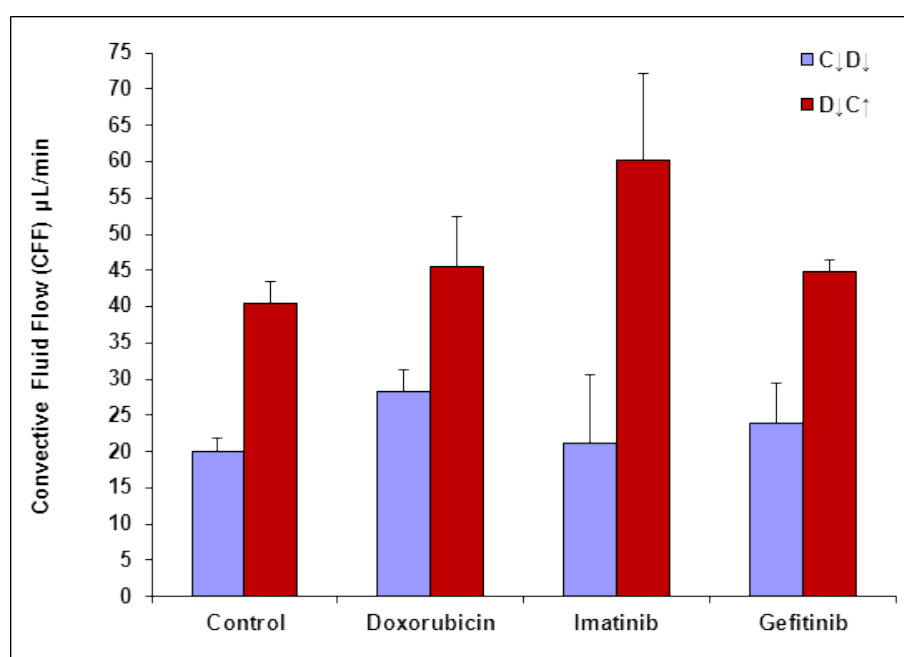


Figure 3-40: Convective fluid flow (CFF) calculated for control (drug-free medium) and for doxorubicin, imatinib and gefitinib 100 μ M penetration through DLD-1 MCL (day-1) using (C \downarrow D \downarrow) and (D \downarrow C \uparrow) penetration assay models. Results represent mean \pm SD for at least 3 independent experiments. $P > 0.05$.

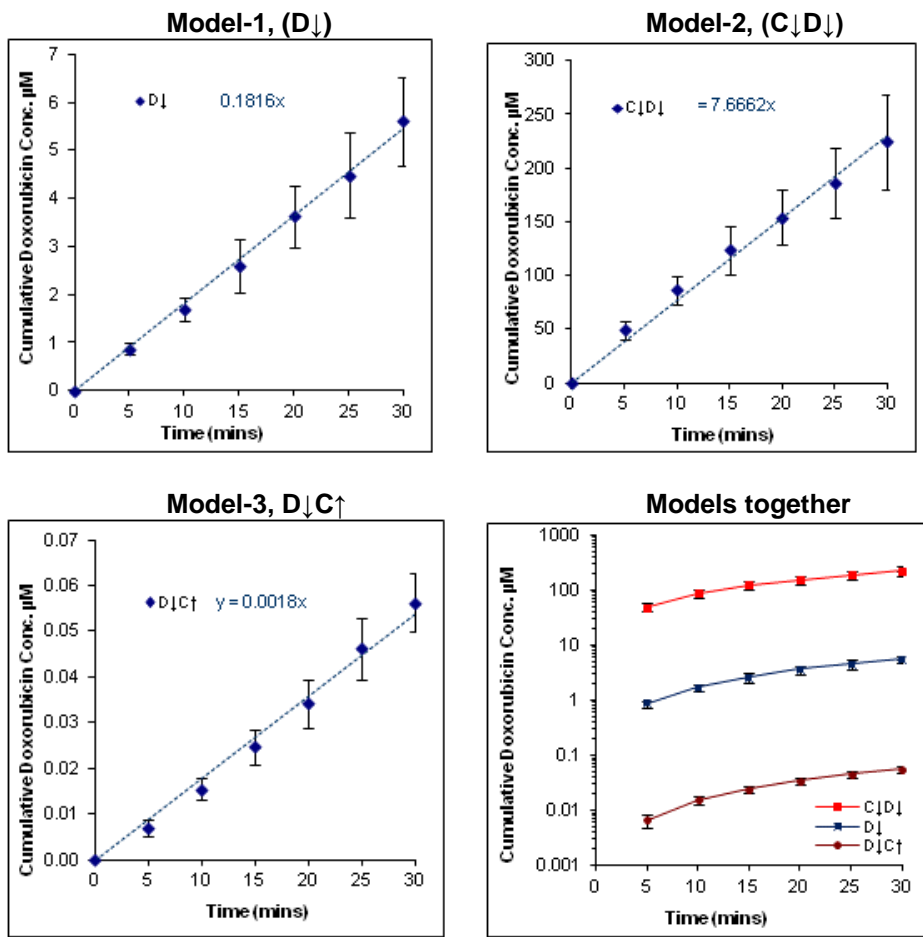


Figure 3-41: Doxorubicin 100 µM penetration results through DLD-1 MCL (Day-1) using the three different penetration models expressed as cumulative concentrations in µM. Results represent mean ± SD for 3 independent experiments.

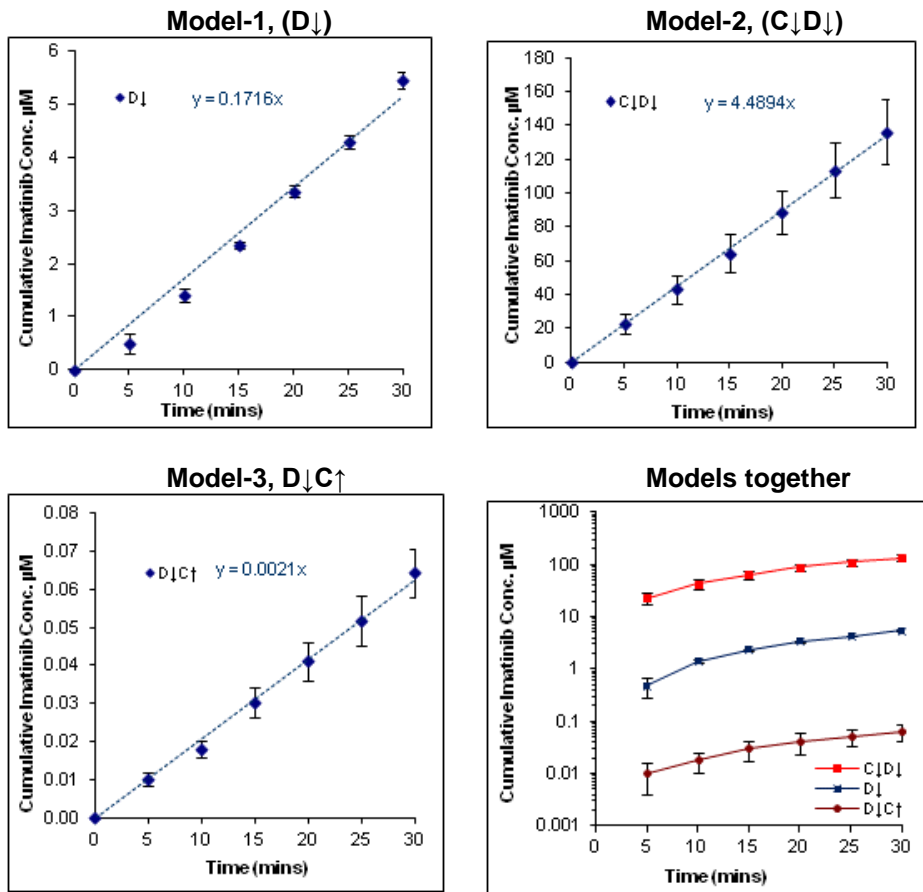


Figure 3-42: Imatinib 100 µM penetration results through DLD-1 MCL (Day-1) using the three different penetration models expressed as cumulative concentrations in µM. Results represent mean ± SD for 3 independent experiments.

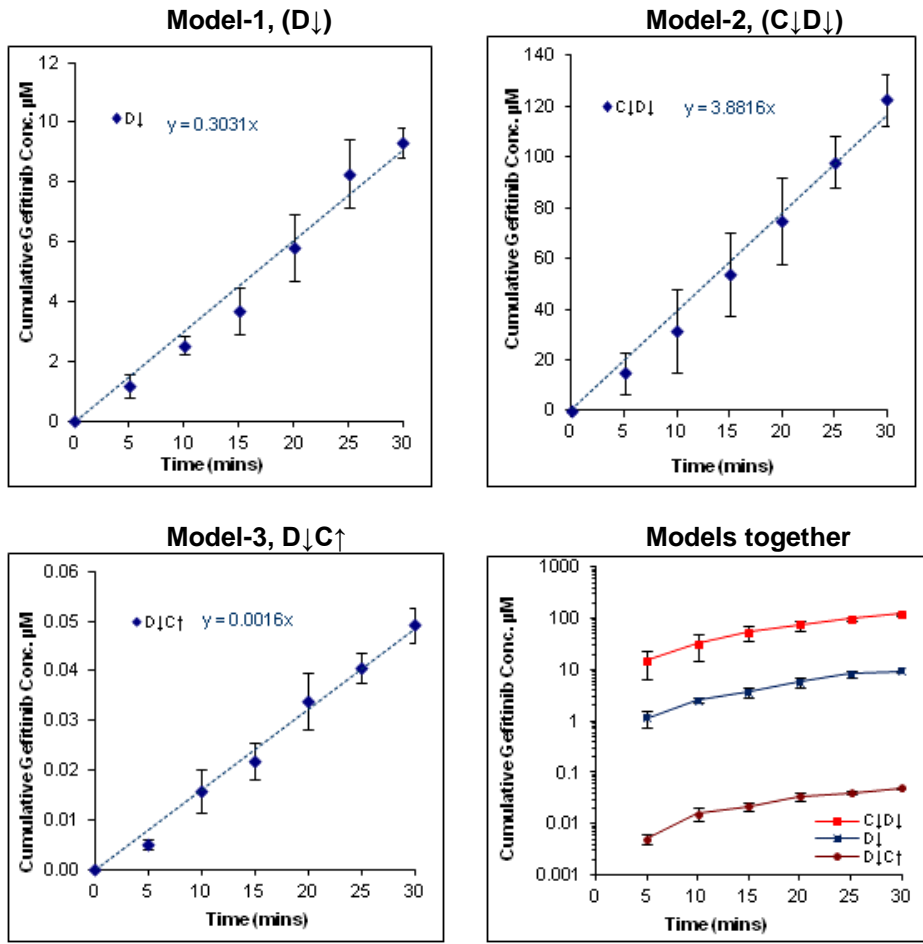
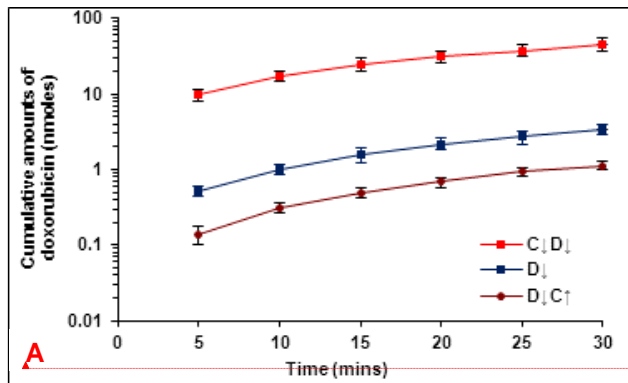
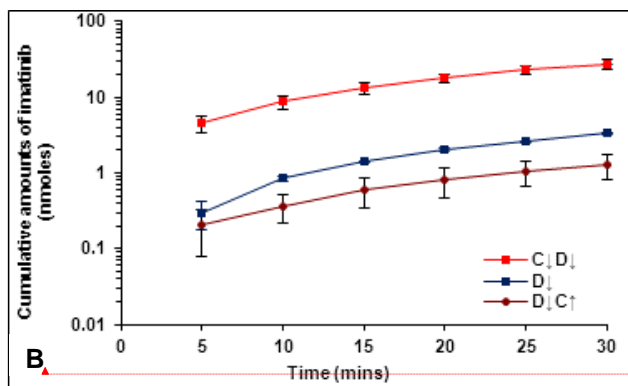


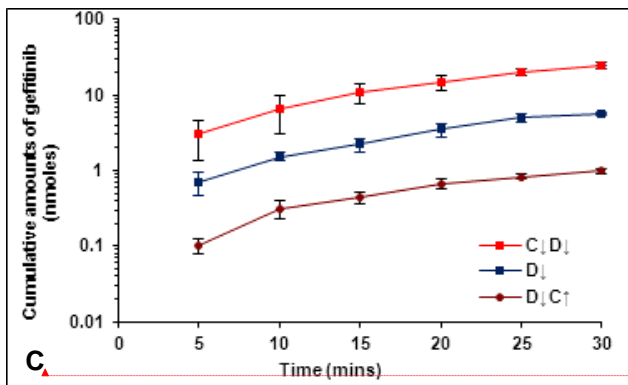
Figure 3-43: Gefitinib 100 μM penetration results through DLD-1 MCL (Day-1) using the three different penetration models expressed as cumulative concentrations in μM. Results represent mean ± SD for 3 independent experiments.



Formatted: Font: (Default) Arial, Bold



Formatted: Font: (Default) Arial, Bold



Formatted: Font: (Default) Arial, Bold

Figure 3-44: Doxorubicin (A), imatinib (B) and gefitinib (C) penetrating amounts through DLD-1 MCL (Day-1) using the three different penetration models expressed as cumulative amounts in (nmoles). Penetration rates were calculated from these figures through their linear regressions (data presented in table 3-12). Results represent mean \pm SD for 3 independent experiments.

Table 3-12: Penetration rates of doxorubicin, imatinib and gefitinib 100 μ M through DLD-1 MCL using the three different penetration models. Results represent mean \pm SD for 3 independent experiments.

Penetration rate (nmole/min)	C↓D↓		D↓		D↓C↑	
	Average	SD	Average	SD	Average	SD
Doxorubicin	1.53	0.17	0.11	0.04	0.04	0.00
Imatinib	0.90	0.24	0.10	0.04	0.04	0.00
Gefitinib	0.78	0.17	0.18	0.04	0.03	0.01

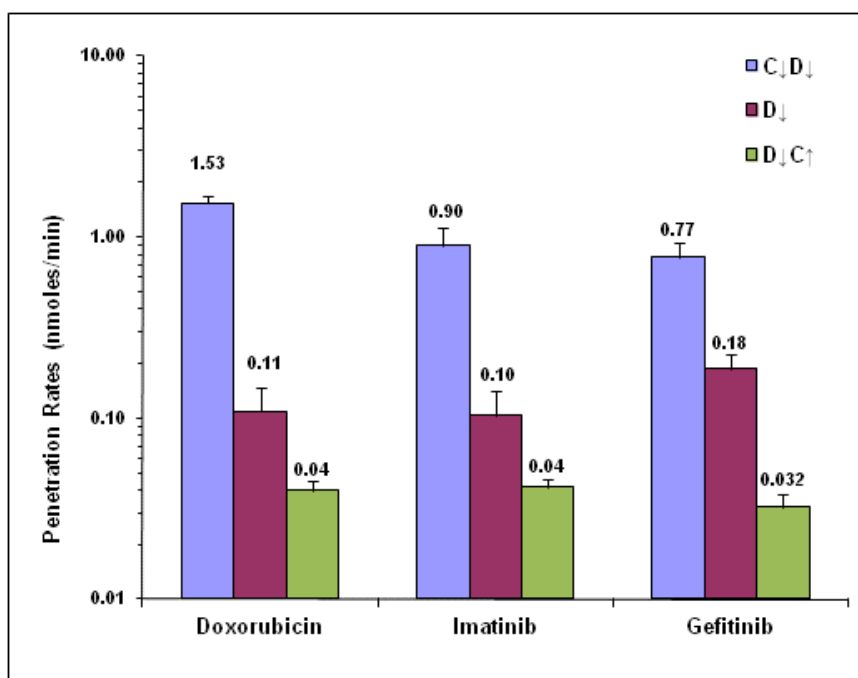


Figure 3-45: Penetration rates of doxorubicin, imatinib and gefitinib 100 μ M using the three different penetration models. Results represent mean \pm SD for 3 independent experiments.

3.8 Influence of concentration versus exposure time on cell survival:

To determine what impact CFF may have on chemosensitivity, cells were exposed to concentrations of drug that represent the amount or concentration of drug crossing the transwell during the experiment. For example, the data presented in figure 3-41 indicates that 112 μM of doxorubicin crossed the membrane within 30 min. Cells were therefore exposed to this concentration of doxorubicin for 30 minutes and cell survival determined by the MTT assay after a 4 day recovery period. Similar experiments were designed using data obtained from the other penetration models. The results of these studies are presented in figures 3-46 to 3-48. Doxorubicin cumulative concentration of 112 μM from model 2 (C \downarrow D \downarrow) was cytotoxic to 76.6% of cells after 30 minutes exposure. For doxorubicin cumulative concentrations collected from the diffusion only model (D \downarrow), were 2.80 μM and this was cytotoxic to 27% of cells. On the other hand doxorubicin cumulative concentration of 0.03 μM collected from model 3 (D \downarrow C \uparrow), did not cause a significant cytotoxicity to the same cell line (figure 3-46). Table 3-13 shows the used concentrations of doxorubicin, imatinib and gefitinib as well as the survival rate $\pm\text{SD}$ after the DLD-1 cells exposure to each one of them. Figures 3-47 and 3-48 represent the results of the same experiment using imatinib, and gefitinib respectively. It was noticed clearly through those figures that apart from gefitinib (C \downarrow D \downarrow) at 61 μM which was cytotoxic to 8% of cells, imatinib and gefitinib at all other concentrations did not cause any significant cytotoxicity.

Table 3-13: Doxorubicin, imatinib and gefitinib cumulative concentrations used for testing concentration VS time effect on DLD-1 survival rates using MTT assay. Those concentrations were retrieved based on the cumulative concentrations analysed post convection plus diffusion (C↓D↓), diffusion only (D↓) and diffusion opposed by convection (D↓C↑) penetration assays.

	C↓D↓	D↓	D↓C↑
Drug	Conc. (µM) / Survival rate ±SD		
Doxorubicin	112 / 23.40±4.68	2.8 / 73.10±6.46	0.03 / 98.95±7.16
Imatinib	68.21 / 99.16±3.52	2.73 / 99.41±3.95	0.08 / 97.46±4.06
Gefitinib	61.34 / 91.74±11.17	5.16 / 94.39±11.15	0.03 / 100.74±4.64

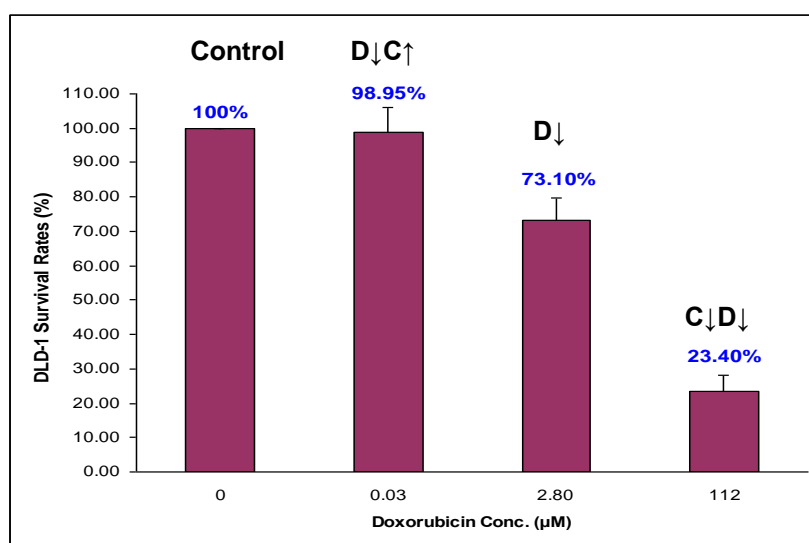


Figure 3-46: Effect of 30 minutes exposure of DLD-1 cells to doxorubicin cumulative concentrations (retrieved from penetration assays) on the cells viability using MTT assay. Results represent mean ± SD for three independent experiments.

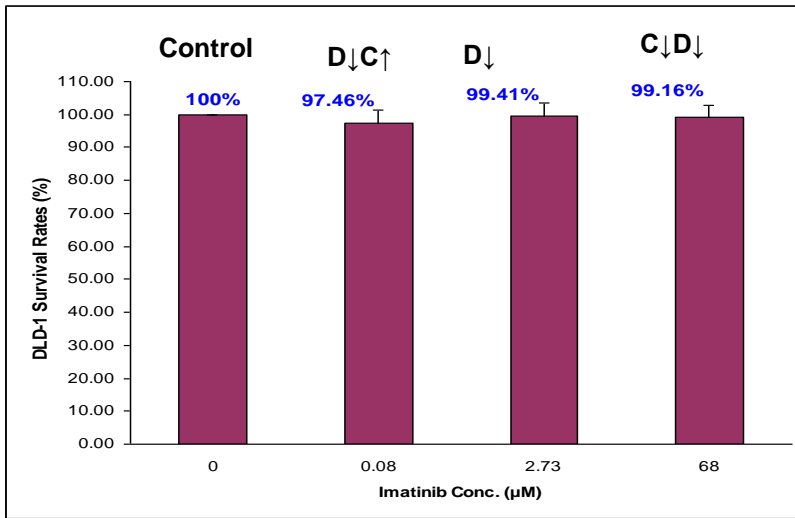


Figure 3-47: Effect of 30 minutes exposure of DLD-1 cells to imatinib cumulative concentrations (retrieved from penetration assays) on the cells viability using MTT assay. Results represent mean \pm SD for three independent experiments.

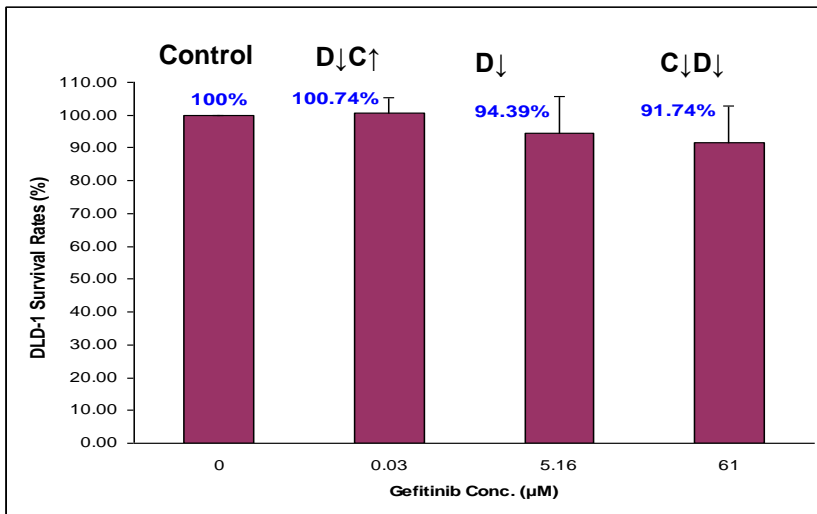


Figure 3-48: Effect of 30 minutes exposure of DLD-1 cells to gefitinib cumulative concentrations (retrieved from penetration assays) on the cells viability using MTT assay. Results represent mean \pm SD for three independent experiments.

3.9 Collagen expression in the MCL using immunohistochemistry (IHC):

Having established that CFF can be generated in our model system, this opens the possibility for future studies designed to manipulate tumour cell / matrix interactions with the aim of modulating CFF. One example of this would be to modulate components of the ECM such as collagen. Preliminary studies are reported here to determine whether or not DLD-1 MCL's secrete collagen. Collagen-IV was chosen as an extracellular matrix target to be modified as it was expected to be one of the MCL extracellular matrix components if DLD-1 MCL can form an extracellular matrix. Immunohistochemistry was used to detect whether collagen-IV was present in DLD-1 MCLs. Archived DLD-1 xenograft tissues (formalin fixed and paraffin embedded tumours) were used as control. Figure 3-49 A, B, C and D, represent the immunohistochemical staining results of collagen-IV expression in DLD-1 xenograft tumours and DLD-1 MCL using Rabbit Polyclonal to Collagen-IV as a primary antibody. Collagen-IV was expressed in DLD-1 xenograft tissues (figure 3-49, B) and the same expression was not detected in the MCLs of DLD-1 (figure 3-49, D).

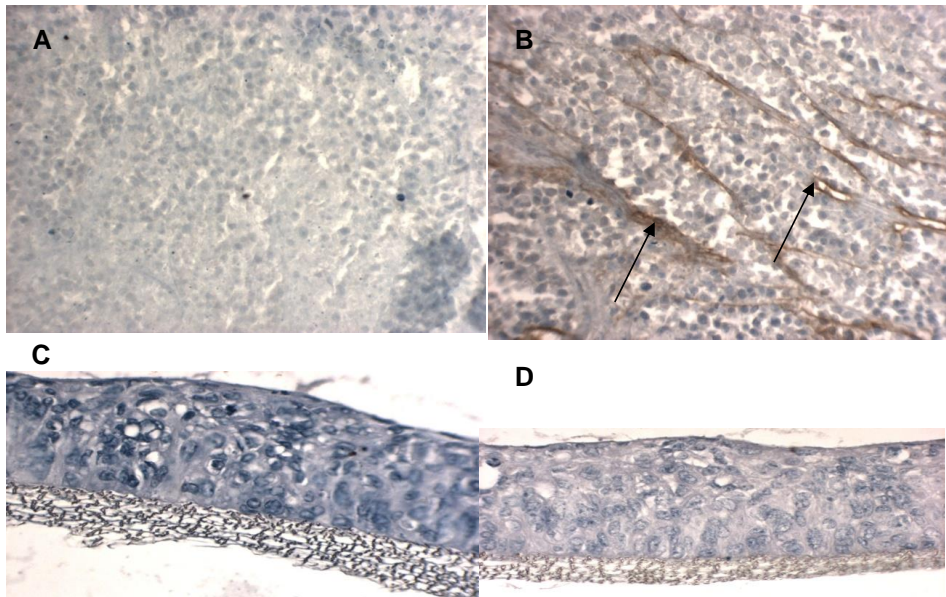


Figure 3-49: Collagen expression in DLD-1 xenograft tumour and in DLD-1 MCL (Day-7). (A) DLD-1 xenograft tumour (Control), (B) DLD-1 xenograft tumour with antibody, (C) DLD-1 MCL Control and (D) DLD-1 MCL with antibody.

4. DISCUSSION AND CONCLUSION:

Poor drug penetration is now recognised as one of the causes of resistance to chemotherapy (Minchinton and Tannock, 2006). The lack of lymphatic drainage together with a heterogenous and leaky vascular supply can lead to the elevation of interstitial fluid pressure (IFP) in solid tumours. One consequence of elevated IFP is that the normal process of convective fluid flow (CFF) through tissues is impeded which is considered a major barrier to drug uptake. Several studies have been conducted and several approaches have been used to study drug penetration into solid tumours. These studies or approaches have almost exclusively used *in vivo* models (Tredan et al., 2007) which are time consuming, expensive and are in conflict with policies on reduction, refinement and replacement of animal experiments.

The aim of this study was to develop a simple *in vitro* model through which drug penetration rates through avascular tissues can be calculated with the specific aim of assessing the impact of CFF on drug penetration through avascular cellular masses. The model is based on the conventional transwell model (Phillips et al., 1998) to assess drug penetration across multicell layers (MCLs) (Figure 2-1). This model was modified and three different penetration models were developed as described below:

Model-1: Diffusion only (D↓), (Figure 2-1). This is where CFF is zero and the drug crosses the MCL via diffusion down a concentration gradient.

Model-2: Convection plus diffusion (C↓D↓), (Figure 2-2). This model is where both CFF and diffusion are driving the drug across the MCL.

Model-3: Diffusion opposing convection (D↓C↑), (Figure 2-3). This is a model where CFF and diffusion are working in opposite directions

In all three models, the arrows in the symbols denote the direction of either diffusion (D) or convection (C).

Before discussing the results of penetration and convection through these three experimental models, it is important to first discuss the preceding experiments which were conducted to characterise and validate the drug penetration models. These experiments include the growth characteristics of cells on the transwell membranes, developing and evaluating various extraction techniques, evaluating analytical methods including limits of detection and limits of quantification, evaluating sampling method that will allow drug penetration rates to be calculated accurately and reproducibly and analysis of the stability of the drugs used under experimental conditions.

4.1 Growth characteristics of cells in monolayer and MCL settings:

4.1.1 Growth curves in monolayer settings:

Growth curves of the two main cell lines in this study (DLD-1 and MCF-7) in monolayer settings were generated and showed lag, log and plateau phases which came in agreement with other studies (Phillips and Clayton, 1997;

Sutherland et al., 1983). These studies were conducted in order to be able to manage cell cultures effectively by adding defined numbers of cells to flasks and subculturing at specified times thereafter. It also allows workers to check for abnormalities in cultures such as mycoplasma contamination. Any disturbance in the growth curve for instance could indicate a problem in the culture. Figure 3-1.

4.1.2 Growth characteristics of cell lines on the transwell membrane and MCL thickness:

DLD-1 and MCF-7 growth on the transwells was also evaluated (figures 3-2 and 3-3). Compared to previous studies (Evans et al., 2009; Phillips et al., 1998) and as expected, DLD-1 and MCF-7 formed MCLs, the thickness of which increased as the incubation time increased. Morphologically, the MCLs were generally of uniform thickness although some undulations in thickness were observed. It was important to carefully look down the light microscope at the day 1 cultures to ensure that an even cell layer was present. Any gaps in the cell layer can be visualised easily using an objective magnification of X20 and these transwells were discarded. Electrical impedance devices can be used to check the integrity of cell layers but histological analysis of cell layers that were checked visually provided a reliable indicator of the integrity of the MCL. Furthermore, trypan blue was used to test the ability of DLD-1 MCL to form a barrier. The penetration of trypan blue was rapid through blank membrane (no cells) but in the presence of a thin MCL of 13.3 μm the penetration of trypan blue was significantly impaired. Impaired trypan blue penetration through the MCL proved that the MCL formed a good barrier but

the blank membrane itself did not. For this reason the MCL can be used to measure drug penetration. It also suggests that movement of drug between cells is comparatively poor.

In addition to DLD-1 and MCF-7 cells, the ability of a panel of other cell lines to form MCLs was also tested. They were selected based on their ability to form spheroids (Friedrich et al., 2007) and on the basis that cells which formed close compact colonies *in vitro* (determined visually) with each other were most likely to form good MCLs. Some of these cells formed MCLs with thicknesses ranging from 20 – 120 μm that were morphologically similar to MCF-7 and DLD-1 cells. These cell lines included; Panc-1, SK-MEL 23, A-2780, M14, SiHa and Caski. In contrast, A-549, 7860, HT-29 and PC3 cell lines formed thin MCLs with gaps between the cells. Others grew as aggregates that were uneven and 'patchy' (HT-29 and PC-3 for example). The results for HT-29 were surprising as this cell line readily forms multicell spheroids that are uniform in shape. In addition, other groups have generated MCLs on transwells using the HT-29 cell line (Hicks et al., 2006; Hicks et al., 2003). The results of this study have shown that whilst several cell lines will form MCLs in the transwell system, others will not readily grow or form uniform MCLs. It is conceivable that inclusion of a matrix which embeds the cells on the transwell could help these cell lines form a MCL but this approach is potentially complex as the matrix itself may form a barrier to drug penetration.

4.2 Extraction techniques and their efficiencies:

As it was expected that a wide range of concentrations would be generated using the three different penetration models, it was necessary to evaluate different extraction techniques. Extraction efficiency, limit of detection, ease of use and cost were the requirements for a suitable extraction technique in this study. Three different extraction techniques were evaluated based on the above requirements. Although SPE is an expensive and time consuming procedure, it was the only technique which capable of concentrating large volumes of sample. For this reason SPE was selected as the technique which gave the lowest limit of detection (Table 3-1), compared to protein precipitation with and without evaporation in which there was no concentration step. Protein precipitation without evaporation was nevertheless used for samples which were expected to give higher concentrations as it was quicker and cheaper.

4.3 Evaluating and validating sampling methods:

During the early stages of this study, penetration assays using model 1 were conducted according to previously published studies (Phillips et al., 1998). Sampling from the bottom chamber occurred by taking 10 μ L samples at various time intervals after addition of drug to the top chamber. At each time point, fresh media replaced the 10 μ L sample so that the volume in the bottom chamber remained constant. As time progressed, the concentration of drug in the top chamber would decrease and this would be matched by an increase in drug concentration in the bottom chamber. The concentration gradient across

the MCL was variable and this sampling method was called VCG denoting variable concentration gradient.

Using this sampling technique, the ability of doxorubicin to cross MCLs was evaluated using an initial concentration of 100, 50 and 25 μM in the top chamber. These concentrations were chosen to check that they can be detected by the analysis method before going to human peak plasma therapeutic level concentrations. Penetration assays were conducted using blank membrane as a control and several thicknesses of DLD-1 and MCF-7 MCLs. Experiments were conducted on days 1, 3, 5, and 7 of DLD-1 growth on the membrane. It was noticed that the penetration curves which were produced by this method were variable even with blank samples (no cells loaded). This level of variability was inconsistent and it made determining the rate of penetration challenging. A variety of possible explanations for this variability were put forward and tested experimentally. One possible explanation was the fact that the transwells used were dehydrated prior to being used in cell culture. It was proposed that air bubbles trapped in the membrane could cause variations in drug penetration. For this reason the experiment was repeated using a hydrated transwell but there was no major change in the shape of the curves (Figure 3-19). The second expected cause of variation in the shape of the plotted curve was the membrane itself. The membrane was collagen coated which could bind doxorubicin and this may be variable. To remove the collagen, the membrane was trypsinized prior to conducting the penetration assay. Although doxorubicin penetration through a trypsinized membrane was faster compared to non-trypsinized which might be

due to drug binding to collagen in non-trypsinized membrane, however, variations and spikes in the results did not disappear (Figure 3-20). The source of error could not be traced despite numerous attempts to resolve this problem. It is likely that the main source of error stems from the fact that the volume of sample taken for analysis is small (10 μ L). Whilst the pipettes were routinely calibrated, the error associated with sampling small volumes is potentially large and this could be a major contributing factor to the experimental variability observed.

Because of the variability obtained with this sampling technique, it was replaced with an alternative method. This method was called the constant concentration gradient or CCG-technique. This technique was reproducible, less time consuming and samples created with this technique could be analysed using any of the previous extraction techniques as the sample volume was 500 μ L instead of the 10 μ L volume used previously. The plotted curves using CCG-technique (Figures 3-24 and 3-25), were linear and reproducible with r^2 of more than 0.95 in all cases. The variability seen in the previous methodology was not observed using this method and it was possible to calculate the penetration rate of doxorubicin through MCLs. Doxorubicin concentrations that are less than 25 μ M can be used and different factors that influence drug penetration such as modifying IFP or ECM components can be quantified using this method.

4.4 Evaluating and validating analysis methods:

Liquid chromatography (LC), liquid chromatography with mass spectrometry (LC/MS) and LC/MS/MS were used to analyse the three drugs which were used in this study. All the three systems were able to give reasonable limits of detection with acceptable precision (Figures 3-8, 3-9 and 3-11 – 3-16 and table 3-1). Results of these three systems were in agreement with other studies that used liquid chromatography to analyse doxorubicin, imatinib and gefitinib in biological samples in spite of the changes in the analysis parameters (Storm et al., 1988; Widmer et al., 2004; Zhao et al., 2005). Use of internal standard helped reduce the variations that could occur during sample extraction from tissue culture medium (Grantab et al., 2006; Zheng et al., 2001). Calibration curves from the three different analysis systems were reproducible and linear with linear regression coefficients of > 0.98 (Figures 3-9, 3-15 and 3-16). The methods described here for the analysis of doxorubicin, imatinib and gefitinib were sensitive and reproducible and therefore suitable for use in the drug penetration assay.

Comment [PKPDpm1]: A high R doesn't necessarily mean they are reproducible, it means they are linear, are you happy with the difference between the two if you are asked.

4.5 Evaluating drugs stability at 37°C:

Doxorubicin, imatinib and gefitinib stabilities in culture medium were assessed at 37°C and the results showed that there was <10% loss after 120 minutes incubation period at 37°C (Figures 3-10 and 3-17). The samples are therefore stable and this simplified sample collection enormously. Despite this, care was always taken when dealing with samples by placing them on ice at all times when conducting an experiment to guarantee drug stability. Stability results

were in agreement with other published studies (Storm et al., 1988; Widmer et al., 2004; Zhao et al., 2005).

Comment [PKPDpml2]: You also examined the stability of Dox with cells present.

4.6 Impact of convective fluid flow (CFF) and diffusion on drug penetration using the three different penetration models:

The ability of drugs to penetrate MCLs of various thicknesses in the presence or absence of CFF is the central issue addressed in this thesis. The ability of doxorubicin, imatinib and gefitinib to penetrate MCLs using the three experimental conditions described above is discussed below.

4.6.1 Diffusion only penetration assays, model-1 (D↓):

Diffusion only penetration assays were performed using the variable concentration gradient (VCG) and constant concentration gradient (CCG) techniques.

4.6.1.1 Penetration of doxorubicin across MCLs using a variable concentration gradient (VCG):

Despite the problems with this approach with regards to variation, some valuable data was obtained that is discussed here. Using the diffusion only penetration assays with VCG technique (section 2.7.1), the penetration rate was proportional to drug concentration and inversely proportional to the MCL thickness. Doxorubicin penetration through membrane alone (no cells seeded) was considerably higher compared to its penetration through multicell layers.

This finding is in agreement with other studies (Evans et al., 2009; Grantab et al., 2006; Phillips et al., 1998; Tunggal et al., 1999). Using this technique, and in spite of the “spiky” curves, it was possible to calculate the penetration rates through blank transwells and through the MCLs. However, the calculated penetration rates using this technique were not reliable because of the noticed variations and spiking in the plotted curves (tables 3-2 to 3-4 and figures 3-22 and 3-23). This approach generated limited data but some general trends were obtained. In particular, drug penetration is inversely proportional to the thickness of the MCL and proportional to drug concentration.

4.6.1.2 Penetration of drugs across MCLs using a constant concentration gradient (CCG):

As discussed above, because of the variability observed in the previous assay, the sampling and experimental design was changed. At each time point, media containing drug in the top chamber was replaced with fresh media containing drug at the original concentration. At the same time, the media in the bottom chamber was changed and replaced with fresh medium. In this way, the concentration gradient between the top and bottom chamber was maintained. By keeping the sampling time short (5 minutes maximum), concentration gradient would not change significantly during each sample point. A further advantage of this technique was that the sample volume used to analyse drug concentration increased from 10 μ L in the previous method to 500 μ L. The sensitivity of the assay then increased significantly.

The results of this modification to the drug penetration assay are presented in figures 3-24 and 3-25. Using this technique, a constant concentration of drug crossed the MCL per unit time which when presented as cumulative concentration against time gave a linear increase in drug concentration (Figure 3-24). The data obtained was significantly better than the previous technique with no major variations observed. Linear regression analysis typically gave regression coefficient values of >0.98 and rates of drug penetration were easily determined from these results. Based on these results, this methodology provides a more reproducible and accurate measure of drug penetration rates.

Analysis of doxorubicin penetration across blank membranes, DLD-1 and MCF-7 MCLs of different thicknesses are presented in figures 3-24 to 3-31 and in tables 3-5 to 3-10. Penetration rates ranged from 0.1016 ± 0.009 to 0.0087 ± 0.0027 nmols/minute for DLD-1 MCLs of 12.91 ± 3.01 and of 69.4 ± 7.4 μm thick respectively. These results are reproducible and demonstrate that an inverse relationship between MCL thickness and doxorubicin penetration exists. Whilst this conclusion is not novel, it is to my knowledge the first time it has been demonstrated here using the constant concentration gradient methodology. The penetration rate of doxorubicin was also concentration dependent as shown in figures 3-27 to 3-31. Using DLD-1 MCL of 12.91 ± 3.01 μm thick, penetration rates of 0.1016 ± 0.0095 , 0.0223 ± 0.0071 and 0.0171 ± 0.0049 were obtained when concentrations of doxorubicin at 100, 50 and 25 μM were applied respectively (Figures 3-28 and 3-30 and Tables 3-5 to 3-7). These results were also reproducible and are consistent with the results of

other studies (Evans et al., 2009; Kyle et al., 2004; Kyle and Minchinton, 1999; Phillips et al., 1998; Tannock et al., 2002; Tunggal et al., 1999; Wilson and Hicks, 1999). Using this methodology, studies were extended to imatinib and gefitinib (Figures 3-42 and 3-43). Using DLD-1 MCLs of 13.01 ± 4.23 and 12.33 ± 2.79 μm thick and $100 \mu\text{M}$ in the top chamber, the penetration rates of imatinib and gefitinib were 0.103 ± 0.04 and 0.18 ± 0.04 nmols/minute respectively (Figure 3-44 and 3-45 and table 3-12).

Using the diffusion only penetration assay model (model 1), the penetration rates of the three drugs through one day old DLD-1 MCL were compared (table 3-12). It was clear that the penetration rate of gefitinib was almost 2 times faster than imatinib and doxorubicin which have mainly shown similar penetration rates. Whilst there are many potential explanations, Gefitinib penetrated faster possibly because it acts on EGFR which is moderately expressed in DLD-1 (Prewett et al., 2002), whereas imatinib acts on and may be bound to c-kit which is expressed in DLD-1 (Ito et al., 1990). Based on the previous results, and as proved by other studies (Minchinton and Tannock, 2006), the poor penetration of doxorubicin may be due to its binding to DNA and the penetration rate decreases as the number of cells (and hence the amount of DNA) increases. Doxorubicin is also a substrate for drug efflux pumps and poor penetration might be also due to the drug being pumped out of cells. Furthermore, cell to cell adhesion forming tight junction or cell to matrix adhesion can also limit doxorubicin, imatinib and gefitinib penetration. As noticed in the histological sections of the MCLs cells were closely packed and previous electron microscopy studies have shown that tight junctions are

Comment [PKPDpm13]: Not sure about this, what about polarity.

formed between cells in DLD1 multicell spheroids (Bibby et al., 1993). This might have been one of the causes of limited penetration of doxorubicin and is in agreement with other studies (Tannock et al., 2002). The other expected cause of limited penetration is probably related to the basic character of doxorubicin (weak base) and its subsequent accumulation in acidic endosomes (Lee and Tannock, 2006; Tunggal et al., 1999). In addition to the role of the MCL in limiting the penetration of doxorubicin, imatinib and gefitinib, the microporous membrane itself has also shown from control experiments (no cells loaded) that it can bind all the three drugs and acts as another barrier which came in agreement with other studies (Tannock et al., 2002).

Whilst the factors that determine drug penetration are complex and varied, these studies provided baseline rates of penetration so that the effect of CFF on drug penetration can be assessed.

4.6.2 Convection plus diffusion penetration assays, model-2 (D↓C↓):

As explained earlier, a drug's ability to leave the blood vessel is dependent on both diffusion and convection (Jain, 1998). Because of the poor lymphatic drainage system in solid tumours, fluids usually build up and IFP increases. As the hydrostatic pressure is variable, there are regions within solid tumours where HP is less than IFP and in this case CFF is from the tumour into the blood vessel. This forms a barrier to drug uptake in these regions. (Heldin et al., 2004).

In the original apparatus which was used to study diffusion dependent penetration, the height of the medium in the top chamber and bottom chamber

Comment [PKPDpm14]: How do these tight junctions compare to an in vivo situation in tumours – a potential question in a viva.

were identical, i.e. there was no pressure gradient (Figure 2-1). By inserting a tube into the transwell (figure 2-2), the fluid level in the top chamber was raised above the bottom chamber and a pressure gradient is therefore generated. The magnitude of this pressure gradient can change by changing the height of media in the tube.

The influence of MCL thickness on CFF was studied using this model by setting the medium height at the top chamber to exert a hydrostatic pressure of 28 mmHg which is comparable to arterial hydrostatic pressure in capillaries (Jain, 1987a). The weight of the fluid in the bottom chamber was measured as a function of time to get the CFF. The results of this study were reproducible and demonstrated that an inverse relationship between the CFF and MCL thickness exists (Figure 3-33). It was clearly noticed that a $41.1 \pm 3.6 \mu\text{m}$ thick MCL was able to completely prevent CFF. This is an interesting result for future studies designed to alter the tumour microenvironment with the aim of enhancing CFF and drug delivery. If cell to cell or cell to matrix interactions can be manipulated, then this assay would be capable of measuring the effect on CFF. This therefore is a novel experimental tool for evaluating such therapeutic strategies. The influence of hydrostatic pressure gradient on CFF was also studied (Figure 3-32) and CFF was proportional to the hydrostatic pressure gradient. These results clearly demonstrate that CFF occurs in the experimental model, the magnitude of which varies depending upon both the thickness of the MCL and the pressure gradient applied.

After checking the ability of this model to create CFF was established, the influence of this CFF on the penetration of drugs through MCLs was studied using doxorubicin, imatinib and gefitinib. Adding these drugs to the top chamber of the model, a physiologically relevant pressure gradient of 28 mmHg was applied on the MCLs to create CFF of 28.41 ± 2.97 , 21.08 ± 9.48 and 24.04 ± 5.49 $\mu\text{L}/\text{min}$ in the case of experiments using doxorubicin, imatinib and gefitinib respectively. This result demonstrates that the drugs themselves do not induce any major changes in CFF. It was clearly noticed that penetration rates were significantly increased in the presence of CFF. Under these experimental conditions, penetration rates for doxorubicin, imatinib and gefitinib were 1.53 ± 0.17 , 0.9 ± 0.24 and 0.78 ± 0.17 nmoles/min respectively (Figure 3-45). There was a 42, 26 and 12 folds increase in the penetration rates of doxorubicin, imatinib and gefitinib respectively in the presence of convection and diffusion compared with the diffusion only model (D \downarrow). This enhancement in drug penetration rates is likely to be caused by CFF 'carrying' drug down the pressure gradient. It is not known whether it is pushing the drug between cells or through cells. This model is similar to what exists in normal situation i.e. non-cancerous tissues where there is high drug concentration in blood driving diffusion into tissues and a pressure gradient which forces CFF from the blood vessel into the tissue. The conclusion here is that the CFF significantly increases the penetration rate of drugs through MCLs. This model was modified in order to represent the situation in a solid tumour where the drug diffusion is opposed by convection coming from solid tumour due to the elevated IFP. This model is discussed in the following section.

4.6.3 Diffusion opposing convection penetration assays, model-3

(D↓C↑):

The above mentioned model was modified to mimic the situation in the solid tumour where the direction of CFF is from the tumour back into the blood vessel. This was achieved by applying a physiologically relevant hydrostatic pressure to the bottom chamber thereby causing CFF to go from the bottom to the top chamber. Addition of drug to the top chamber now puts diffusion driven drug penetration in opposition to the direction of CFF (figure 2-3). The experimental conditions in this model were that one day old DLD-1 MCLs were treated with doxorubicin, imatinib and gefitinib (at 100 μ M). Drugs were added to the top chambers and their diffusion was opposed by hydrostatic pressure and CFF (from bottom chamber) of 45.57 ± 6.94 , 60.23 ± 11.89 and 44.90 ± 1.65 μ L/min in case of doxorubicin, imatinib and gefitinib respectively (Figure 3-40). Using this model, penetration rates of doxorubicin, imatinib and gefitinib respectively were 0.04 ± 0 , 0.04 ± 0 and 0.03 ± 0.01 nmoles/min as presented in figure 3-45. The penetration rate of these drugs is therefore significantly reduced when CFF opposes drug diffusion.

Whilst this assay is technically feasible, it is more demanding than models 1 and 2. The main disadvantage with this model was that at each sampling point, the entire bottom chamber had to be replaced and this was time consuming. In order to simplify this model and reduce the time required to obtain samples, it was further modified by adding the drug to the bottom chamber and drug concentration in the top chamber was measured (i.e. D↑C↓) as presented in figure 2-4. The hydrostatic pressure from the top to the

bottom chamber is applied using 13 mL of medium which exerts a physiologically relevant pressure of 28 mmHg similar to that used in the convection plus diffusion model. With this model, doxorubicin flowed from the bottom chamber to the top chamber at rates of 0.08 ± 0.02 nmoles/min and CFF from top to bottom chamber was 26.7 ± 3.9 μ L/min. The penetration rate with this model was also significantly lower compared to the diffusion only model. The advantage of this model is that it reduces the sampling time considerably but the main disadvantage of this model is that there is no proper stirring in the top chamber.

Comment [PKPDpm15]: Preventing the formation of vortices.?

The results of the three models have clearly proved that CFF significantly affects drug penetration rates. It was clearly noticed that drug penetration was enhanced in the presence of CFF. In contrast, drug penetration was dramatically limited and hindered when diffusion was opposed by CFF. These results came in agreement with the results of the *in vivo* convection enhanced delivery experiments which were conducted by Bobo, Lidar and Mardor (Bobo et al., 1994; Lidar et al., 2004; Mardor et al., 2005). Whilst different *in vivo* methodologies were used, the aim of which was studying the influence of convection on improving drug delivery was the same. The results of the Bobo, Lidar and Mardor studies have also added and proved that convection can also be used to enhance drug distribution into solid tumours with the advantage of avoiding systemic toxicity. These conclusions can strengthen the importance of designing simple *in vitro* models for studying the impact of CFF on drug penetration.

Comment [PKPDpm16]: Need expanding. There is an obvious question in a viva here.

Different strategies can be used to improve drug penetration and lethality to cells. These strategies include modification of the factors that limit drug penetration. For example, the extracellular matrix is significantly altered in solid tumours and it may provide a barrier by sequestering drug via protein binding mechanisms. It also contributes significantly to increased rigidity of tumours thereby preventing the increased interstitial fluid pressure from dissipating. There is considerable interest in developing novel strategies that target the cellular and/or extracellular microenvironment of tumours. The experimental models described in this thesis could be used to evaluate therapeutic strategies designed to modify the tumour microenvironment with the aim of re-establishing CFF therefore enhancing the delivery of a partner therapeutic. This is the first report of an *in vitro* model that can address this issue and further studies to explore other applications (e.g. co-culturing with stromal fibroblasts to form more complex MCLs) are warranted.

4.7 Concentration versus time effect on cell survival:

Having established that CFF influences drug penetration, an obvious question to ask was what impact does CFF have on the sensitivity of cells to the drugs? Cells were exposed to concentrations of drugs (Table 3-13) that represent the amounts of drugs which penetrated through the MCL in each model. As the length of the experiment was 30 minutes, cells were exposed to these concentrations for this period of time to determine the concentration versus time effect on the cell survival. DLD-1 cells were exposed to doxorubicin, imatinib and gefitinib in separate experiments using three different

concentrations of each drug, each of which represented the concentration of drug which penetrated DLD1 MCLs using the three experimental models. Cells were sensitive to the three different concentrations of doxorubicin (Figure 3-46) however; imatinib and gefitinib (Figures 3-47 and 3-48) did not show significant toxicity to the same cell line.

In the three experimental models, the concentrations of doxorubicin that penetrated the MCL in 30 minutes were 112, 2.8 and 0.03 μM for C \downarrow D \downarrow , D \downarrow and D \downarrow C \uparrow models respectively table 3-13. Using these concentrations, the % cell kill was 76.6, 27 and 1% which clearly demonstrates that the direction of CFF not only impacts upon drug penetration but it also affects cell response. This conclusion is pharmacologically obvious but it clearly demonstrates that CFF can have a significant effect on cellular response. The same experiments conducted using imatinib and gefitinib were not conclusive as both drugs are not very active at the concentrations used.

4.8 Modifying ECM components as a strategy to improve CFF:

The last two models in this study proved the ability of CFF to enhance drug penetration through MCLs. For this reason, thinking of strategies to improve CFF would enhance drug penetration through MCL. As stated above, one of the strategies to think of was to modify the MCL extracellular matrix (ECM) components assuming that the MCL can include an ECM. Collagen is known to be one of the components of ECM. In this study, an experiment was

conducted to check whether or not DLD-1 MCL can secrete collagen. The hypothesis on which this experiment built was that if DLD-1 MCL expresses collagen, then if this collagen was degraded enzymatically, that might enhance CFF through MCL and hence improve drug penetration. There are several types of collagen and collagen type-IV was chosen for this experiment (Tannock et al., 2002). Immunohistochemistry was used to detect whether or not collagen-IV was present in DLD-1 MCLs. DLD-1 xenograft tissues were used as control. Immunohistochemical staining has expressed collagen-IV only in DLD-1 xenograft tissues but this expression was not noticed in DLD-1 MCL as presented in figure 3-49. This suggests that DLD-1 MCL might not be secreting this type of collagen or that it might be secreting another ECM component such as laminin or fibronectin which needs to be tested using another specific antibody. These results can be compared with Tannocks team results (Tannock et al., 2002) which have shown the presence of an ECM containing both laminin and collagen type-I in the MCLs of MGH-U1 tumour (Human bladder carcinoma). However, Tannocks and his team results were in agreement with what was achieved in this study through proving the absence of collagen-IV in MGH-U1 MCLs although it was present in tumour sections. Due to time limitation, this experiment was not further investigated and it can be further investigated in the future. Future work should be conducted to characterise ECM formation in MCLs using antibody against ECM component such as laminin or fibronectin or even another type of collagen. Subsequent studies designed to degrade the ECM as a means of enhancing CFF and drug delivery would therefore be possible.

4.9 Limitations of the study:

The experimental models described in this study are simple *in vitro* models that are capable of assessing drug penetration through multicell layers and assessing the impact of CFF on drug penetration. To my knowledge, no previous study has been able to assess CFF or to calculate its effects on penetration rates *in vitro*. These models provide a novel strategy to assess the effect of modifying IFP in order to assess the effect of CFF on drug penetration. Whilst there are many attractive features to this model, it is true that there are limitations. These include the inability to mimic or represent the vascular part of the solid tumour and being *in vitro* models, they are unable to represent the full classical PK/PD properties of the used drugs. This especially includes drug metabolism process which is considered an essential part of the drug PK properties. The preliminary studies reported here also suggest that DLD-1 cells cannot form a collagen-IV containing ECM but further studies are needed to examine whether other ECM components are secreted. Other studies (Tannock et al., 2002) have indeed proved that MCL can form an ECM. Despite these limitations, the experimental models described here are novel and within the limitations of this approach, can be used to study the impact of CFF on drug penetration and its possible therapeutic manipulation.

4.10 Conclusion:

Solid tumour resistance to chemotherapy occurs due to several factors. Although cellular and genetic causes of resistance have been proved, resistance due to limited drug delivery has also been proved to contribute to chemotherapy resistance. Developing strategies to improve drug delivery to solid tumours is therefore important and is a fundamental requirement for efficacy. As drug delivery depends mainly on convection and diffusion, one of the strategies to be followed is to improve convective fluid flow (CFF) to solid tumours but this field is currently limited by the absence of *in vitro* models capable of measuring CFF and its effects on drug penetration. In this study, simple *in vitro* models were developed to study drug penetration through MCL. These models were modified to allow CFF and penetration rates to be calculated. It was proved in this study that CFF has a significant impact on drug penetration. The model itself is flexible and can be modified further to incorporate several other features of tumour biology such as the presence of an ECM and co-cultures with stromal fibroblasts. It is limited by the fact that it does not incorporate the tumour vasculature although it is feasible to culture HUVEC or other endothelial cell lines in the transwell. CFF in the presence or absence of VEGF could therefore be studied and it is feasible to use such a model to study strategies aimed at 'normalising' the vascular supply to tumours. This proposal clearly requires further study.

In conclusion, the results of this study illustrate the importance of convective fluid flow for effective drug delivery. In tumours where the convective flow is

reduced or reversed due to elevated tumour IFP, drug delivery is impaired. Strategies designed to enhance convective flow by manipulation of tumour cell or tumour/stroma interactions could enhance drug uptake and this model provides a 'tool' for evaluating such strategies. The limitation of the model is that it does not mimic the role played by the microvasculature in generating elevated interstitial fluid pressures in tumours.

5. REFERENCES

- Alagkiozidis, I., Facciabene, A., Tsiatas, M., Carpenito, C., Benencia, F., Adams, S., Jonak, Z., June, C.H., Powell, D.J., Jr., and Coukos, G. (2011). Time-dependent cytotoxic drugs selectively cooperate with IL-18 for cancer chemo-immunotherapy. *J Transl Med* 9, 77.
- Ali, S., and Coombes, R.C. (2002). Endocrine-responsive breast cancer and strategies for combating resistance. *Nat Rev Cancer* 2, 101-112.
- Ansiaux, R., Baudalet, C., Cron, G.O., Segers, J., Dessy, C., Martinive, P., De Wever, J., Verrax, J., Wauthier, V., Beghein, N., *et al.* (2006). Botulinum toxin potentiates cancer radiotherapy and chemotherapy. *Clin Cancer Res* 12, 1276-1283.
- Ansiaux, R., and Gallez, B. (2007). Use of botulinum toxins in cancer therapy. *Expert Opin Investig Drugs* 16, 209-218.
- Arkenau, H.T., Brunetto, A.T., Barriuso, J., Olmos, D., Eaton, D., de Bono, J., Judson, I., and Kaye, S. (2009). Clinical benefit of new targeted agents in phase I trials in patients with advanced colorectal cancer. *Oncology* 76, 151-156.
- Aukland, K., and Reed, R.K. (1993). Interstitial-lymphatic mechanisms in the control of extracellular fluid volume. *Physiol Rev* 73, 1-78.
- Baudry, N., and Vicaut, E. (1993). Role of nitric oxide in effects of tumor necrosis factor-alpha on microcirculation in rat. *J Appl Physiol* 75, 2392-2399.
- Baumgartner, G., Gomar-Hoss, C., Sakr, L., Ulsperger, E., and Wogritsch, C. (1998). The impact of extracellular matrix on the chemoresistance of solid

tumors--experimental and clinical results of hyaluronidase as additive to cytostatic chemotherapy. *Cancer Lett* 131, 85-99.

Baxter, L.T., and Jain, R.K. (1989). Transport of fluid and macromolecules in tumors. I. Role of interstitial pressure and convection. *Microvasc Res* 37, 77-104.

Baxter, L.T., and Jain, R.K. (1991). Transport of fluid and macromolecules in tumors. III. Role of binding and metabolism. *Microvasc Res* 41, 5-23.

Bibby, M., Cronin, B., and Phillips, R. (1993). Evaluation of the cytotoxicity of the indoloquinone eo9 in a human colon adenocarcinoma model. *Int J Oncol* 3, 661-666.

Bleumer, I., Oosterwijk, E., Oosterwijk-Wakka, J.C., Voller, M.C., Melchior, S., Warnaar, S.O., Mala, C., Beck, J., and Mulders, P.F. (2006). A clinical trial with chimeric monoclonal antibody WX-G250 and low dose interleukin-2 pulsing scheme for advanced renal cell carcinoma. *J Urol* 175, 57-62.

Bobo, R.H., Laske, D.W., Akbasak, A., Morrison, P.F., Dedrick, R.L., and Oldfield, E.H. (1994). Convection-enhanced delivery of macromolecules in the brain. *Proc Natl Acad Sci U S A* 91, 2076-2080.

Brenner, H. (2002). Long-term survival rates of cancer patients achieved by the end of the 20th century: a period analysis. *Lancet* 360, 1131-1135.

Brindle, K. (2008). New approaches for imaging tumour responses to treatment. *Nat Rev Cancer* 8, 94-107.

Brown, E., McKee, T., diTomaso, E., Pluen, A., Seed, B., Boucher, Y., and Jain, R.K. (2003). Dynamic imaging of collagen and its modulation in tumors in vivo using second-harmonic generation. *Nat Med* 9, 796-800.

Brown, J.M. (1999). The hypoxic cell: a target for selective cancer therapy--eighteenth Bruce F. Cain Memorial Award lecture. *Cancer Res* 59, 5863-5870.

Brown, J.M., and Wilson, W.R. (2004). Exploiting tumour hypoxia in cancer treatment. *Nat Rev Cancer* 4, 437-447.

Brunstein, F., Eggermont, A.M., de Wiel-Ambagtsheer, G., van Tiel, S.T., Rens, J., and ten Hagen, T.L. (2007). Synergistic antitumor effects of histamine plus melphalan in isolated hepatic perfusion for liver metastases. *Ann Surg Oncol* 14, 795-801.

Brunstein, F., Rens, J., van Tiel, S.T., Eggermont, A.M., and ten Hagen, T.L. (2006). Histamine, a vasoactive agent with vascular disrupting potential, improves tumour response by enhancing local drug delivery. *Br J Cancer* 95, 1663-1669.

Camma, C., Giunta, M., Fiorica, F., Pagliaro, L., Craxi, A., and Cottone, M. (2000). Preoperative radiotherapy for resectable rectal cancer: A meta-analysis. *JAMA* 284, 1008-1015.

Chary, S.R., and Jain, R.K. (1989). Direct measurement of interstitial convection and diffusion of albumin in normal and neoplastic tissues by fluorescence photobleaching. *Proc Natl Acad Sci U S A* 86, 5385-5389.

Chen, K., and Chen, X. (2011). Integrin targeted delivery of chemotherapeutics. *Theranostics* 1, 189-200.

Chowdhury, S., Larkin, J.M., and Gore, M.E. (2008). Recent advances in the treatment of renal cell carcinoma and the role of targeted therapies. *Eur J Cancer* 44, 2152-2161.

Cohen, M.H., Cortazar, P., Justice, R., and Pazdur, R. (2010). Approval summary: imatinib mesylate in the adjuvant treatment of malignant gastrointestinal stromal tumors. *Oncologist* 15, 300-307.

Cowan, D.S., Hicks, K.O., and Wilson, W.R. (1996). Multicellular membranes as an in vitro model for extravascular diffusion in tumours. *Br J Cancer Suppl* 27, S28-31.

Cowan, D.S., and Tannock, I.F. (2001). Factors that influence the penetration of methotrexate through solid tissue. *Int J Cancer* 91, 120-125.

Croce, C.M. (2008). Oncogenes and cancer. *N Engl J Med* 358, 502-511.

Croix, B.S., Rak, J.W., Kapitan, S., Sheehan, C., Graham, C.H., and Kerbel, R.S. (1996). Reversal by hyaluronidase of adhesion-dependent multicellular drug resistance in mammary carcinoma cells. *J Natl Cancer Inst* 88, 1285-1296.

Cron, G.O., Beghein, N., Ansiaux, R., Martinive, P., Feron, O., and Gallez, B. (2008). ¹⁹F NMR in vivo spectroscopy reflects the effectiveness of perfusion-enhancing vascular modifiers for improving gemcitabine chemotherapy. *Magn Reson Med* 59, 19-27.

Curnis, F., Sacchi, A., and Corti, A. (2002). Improving chemotherapeutic drug penetration in tumors by vascular targeting and barrier alteration. *J Clin Invest* 110, 475-482.

Curti, B.D., Urba, W.J., Alvord, W.G., Janik, J.E., Smith, J.W., 2nd, Madara, K., and Longo, D.L. (1993). Interstitial pressure of subcutaneous nodules in melanoma and lymphoma patients: changes during treatment. *Cancer Res* 53, 2204-2207.

de Gramont, A., Bosset, J.F., Milan, C., Rougier, P., Bouche, O., Etienne, P.L., Morvan, F., Louvet, C., Guillot, T., Francois, E., *et al.* (1997). Randomized trial comparing monthly low-dose leucovorin and fluorouracil bolus with bimonthly high-dose leucovorin and fluorouracil bolus plus continuous infusion for advanced colorectal cancer: a French intergroup study. *J Clin Oncol* 15, 808-815.

de Groot, J.F., and Yung, W.K. (2008). Bevacizumab and irinotecan in the treatment of recurrent malignant gliomas. *Cancer J* 14, 279-285.

de Wilt, J.H., ten Hagen, T.L., de Boeck, G., van Tiel, S.T., de Bruijn, E.A., and Eggermont, A.M. (2000). Tumour necrosis factor alpha increases melphalan concentration in tumour tissue after isolated limb perfusion. *Br J Cancer* 82, 1000-1003.

Deroose, J.P., Grunhagen, D.J., van Geel, A.N., de Wilt, J.H., Eggermont, A.M., and Verhoef, C. (2011). Long-term outcome of isolated limb perfusion with tumour necrosis factor-alpha for patients with melanoma in-transit metastases. *Br J Surg* 98, 1573-1580.

Dexter, D.L., Barbosa, J.A., and Calabresi, P. (1979). N,N-dimethylformamide-induced alteration of cell culture characteristics and loss of tumorigenicity in cultured human colon carcinoma cells. *Cancer Res* 39, 1020-1025.

Di Paolo, A. (2004). Liposomal anticancer therapy: pharmacokinetic and clinical aspects. *J Chemother* 16 Suppl 4, 90-93.

Doll, R., and Peto, R. (1981). The causes of cancer: quantitative estimates of avoidable risks of cancer in the United States today. *J Natl Cancer Inst* 66, 1191-1308.

Dreher, M.R., Liu, W., Michelich, C.R., Dewhirst, M.W., Yuan, F., and Chilkoti, A. (2006). Tumor vascular permeability, accumulation, and penetration of macromolecular drug carriers. *J Natl Cancer Inst* 98, 335-344.

Dunehoo, A.L., Anderson, M., Majumdar, S., Kobayashi, N., Berkland, C., and Siahaan, T.J. (2006). Cell adhesion molecules for targeted drug delivery. *J Pharm Sci* 95, 1856-1872.

Durand, R.E. (1989). Distribution and activity of antineoplastic drugs in a tumor model. *J Natl Cancer Inst* 81, 146-152.

Durand, R.E. (1990). Slow penetration of anthracyclines into spheroids and tumors: a therapeutic advantage? *Cancer Chemother Pharmacol* 26, 198-204.

Eckhardt, S. (2006). Molecular targeted therapy: a strategy of disillusion or optimism? *J Lab Clin Med* 147, 108-113.

Eikenes, L., Bruland, O.S., Brekken, C., and Davies Cde, L. (2004). Collagenase increases the transcapillary pressure gradient and improves the uptake and distribution of monoclonal antibodies in human osteosarcoma xenografts. *Cancer Res* 64, 4768-4773.

Eikenes, L., Tari, M., Tufto, I., Bruland, O.S., and de Lange Davies, C. (2005). Hyaluronidase induces a transcapillary pressure gradient and improves the distribution and uptake of liposomal doxorubicin (Caelyx) in human osteosarcoma xenografts. *Br J Cancer* 93, 81-88.

Emerich, D.F., Dean, R.L., Snodgrass, P., Lafreniere, D., Agostino, M., Wiens, T., Xiong, H., Hasler, B., Marsh, J., Pink, M., *et al.* (2001a). Bradykinin modulation of tumor vasculature: II. activation of nitric oxide and phospholipase A2/prostaglandin signaling pathways synergistically modifies

vascular physiology and morphology to enhance delivery of chemotherapeutic agents to tumors. *J Pharmacol Exp Ther* 296, 632-641.

Emerich, D.F., Snodgrass, P., Dean, R.L., Lafreniere, D., Agostino, M., Wiens, T., Xiong, H., Hasler, B., Marsh, J., Pink, M., *et al.* (2001b). Bradykinin modulation of tumor vasculature: I. Activation of B2 receptors increases delivery of chemotherapeutic agents into solid peripheral tumors, enhancing their efficacy. *J Pharmacol Exp Ther* 296, 623-631.

Evans, C.J., Phillips, R.M., Jones, P.F., Loadman, P.M., Sleeman, B.D., Twelves, C.J., and Smye, S.W. (2009). A mathematical model of doxorubicin penetration through multicellular layers. *J Theor Biol* 257, 598-608.

Eytan, G.D. (2005). Mechanism of multidrug resistance in relation to passive membrane permeation. *Biomed Pharmacother* 59, 90-97.

Fagan-Dubin, L. (1979). Causes of cancer. *Cancer Nurs* 2, 435-441.

Fearon, E.R., and Vogelstein, B. (1990). A genetic model for colorectal tumorigenesis. *Cell* 61, 759-767.

Fogh, J., Fogh, J.M., and Orfeo, T. (1977). One hundred and twenty-seven cultured human tumor cell lines producing tumors in nude mice. *J Natl Cancer Inst* 59, 221-226.

Franceschi, S., Dal Maso, L., Arniani, S., Crosignani, P., VerCELLI, M., Simonato, L., Falcini, F., Zanetti, R., Barchielli, A., Serraino, D., *et al.* (1998). Risk of cancer other than Kaposi's sarcoma and non-Hodgkin's lymphoma in persons with AIDS in Italy. Cancer and AIDS Registry Linkage Study. *Br J Cancer* 78, 966-970.

Friedl, F., Kimura, I., Osato, T., and Ito, Y. (1970). Studies on a new human cell line (SiHa) derived from carcinoma of uterus. I. Its establishment and morphology. *Proc Soc Exp Biol Med* 135, 543-545.

Friedrich, J., Ebner, R., and Kunz-Schughart, L.A. (2007). Experimental anti-tumor therapy in 3-D: spheroids--old hat or new challenge? *Int J Radiat Biol* 83, 849-871.

Ganapathy, A., Paterson, I.C., Prime, S.S., Eveson, J.W., Pring, M., Price, N., Threadgold, S.P., and Davies, M. (2010). TGF-beta inhibits metastasis in late stage human squamous cell carcinoma of the skin by a mechanism that does not involve Id1. *Cancer Lett* 298, 107-118.

Garattini, S. (2007). Pharmacokinetics in cancer chemotherapy. *Eur J Cancer* 43, 271-282.

Gerweck, L.E., Vijayappa, S., and Kozin, S. (2006). Tumor pH controls the in vivo efficacy of weak acid and base chemotherapeutics. *Mol Cancer Ther* 5, 1275-1279.

Gharib, M.I., and Burnett, A.K. (2002). Chemotherapy-induced cardiotoxicity: current practice and prospects of prophylaxis. *Eur J Heart Fail* 4, 235-242.

Gianni, A.M., and Piccart, M.J. (2000). Optimising chemotherapy dose density and dose intensity. new strategies to improve outcomes in adjuvant therapy for breast cancer. *Eur J Cancer* 36 *Suppl* 1, S1-3.

Giard, D.J., Aaronson, S.A., Todaro, G.J., Arnstein, P., Kersey, J.H., Dosik, H., and Parks, W.P. (1973). In vitro cultivation of human tumors: establishment of cell lines derived from a series of solid tumors. *J Natl Cancer Inst* 51, 1417-1423.

Gilman, G.a. (2006). Goodman and Gilman's the pharmacological basis of therapeutics (Parker in Books).

Goldman, J.M., and Melo, J.V. (2001). Targeting the BCR-ABL tyrosine kinase in chronic myeloid leukemia. *N Engl J Med* 344, 1084-1086.

Goodman, T.T., Olive, P.L., and Pun, S.H. (2007). Increased nanoparticle penetration in collagenase-treated multicellular spheroids. *Int J Nanomedicine* 2, 265-274.

Gottesman, M.M. (1993). How cancer cells evade chemotherapy: sixteenth Richard and Hinda Rosenthal Foundation Award Lecture. *Cancer research* 53, 747-754.

Grantab, R., Sivananthan, S., and Tannock, I.F. (2006). The penetration of anticancer drugs through tumor tissue as a function of cellular adhesion and packing density of tumor cells. *Cancer Res* 66, 1033-1039.

Griffon-Etienne, G., Boucher, Y., Brekken, C., Suit, H.D., and Jain, R.K. (1999). Taxane-induced apoptosis decompresses blood vessels and lowers interstitial fluid pressure in solid tumors: clinical implications. *Cancer Res* 59, 3776-3782.

Grunhagen, D.J., de Wilt, J.H., Graveland, W.J., van Geel, A.N., and Eggermont, A.M. (2006). The palliative value of tumor necrosis factor alpha-based isolated limb perfusion in patients with metastatic sarcoma and melanoma. *Cancer* 106, 156-162.

Gutmann, R., Leunig, M., Feyh, J., Goetz, A.E., Messmer, K., Kastenbauer, E., and Jain, R.K. (1992). Interstitial hypertension in head and neck tumors in patients: correlation with tumor size. *Cancer Res* 52, 1993-1995.

Hanahan, D., and Weinberg, R.A. (2000). The hallmarks of cancer. *Cell* 100, 57-70.

Hanahan, D., and Weinberg, R.A. (2011). Hallmarks of cancer: the next generation. *Cell* 144, 646-674.

Heldin, C.H., Rubin, K., Pietras, K., and Ostman, A. (2004). High interstitial fluid pressure - an obstacle in cancer therapy. *Nat Rev Cancer* 4, 806-813.

Helmlinger, G., Yuan, F., Dellian, M., and Jain, R.K. (1997). Interstitial pH and pO₂ gradients in solid tumors in vivo: high-resolution measurements reveal a lack of correlation. *Nat Med* 3, 177-182.

Henneberry, H.P., and Aherne, G.W. (1992). Visualisation of doxorubicin in human and animal tissues and in cell cultures by immunogold-silver staining. *Br J Cancer* 65, 82-86.

Herbst, R.S., Ansari, R., Bustin, F., Flynn, P., Hart, L., Otterson, G.A., Vlahovic, G., Soh, C.H., O'Connor, P., and Hainsworth, J. (2011). Efficacy of bevacizumab plus erlotinib versus erlotinib alone in advanced non-small-cell lung cancer after failure of standard first-line chemotherapy (BeTa): a double-blind, placebo-controlled, phase 3 trial. *Lancet* 377, 1846-1854.

Herbst, R.S., O'Neill, V.J., Fehrenbacher, L., Belani, C.P., Bonomi, P.D., Hart, L., Melnyk, O., Ramies, D., Lin, M., and Sandler, A. (2007). Phase II study of efficacy and safety of bevacizumab in combination with chemotherapy or erlotinib compared with chemotherapy alone for treatment of recurrent or refractory non small-cell lung cancer. *J Clin Oncol* 25, 4743-4750.

Hicks, K.O., Pruijn, F.B., Secomb, T.W., Hay, M.P., Hsu, R., Brown, J.M., Denny, W.A., Dewhurst, M.W., and Wilson, W.R. (2006). Use of three-

dimensional tissue cultures to model extravascular transport and predict in vivo activity of hypoxia-targeted anticancer drugs. *J Natl Cancer Inst* 98, 1118-1128.

Hicks, K.O., Pruijn, F.B., Sturman, J.R., Denny, W.A., and Wilson, W.R. (2003). Multicellular resistance to tirapazamine is due to restricted extravascular transport: a pharmacokinetic/pharmacodynamic study in HT29 multicellular layer cultures. *Cancer Res* 63, 5970-5977.

Hicks, K.O., Siim, B.G., Pruijn, F.B., and Wilson, W.R. (2004). Oxygen dependence of the metabolic activation and cytotoxicity of tirapazamine: implications for extravascular transport and activity in tumors. *Radiat Res* 161, 656-666.

Higgins, G.A., Humphrey, E.W., Dwight, R.W., Roswit, B., Lee, L.E., Jr., and Keehn, R.J. (1986). Preoperative radiation and surgery for cancer of the rectum. Veterans Administration Surgical Oncology Group Trial II. *Cancer* 58, 352-359.

Horsman, M.R., and Siemann, D.W. (2006). Pathophysiologic effects of vascular-targeting agents and the implications for combination with conventional therapies. *Cancer Res* 66, 11520-11539.

Hurwitz, H., Fehrenbacher, L., Novotny, W., Cartwright, T., Hainsworth, J., Heim, W., Berlin, J., Baron, A., Griffing, S., Holmgren, E., *et al.* (2004). Bevacizumab plus irinotecan, fluorouracil, and leucovorin for metastatic colorectal cancer. *N Engl J Med* 350, 2335-2342.

Hynes, R.O., and Zhao, Q. (2000). The evolution of cell adhesion. *J Cell Biol* 150, F89-96.

Inch, W.R., McCredie, J.A., and Sutherland, R.M. (1970). Growth of nodular carcinomas in rodents compared with multi-cell spheroids in tissue culture. *Growth* 34, 271-282.

Ito, M., Yoshida, K., Kyo, E., Ayhan, A., Nakayama, H., Yasui, W., Ito, H., and Tahara, E. (1990). Expression of several growth factors and their receptor genes in human colon carcinomas. *Virchows Arch B Cell Pathol Incl Mol Pathol* 59, 173-178.

Iyer, A.K., Khaled, G., Fang, J., and Maeda, H. (2006). Exploiting the enhanced permeability and retention effect for tumor targeting. *Drug Discov Today* 11, 812-818.

Jacobson, A., Salnikov, A., Lammerts, E., Roswall, P., Sundberg, C., Heldin, P., Rubin, K., and Heldin, N.E. (2003). Hyaluronan content in experimental carcinoma is not correlated to interstitial fluid pressure. *Biochem Biophys Res Commun* 305, 1017-1023.

Jain, R.K. (1987a). Transport of molecules across tumor vasculature. *Cancer Metastasis Rev* 6, 559-593.

Jain, R.K. (1987b). Transport of molecules in the tumor interstitium: a review. *Cancer Res* 47, 3039-3051.

Jain, R.K. (1998). Delivery of molecular and cellular medicine to solid tumors. *J Control Release* 53, 49-67.

Jain, R.K. (2001). Normalizing tumor vasculature with anti-angiogenic therapy: a new paradigm for combination therapy. *Nat Med* 7, 987-989.

Jain, R.K. (2005). Normalization of tumor vasculature: an emerging concept in antiangiogenic therapy. *Science* 307, 58-62.

Jain, R.K., and Baxter, L.T. (1988). Mechanisms of heterogeneous distribution of monoclonal antibodies and other macromolecules in tumors: significance of elevated interstitial pressure. *Cancer Res* 48, 7022-7032.

Jain, R.K., and Stylianopoulos, T. (2010). Delivering nanomedicine to solid tumors. *Nat Rev Clin Oncol* 7, 653-664.

Jang, S.H., Wientjes, M.G., Lu, D., and Au, J.L. (2003). Drug delivery and transport to solid tumors. *Pharm Res* 20, 1337-1350.

Jayson, G.C., Parker, G.J., Mullamitha, S., Valle, J.W., Saunders, M., Broughton, L., Lawrance, J., Carrington, B., Roberts, C., Issa, B., *et al.* (2005). Blockade of platelet-derived growth factor receptor-beta by CDP860, a humanized, PEGylated di-Fab', leads to fluid accumulation and is associated with increased tumor vascularized volume. *J Clin Oncol* 23, 973-981.

Jemal, A., Bray, F., Center, M.M., Ferlay, J., Ward, E., and Forman, D. (2011). Global cancer statistics. *CA Cancer J Clin* 61, 69-90.

Jemal, A., Siegel, R., Xu, J., and Ward, E. (2010). Cancer statistics, 2010. *CA Cancer J Clin* 60, 277-300.

Joensuu, H. (2008). Systemic chemotherapy for cancer: from weapon to treatment. *Lancet Oncol* 9, 304.

Kaighn, M.E., Narayan, K.S., Ohnuki, Y., Lechner, J.F., and Jones, L.W. (1979). Establishment and characterization of a human prostatic carcinoma cell line (PC-3). *Investigative urology* 17, 16-23.

Kane, R.C., Farrell, A.T., Madabushi, R., Booth, B., Chattopadhyay, S., Sridhara, R., Justice, R., and Pazdur, R. (2009). Sorafenib for the treatment of unresectable hepatocellular carcinoma. *Oncologist* 14, 95-100.

Kantarjian, H., Shah, N.P., Hochhaus, A., Cortes, J., Shah, S., Ayala, M., Moiraghi, B., Shen, Z., Mayer, J., Pasquini, R., *et al.* (2010). Dasatinib versus imatinib in newly diagnosed chronic-phase chronic myeloid leukemia. *N Engl J Med* 362, 2260-2270.

Kerr, D.J., and Kaye, S.B. (1987). Aspects of cytotoxic drug penetration, with particular reference to anthracyclines. *Cancer Chemother Pharmacol* 19, 1-5.

Kim, H.P., Han, S.W., Kim, S.H., Im, S.A., Oh, D.Y., Bang, Y.J., and Kim, T.Y. (2008). Combined lapatinib and cetuximab enhance cytotoxicity against gefitinib-resistant lung cancer cells. *Mol Cancer Ther* 7, 607-615.

Kimble, M.A.K. (2004). *Applied therapeutics, the clinical use of drugs*, 8 edn.

Kirkwood, J. (2002). Cancer immunotherapy: the interferon-alpha experience. *Semin Oncol* 29, 18-26.

Kohno, N., Ohnuma, T., and Truog, P. (1994). Effects of hyaluronidase on doxorubicin penetration into squamous carcinoma multicellular tumor spheroids and its cell lethality. *J Cancer Res Clin Oncol* 120, 293-297.

Kontermann, R.E. (2006). Immunoliposomes for cancer therapy. *Curr Opin Mol Ther* 8, 39-45.

Kozin, S.V., Shkarin, P., and Gerweck, L.E. (2001). The cell transmembrane pH gradient in tumors enhances cytotoxicity of specific weak acid chemotherapeutics. *Cancer Res* 61, 4740-4743.

Kristensen, C.A., Nozue, M., Boucher, Y., and Jain, R.K. (1996). Reduction of interstitial fluid pressure after TNF-alpha treatment of three human melanoma xenografts. *Br J Cancer* 74, 533-536.

Kristjansen, P.E., Boucher, Y., and Jain, R.K. (1993). Dexamethasone reduces the interstitial fluid pressure in a human colon adenocarcinoma xenograft. *Cancer research* 53, 4764-4766.

Kuh, H.J., Jang, S.H., Wientjes, M.G., Weaver, J.R., and Au, J.L. (1999). Determinants of paclitaxel penetration and accumulation in human solid tumor. *J Pharmacol Exp Ther* 290, 871-880.

Kyle, A.H., Huxham, L.A., Chiam, A.S., Sim, D.H., and Minchinton, A.I. (2004). Direct assessment of drug penetration into tissue using a novel application of three-dimensional cell culture. *Cancer Res* 64, 6304-6309.

Kyle, A.H., Huxham, L.A., Yeoman, D.M., and Minchinton, A.I. (2007). Limited tissue penetration of taxanes: a mechanism for resistance in solid tumors. *Clin Cancer Res* 13, 2804-2810.

Kyle, A.H., and Minchinton, A.I. (1999). Measurement of delivery and metabolism of tirapazamine to tumour tissue using the multilayered cell culture model. *Cancer Chemother Pharmacol* 43, 213-220.

Lammerts, E., Roswall, P., Sundberg, C., Gotwals, P.J., Kotliansky, V.E., Reed, R.K., Heldin, N.E., and Rubin, K. (2002). Interference with TGF-beta1 and -beta3 in tumor stroma lowers tumor interstitial fluid pressure independently of growth in experimental carcinoma. *Int J Cancer* 102, 453-462.

Lankelma, J., Dekker, H., Luque, F.R., Luykx, S., Hoekman, K., van der Valk, P., van Diest, P.J., and Pinedo, H.M. (1999). Doxorubicin gradients in human breast cancer. *Clin Cancer Res* 5, 1703-1707.

Lee, C.M., and Tannock, I.F. (2006). Inhibition of endosomal sequestration of basic anticancer drugs: influence on cytotoxicity and tissue penetration. *Br J Cancer* 94, 863-869.

Lee, I., Boucher, Y., and Jain, R.K. (1992). Nicotinamide can lower tumor interstitial fluid pressure: mechanistic and therapeutic implications. *Cancer Res* 52, 3237-3240.

Less, J.R., Posner, M.C., Boucher, Y., Borochoviz, D., Wolmark, N., and Jain, R.K. (1992). Interstitial hypertension in human breast and colorectal tumors. *Cancer Res* 52, 6371-6374.

Leu, A.J., Berk, D.A., Lymboussaki, A., Alitalo, K., and Jain, R.K. (2000). Absence of functional lymphatics within a murine sarcoma: a molecular and functional evaluation. *Cancer Res* 60, 4324-4327.

Lewis, L.D., Benin, A., Szumlanski, C.L., Otterness, D.M., Lennard, L., Weinshilboum, R.M., and Nierenberg, D.W. (1997). Olsalazine and 6-mercaptopurine-related bone marrow suppression: a possible drug-drug interaction. *Clin Pharmacol Ther* 62, 464-475.

Li, C., Newman, R.A., Wu, Q.P., Ke, S., Chen, W., Hutto, T., Kan, Z., Brannan, M.D., Charnsangavej, C., and Wallace, S. (2000). Biodistribution of paclitaxel and poly(L-glutamic acid)-paclitaxel conjugate in mice with ovarian OCa-1 tumor. *Cancer Chemother Pharmacol* 46, 416-422.

Li, H.P., Li, X., He, G.J., Yi, X.H., and Kaplan, A.P. (2004). The influence of dexamethasone on the proliferation and apoptosis of pulmonary inflammatory cells in bleomycin-induced pulmonary fibrosis in rats. *Respirology* 9, 25-32.

Lidar, Z., Mardor, Y., Jonas, T., Pfeffer, R., Faibel, M., Nass, D., Hadani, M., and Ram, Z. (2004). Convection-enhanced delivery of paclitaxel for the treatment of recurrent malignant glioma: a phase I/II clinical study. *J Neurosurg* 100, 472-479.

Lieber, M., Mazzetta, J., Nelson-Rees, W., Kaplan, M., and Todaro, G. (1975). Establishment of a continuous tumor-cell line (panc-1) from a human carcinoma of the exocrine pancreas. *Int J Cancer* 15, 741-747.

Liu, X., Chen, C., and Smith, B.J. (2008). Progress in brain penetration evaluation in drug discovery and development. *J Pharmacol Exp Ther* 325, 349-356.

Lokich, J., and Anderson, N. (1997). Dose intensity for bolus versus infusion chemotherapy administration: review of the literature for 27 anti-neoplastic agents. *Ann Oncol* 8, 15-25.

Maeda, H. (2010a). Nitroglycerin enhances vascular blood flow and drug delivery in hypoxic tumor tissues: analogy between angina pectoris and solid tumors and enhancement of the EPR effect. *J Control Release* 142, 296-298.

Maeda, H. (2010b). Tumor-selective delivery of macromolecular drugs via the EPR effect: background and future prospects. *Bioconjug Chem* 21, 797-802.

Maemondo, M., Inoue, A., Kobayashi, K., Sugawara, S., Oizumi, S., Isobe, H., Gemma, A., Harada, M., Yoshizawa, H., Kinoshita, I., *et al.* (2010). Gefitinib or chemotherapy for non-small-cell lung cancer with mutated EGFR. *N Engl J Med* 362, 2380-2388.

Malvezzi, M., Arfe, A., Bertuccio, P., Levi, F., La Vecchia, C., and Negri, E. European cancer mortality predictions for the year 2011. *Ann Oncol* 22, 947-956.

Malvezzi, M., Arfe, A., Bertuccio, P., Levi, F., La Vecchia, C., and Negri, E. (2011). European cancer mortality predictions for the year 2011. *Ann Oncol* 22, 947-956.

Mardor, Y., Rahav, O., Zauberman, Y., Lidar, Z., Ocherashvili, A., Daniels, D., Roth, Y., Maier, S.E., Orenstein, A., and Ram, Z. (2005). Convection-enhanced drug delivery: increased efficacy and magnetic resonance image monitoring. *Cancer Res* 65, 6858-6863.

Mauriac, L., MacGrogan, G., Avril, A., Durand, M., Floquet, A., Debled, M., Dilhuydy, J.M., and Bonichon, F. (1999). Neoadjuvant chemotherapy for operable breast carcinoma larger than 3 cm: a unicentre randomized trial with a 124-month median follow-up. Institut Bergonie Bordeaux Groupe Sein (IBBGS). *Ann Oncol* 10, 47-52.

Mazzeo, F., Berliere, M., Kerger, J., Squifflet, J., Duck, L., D'Hondt, V., Humblet, Y., Donnez, J., and Machiels, J.P. (2003). Neoadjuvant chemotherapy followed by surgery and adjuvant chemotherapy in patients with primarily unresectable, advanced-stage ovarian cancer. *Gynecol Oncol* 90, 163-169.

McGrogan, B.T., Gilmartin, B., Carney, D.N., and McCann, A. (2008). Taxanes, microtubules and chemoresistant breast cancer. *Biochim Biophys Acta* 1785, 96-132.

McKeage, M.J. (2011). Clinical trials of vascular disrupting agents in advanced non--small-cell lung cancer. *Clin Lung Cancer* 12, 143-147.

McKeage, M.J., Reck, M., Jameson, M.B., Rosenthal, M.A., Gibbs, D., Mainwaring, P.N., Freitag, L., Sullivan, R., and Von Pawel, J. (2009). Phase II study of ASA404 (vadimezan, 5,6-dimethylxanthenone-4-acetic acid/DMXAA) 1800mg/m(2) combined with carboplatin and paclitaxel in previously untreated advanced non-small cell lung cancer. *Lung Cancer* 65, 192-197.

McKee, T.D., Grandi, P., Mok, W., Alexandrakis, G., Insin, N., Zimmer, J.P., Bawendi, M.G., Boucher, Y., Breakefield, X.O., and Jain, R.K. (2006). Degradation of fibrillar collagen in a human melanoma xenograft improves the efficacy of an oncolytic herpes simplex virus vector. *Cancer Res* 66, 2509-2513.

Melisi, D., Ishiyama, S., Scwabas, G.M., Fleming, J.B., Xia, Q., Tortora, G., Abbruzzese, J.L., and Chiao, P.J. (2008). LY2109761, a novel transforming growth factor beta receptor type I and type II dual inhibitor, as a therapeutic approach to suppressing pancreatic cancer metastasis. *Mol Cancer Ther* 7, 829-840.

Mihich, E. (2000). Historical overview of biologic response modifiers. *Cancer Invest* 18, 456-466.

Milosevic, M., Fyles, A., Hedley, D., Pintilie, M., Levin, W., Manchul, L., and Hill, R. (2001). Interstitial fluid pressure predicts survival in patients with cervix cancer independent of clinical prognostic factors and tumor oxygen measurements. *Cancer Res* 61, 6400-6405.

- Minchinton, A.I., and Tannock, I.F. (2006). Drug penetration in solid tumours. *Nat Rev Cancer* 6, 583-592.
- Montesano, R., and Hall, J. (2001). Environmental causes of human cancers. *Eur J Cancer* 37 *Suppl* 8, S67-87.
- Mosmann, T. (1983). Rapid colorimetric assay for cellular growth and survival: application to proliferation and cytotoxicity assays. *Journal of immunological methods* 65, 55-63.
- Mouches, C., and Bove, J.M. (1983). A plasmid from *S. citri* strain M14 hybridizes with extrachromosomal DNAs from other spiroplasmas, including corn stunt spiroplasma E275, tick spiroplasma 277F, and coco spiroplasma N525. *The Yale journal of biology and medicine* 56, 723-727.
- Muller, M., Mader, R.M., Steiner, B., Steger, G.G., Jansen, B., Gnant, M., Helbich, T., Jakesz, R., Eichler, H.G., and Blochl-Daum, B. (1997). 5-fluorouracil kinetics in the interstitial tumor space: clinical response in breast cancer patients. *Cancer Res* 57, 2598-2601.
- Nagula, S., Ishill, N., Nash, C., Markowitz, A.J., Schattner, M.A., Temple, L., Weiser, M.R., Thaler, H.T., Zauber, A., and Gerdes, H. (2010). Quality of life and symptom control after stent placement or surgical palliation of malignant colorectal obstruction. *J Am Coll Surg* 210, 45-53.
- Nederman, T., and Carlsson, J. (1984). Penetration and binding of vinblastine and 5-fluorouracil in cellular spheroids. *Cancer Chemother Pharmacol* 13, 131-135.
- Nederman, T., and Twentyman, P. (1984). Spheroids for studies of drug effects. *Recent Results Cancer Res* 95, 84-102.

Netti, P.A., Berk, D.A., Swartz, M.A., Grodzinsky, A.J., and Jain, R.K. (2000). Role of extracellular matrix assembly in interstitial transport in solid tumors. *Cancer Res* 60, 2497-2503.

Newman, E.M., Lu, Y., Kashani-Sabet, M., Kesavan, V., and Scanlon, K.J. (1988). Mechanisms of cross-resistance to methotrexate and 5-fluorouracil in an A2780 human ovarian carcinoma cell subline resistant to cisplatin. *Biochemical pharmacology* 37, 443-447.

Nishida, T., Kanda, T., Nishitani, A., Takahashi, T., Nakajima, K., Ishikawa, T., and Hirota, S. (2008). Secondary mutations in the kinase domain of the KIT gene are predominant in imatinib-resistant gastrointestinal stromal tumor. *Cancer Sci* 99, 799-804.

Nyman, D.W., Campbell, K.J., Hersh, E., Long, K., Richardson, K., Trieu, V., Desai, N., Hawkins, M.J., and Von Hoff, D.D. (2005). Phase I and pharmacokinetics trial of ABI-007, a novel nanoparticle formulation of paclitaxel in patients with advanced nonhematologic malignancies. *J Clin Oncol* 23, 7785-7793.

O'Dwyer, P.J., Manola, J., Valone, F.H., Ryan, L.M., Hines, J.D., Wadler, S., Haller, D.G., Arbuck, S.G., Weiner, L.M., Mayer, R.J., *et al.* (2001). Fluorouracil modulation in colorectal cancer: lack of improvement with N - phosphonoacetyl- I -aspartic acid or oral leucovorin or interferon, but enhanced therapeutic index with weekly 24-hour infusion schedule--an Eastern Cooperative Oncology Group/Cancer and Leukemia Group B Study. *J Clin Oncol* 19, 2413-2421.

Ozols, R.F., Locker, G.Y., Doroshow, J.H., Grotzinger, K.R., Myers, C.E., and Young, R.C. (1979). Pharmacokinetics of adriamycin and tissue penetration in murine ovarian cancer. *Cancer Res* 39, 3209-3214.

Padera, T.P., Stoll, B.R., Tooredman, J.B., Capen, D., di Tomaso, E., and Jain, R.K. (2004). Pathology: cancer cells compress intratumour vessels. *Nature* 427, 695.

Pankovich, J.M., and Jimbow, K. (1991). Tyrosine transport in a human melanoma cell line as a basis for selective transport of cytotoxic analogues. *The Biochemical journal* 280 (Pt 3), 721-725.

Pattillo, R.A., Husa, R.O., Story, M.T., Ruckert, A.C., Shalaby, M.R., and Mattingly, R.F. (1977). Tumor antigen and human chorionic gonadotropin in CaSki cells: a new epidermoid cervical cancer cell line. *Science* 196, 1456-1458.

Pavalko, F.M., and Otey, C.A. (1994). Role of adhesion molecule cytoplasmic domains in mediating interactions with the cytoskeleton. *Proc Soc Exp Biol Med* 205, 282-293.

Perentes, J.Y., McKee, T.D., Ley, C.D., Mathiew, H., Dawson, M., Padera, T.P., Munn, L.L., Jain, R.K., and Boucher, Y. (2009). In vivo imaging of extracellular matrix remodeling by tumor-associated fibroblasts. *Nat Methods* 6, 143-145.

Peters, C.E., Chaplin, D.J., and Hirst, D.G. (1997). Nicotinamide reduces tumour interstitial fluid pressure in a dose- and time-dependent manner. *Br J Radiol* 70, 160-167.

Phillips, R.M., and Clayton, M.R. (1997). Plateau-phase cultures: an experimental model for identifying drugs which are bioactivated within the microenvironment of solid tumours. *Br J Cancer* 75, 196-201.

Phillips, R.M., Loadman, P.M., and Cronin, B.P. (1998). Evaluation of a novel in vitro assay for assessing drug penetration into avascular regions of tumours. *Br J Cancer* 77, 2112-2119.

Pietras, K., Rubin, K., Sjoblom, T., Buchdunger, E., Sjoquist, M., Heldin, C.H., and Ostman, A. (2002). Inhibition of PDGF receptor signaling in tumor stroma enhances antitumor effect of chemotherapy. *Cancer Res* 62, 5476-5484.

Pietras, K., Stumm, M., Hubert, M., Buchdunger, E., Rubin, K., Heldin, C.H., McSheehy, P., Wartmann, M., and Ostman, A. (2003). STI571 enhances the therapeutic index of epothilone B by a tumor-selective increase of drug uptake. *Clin Cancer Res* 9, 3779-3787.

Pillwein, K., Fuiko, R., Slavic, I., Czech, T., Hawliczek, G., Bernhardt, G., Nirnberger, G., and Koller, U. (1998). Hyaluronidase additional to standard chemotherapy improves outcome for children with malignant brain tumors. *Cancer Lett* 131, 101-108.

Podobnik, B., Sersa, G., and Miklavcic, D. (2001). Effect of hydralazine on interstitial fluid pressure in experimental tumours and in normal tissue. *In Vivo* 15, 417-424.

Presant, C.A., Wolf, W., Waluch, V., Wiseman, C., Kennedy, P., Blayney, D., and Brechner, R.R. (1994). Association of intratumoral pharmacokinetics of fluorouracil with clinical response. *Lancet* 343, 1184-1187.

Prewett, M.C., Hooper, A.T., Bassi, R., Ellis, L.M., Waksal, H.W., and Hicklin, D.J. (2002). Enhanced antitumor activity of anti-epidermal growth factor receptor monoclonal antibody IMC-C225 in combination with irinotecan (CPT-11) against human colorectal tumor xenografts. *Clin Cancer Res* 8, 994-1003.

Primeau, A.J., Rendon, A., Hedley, D., Lilge, L., and Tannock, I.F. (2005). The distribution of the anticancer drug Doxorubicin in relation to blood vessels in solid tumors. *Clin Cancer Res* 11, 8782-8788.

Regev, R., Katzir, H., Yeheskely-Hayon, D., and Eytan, G.D. (2007). Modulation of P-glycoprotein-mediated multidrug resistance by acceleration of passive drug permeation across the plasma membrane. *FEBS J* 274, 6204-6214.

Rentsch, K.M., Schwendener, R.A., Pestalozzi, B.C., Sauter, C., Wunderli-Allenspach, H., and Hanseler, E. (1998). Pharmacokinetic studies of mitoxantrone and one of its metabolites in serum and urine in patients with advanced breast cancer. *Eur J Clin Pharmacol* 54, 83-89.

Rischin, D., Peters, L.J., O'Sullivan, B., Giralt, J., Fisher, R., Yuen, K., Trotti, A., Bernier, J., Bourhis, J., Ringash, J., *et al.* (2010). Tirapazamine, cisplatin, and radiation versus cisplatin and radiation for advanced squamous cell carcinoma of the head and neck (TROG 02.02, HeadSTART): a phase III trial of the Trans-Tasman Radiation Oncology Group. *J Clin Oncol* 28, 2989-2995.

Roca, J.M., Alonso, V., Pericay, C., Escudero, P., Salud, A., Losa, F., Lopez, L.J., Guasch, I., Mendez, M., Quintero-Aldana, G., *et al.* (2010). Cetuximab given every 2 weeks plus irinotecan is an active and safe option for previously treated patients with metastatic colorectal cancer. *Chemotherapy* 56, 142-146.

Rochlitz, C.F. (2001). Gene therapy of cancer. *Swiss Med Wkly* 131, 4-9.

Rubin, K., Sjoquist, M., Gustafsson, A.M., Isaksson, B., Salvessen, G., and Reed, R.K. (2000). Lowering of tumoral interstitial fluid pressure by prostaglandin E(1) is paralleled by an increased uptake of (51)Cr-EDTA. *Int J Cancer* 86, 636-643.

Salnikov, A.V., Iversen, V.V., Koisti, M., Sundberg, C., Johansson, L., Stuhr, L.B., Sjoquist, M., Ahlstrom, H., Reed, R.K., and Rubin, K. (2003). Lowering of tumor interstitial fluid pressure specifically augments efficacy of chemotherapy. *FASEB J* 17, 1756-1758.

Salnikov, A.V., Roswall, P., Sundberg, C., Gardner, H., Heldin, N.E., and Rubin, K. (2005). Inhibition of TGF-beta modulates macrophages and vessel maturation in parallel to a lowering of interstitial fluid pressure in experimental carcinoma. *Lab Invest* 85, 512-521.

Sandler, A., Gray, R., Perry, M.C., Brahmer, J., Schiller, J.H., Dowlati, A., Lilienbaum, R., and Johnson, D.H. (2006). Paclitaxel-carboplatin alone or with bevacizumab for non-small-cell lung cancer. *N Engl J Med* 355, 2542-2550.

Sarin, H., Kanevsky, A.S., Fung, S.H., Butman, J.A., Cox, R.W., Glen, D., Reynolds, R., and Auh, S. (2009). Metabolically stable bradykinin B2 receptor agonists enhance transvascular drug delivery into malignant brain tumors by increasing drug half-life. *J Transl Med* 7, 33.

Scartozzi, M., Bearzi, I., Mandolesi, A., Giampieri, R., Faloppi, L., Galizia, E., Loupakis, F., Zaniboni, A., Zorzi, F., Biscotti, T., *et al.* (2011). Epidermal growth factor receptor (EGFR) gene promoter methylation and cetuximab treatment in colorectal cancer patients. *Br J Cancer* 104, 1786-1790.

Segers, J., Di Fazio, V., Ansiaux, R., Martinive, P., Feron, O., Wallemacq, P., and Gallez, B. (2006). Potentiation of cyclophosphamide chemotherapy using the anti-angiogenic drug thalidomide: importance of optimal scheduling to exploit the 'normalization' window of the tumor vasculature. *Cancer Lett* 244, 129-135.

Seibold, J.R., Korn, J.H., Simms, R., Clements, P.J., Moreland, L.W., Mayes, M.D., Furst, D.E., Rothfield, N., Steen, V., Weisman, M., *et al.* (2000). Recombinant human relaxin in the treatment of scleroderma. A randomized, double-blind, placebo-controlled trial. *Ann Intern Med* 132, 871-879.

Sepulveda, C., Marlin, A., Yoshida, T., and Ullrich, A. (2002). Palliative Care: the World Health Organization's global perspective. *J Pain Symptom Manage* 24, 91-96.

Shubik, P. (1982). Vascularization of tumors: a review. *J Cancer Res Clin Oncol* 103, 211-226.

Siemann, D.W. (2011). The unique characteristics of tumor vasculature and preclinical evidence for its selective disruption by Tumor-Vascular Disrupting Agents. *Cancer Treat Rev* 37, 63-74.

Siemann, D.W., Bibby, M.C., Dark, G.G., Dicker, A.P., Eskens, F.A., Horsman, M.R., Marme, D., and Lorusso, P.M. (2005). Differentiation and definition of vascular-targeted therapies. *Clin Cancer Res* 11, 416-420.

Siemann, D.W., Chaplin, D.J., and Walicke, P.A. (2009). A review and update of the current status of the vasculature-disabling agent combretastatin-A4 phosphate (CA4P). *Expert Opin Investig Drugs* 18, 189-197.

Slamon, D., Eiermann, W., Robert, N., Pienkowski, T., Martin, M., Press, M., Mackey, J., Glaspy, J., Chan, A., Pawlicki, M., *et al.* (2011). Adjuvant trastuzumab in HER2-positive breast cancer. *N Engl J Med* 365, 1273-1283.

Soria, J.C., Blay, J.Y., Spano, J.P., Pivot, X., Coscas, Y., and Khayat, D. (2011). Added value of molecular targeted agents in oncology. *Ann Oncol* 22, 1703-1716.

Soule, H.D., Vazquez, J., Long, A., Albert, S., and Brennan, M. (1973). A human cell line from a pleural effusion derived from a breast carcinoma. *J Natl Cancer Inst* 51, 1409-1416.

Starling, N., Hawkes, E.A., Chau, I., Watkins, D., Thomas, J., Webb, J., Brown, G., Thomas, K., Barbachano, Y., Oates, J., *et al.* (2011). A dose escalation study of gemcitabine plus oxaliplatin in combination with imatinib for gemcitabine-refractory advanced pancreatic adenocarcinoma. *Ann Oncol*.

Storm, G., Steerenberg, P.A., van Borssum Waalkes, M., Emmen, F., and Crommelin, D.J. (1988). Potential pitfalls in in vitro antitumor activity testing of free and liposome-entrapped doxorubicin. *J Pharm Sci* 77, 823-830.

Stuhr, L.E., Salnikov, A.V., Iversen, V.V., Salvesen, G., Rubin, K., and Reed, R.K. (2006). High-dose, short-term, anti-inflammatory treatment with dexamethasone reduces growth and augments the effects of 5-fluorouracil on dimethyl-alpha-benzanthracene-induced mammary tumors in rats. *Scand J Clin Lab Invest* 66, 477-486.

Sutherland, R.L., Hall, R.E., and Taylor, I.W. (1983). Cell proliferation kinetics of MCF-7 human mammary carcinoma cells in culture and effects of tamoxifen on exponentially growing and plateau-phase cells. *Cancer Res* 43, 3998-4006.

Sutherland, R.M. (1988). Cell and environment interactions in tumor microregions: the multicell spheroid model. *Science* 240, 177-184.

Sutherland, R.M., Eddy, H.A., Bareham, B., Reich, K., and Vanantwerp, D. (1979). Resistance to adriamycin in multicellular spheroids. *Int J Radiat Oncol Biol Phys* 5, 1225-1230.

Swabb, E.A., Wei, J., and Gullino, P.M. (1974). Diffusion and convection in normal and neoplastic tissues. *Cancer Res* 34, 2814-2822.

Syed, S., Takimoto, C., Hidalgo, M., Rizzo, J., Kuhn, J.G., Hammond, L.A., Schwartz, G., Tolcher, A., Patnaik, A., Eckhardt, S.G., *et al.* (2004). A phase I and pharmacokinetic study of Col-3 (Metastat), an oral tetracycline derivative with potent matrix metalloproteinase and antitumor properties. *Clin Cancer Res* 10, 6512-6521.

Taghian, A.G., Abi-Raad, R., Assaad, S.I., Casty, A., Ancukiewicz, M., Yeh, E., Molokhia, P., Attia, K., Sullivan, T., Kuter, I., *et al.* (2005). Paclitaxel decreases the interstitial fluid pressure and improves oxygenation in breast cancers in patients treated with neoadjuvant chemotherapy: clinical implications. *J Clin Oncol* 23, 1951-1961.

Talpaz, M., Shah, N.P., Kantarjian, H., Donato, N., Nicoll, J., Paquette, R., Cortes, J., O'Brien, S., Nicaise, C., Bleickardt, E., *et al.* (2006). Dasatinib in imatinib-resistant Philadelphia chromosome-positive leukemias. *N Engl J Med* 354, 2531-2541.

Tannock, I.F., Lee, C.M., Tunggal, J.K., Cowan, D.S., and Egorin, M.J. (2002). Limited penetration of anticancer drugs through tumor tissue: a potential cause of resistance of solid tumors to chemotherapy. *Clin Cancer Res* 8, 878-884.

Tannock, I.F., and Rotin, D. (1989). Acid pH in tumors and its potential for therapeutic exploitation. *Cancer Res* 49, 4373-4384.

Tol, J., and Punt, C.J. (2010). Monoclonal antibodies in the treatment of metastatic colorectal cancer: a review. *Clin Ther* 32, 437-453.

Tong, R.T., Boucher, Y., Kozin, S.V., Winkler, F., Hicklin, D.J., and Jain, R.K. (2004). Vascular normalization by vascular endothelial growth factor receptor 2 blockade induces a pressure gradient across the vasculature and improves drug penetration in tumors. *Cancer Res* 64, 3731-3736.

Torchilin, V. (2011). Tumor delivery of macromolecular drugs based on the EPR effect. *Adv Drug Deliv Rev* 63, 131-135.

Tredan, O., Galmarini, C.M., Patel, K., and Tannock, I.F. (2007). Drug resistance and the solid tumor microenvironment. *J Natl Cancer Inst* 99, 1441-1454.

Tunggal, J.K., Cowan, D.S., Shaikh, H., and Tannock, I.F. (1999). Penetration of anticancer drugs through solid tissue: a factor that limits the effectiveness of chemotherapy for solid tumors. *Clin Cancer Res* 5, 1583-1586.

Upton, R.N. (2007). Cerebral uptake of drugs in humans. *Clin Exp Pharmacol Physiol* 34, 695-701.

Vail, D.M., Amantea, M.A., Colbern, G.T., Martin, F.J., Hilger, R.A., and Working, P.K. (2004). Pegylated liposomal doxorubicin: proof of principle using preclinical animal models and pharmacokinetic studies. *Semin Oncol* 31, 16-35.

Vlahovic, G., Rabbani, Z.N., Herndon, J.E., 2nd, Dewhirst, M.W., and Vujaskovic, Z. (2006). Treatment with Imatinib in NSCLC is associated with

decrease of phosphorylated PDGFR-beta and VEGF expression, decrease in interstitial fluid pressure and improvement of oxygenation. *Br J Cancer* 95, 1013-1019.

Vukovic, V., and Tannock, I.F. (1997). Influence of low pH on cytotoxicity of paclitaxel, mitoxantrone and topotecan. *Br J Cancer* 75, 1167-1172.

Wedding, U., Honecker, F., Bokemeyer, C., Pientka, L., and Hoffken, K. (2007). Tolerance to chemotherapy in elderly patients with cancer. *Cancer Control* 14, 44-56.

Weinberg, R.A. (1996). How cancer arises. *Sci Am* 275, 62-70.

West, G.W., Weichselbaum, R., and Little, J.B. (1980). Limited penetration of methotrexate into human osteosarcoma spheroids as a proposed model for solid tumor resistance to adjuvant chemotherapy. *Cancer Res* 40, 3665-3668.

Widmer, N., Beguin, A., Rochat, B., Buclin, T., Kovacsics, T., Duchosal, M.A., Leyvraz, S., Rosselet, A., Biollaz, J., and Decosterd, L.A. (2004). Determination of imatinib (Gleevec) in human plasma by solid-phase extraction-liquid chromatography-ultraviolet absorbance detection. *J Chromatogr B Analyt Technol Biomed Life Sci* 803, 285-292.

Wildiers, H., Guetens, G., De Boeck, G., Verbeken, E., Landuyt, B., Landuyt, W., de Bruijn, E.A., and van Oosterom, A.T. (2003). Effect of anti-vascular endothelial growth factor treatment on the intratumoral uptake of CPT-11. *Br J Cancer* 88, 1979-1986.

Williams, R.D., Elliott, A.Y., Stein, N., and Fraley, E.E. (1976). In vitro cultivation of human renal cell cancer. I. Establishment of cells in culture. *In vitro* 12, 623-627.

Wilson, W.R., and Hicks, K.O. (1999). Measurement of extravascular drug diffusion in multicellular layers. *Br J Cancer* 79, 1623-1626.

Wong, P., Lee, C., and Tannock, I.F. (2005). Reduction of intracellular pH as a strategy to enhance the pH-dependent cytotoxic effects of melphalan for human breast cancer cells. *Clin Cancer Res* 11, 3553-3557.

Yarden, Y. (2001). The EGFR family and its ligands in human cancer. signalling mechanisms and therapeutic opportunities. *Eur J Cancer* 37 *Suppl* 4, S3-8.

Zhao, M., Hartke, C., Jimeno, A., Li, J., He, P., Zabelina, Y., Hidalgo, M., and Baker, S.D. (2005). Specific method for determination of gefitinib in human plasma, mouse plasma and tissues using high performance liquid chromatography coupled to tandem mass spectrometry. *J Chromatogr B Analyt Technol Biomed Life Sci* 819, 73-80.

Zheng, J.H., Chen, C.T., Au, J.L., and Wientjes, M.G. (2001). Time- and concentration-dependent penetration of doxorubicin in prostate tumors. *AAPS PharmSci* 3, E15.

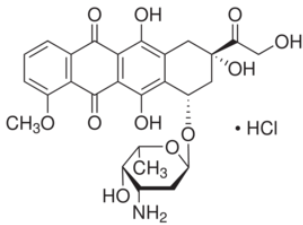
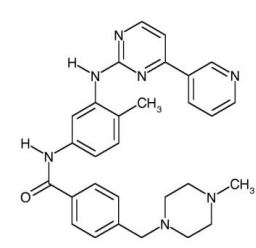
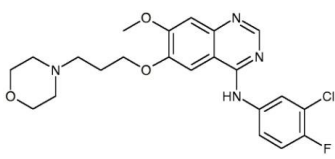
Zheng, X., Goins, B.A., Cameron, I.L., Santoyo, C., Bao, A., Frohlich, V.C., and Fullerton, G.D. (2011). Ultrasound-guided intratumoral administration of collagenase-2 improved liposome drug accumulation in solid tumor xenografts. *Cancer Chemother Pharmacol* 67, 173-182.

Zlotecki, R.A., Baxter, L.T., Boucher, Y., and Jain, R.K. (1995). Pharmacologic modification of tumor blood flow and interstitial fluid pressure in a human tumor xenograft: network analysis and mechanistic interpretation. *Microvasc Res* 50, 429-443.

Zondor, S.D., and Medina, P.J. (2004). Bevacizumab: an angiogenesis inhibitor with efficacy in colorectal and other malignancies. *Ann Pharmacother* 38, 1258-1264.

6. APPENDICES:

6.1 Appendix 1: Chemical structures and molecular weights of doxorubicin, imatinib and gefitinib:

Drug	Chemical structure	Molecular weight (g/L)
Doxorubicin	$C_{27}H_{29}NO_{11} \cdot HCl$ 	579.98
Imatinib	$C_{29}H_{31}N_7O$ 	493.6
Gefitinib	$C_{22}H_{24}ClFN_4O_3$ 	446.9

6.2 Appendix 2:

Summary of various analysis conditions used for doxorubicin, imatinib and gefitinib in the three different penetration systems:

Variable	Model	Drugs (100µM)		
		Doxorubicin	Imatinib	Gefitinib
Analysed sample (µL) + Internal standard (µL)	C↓D↓	100 + 100	100 + 300	100 + 300
	D↓	500 + 100	100 + 300	100 + 300
	D↓C↑	900+100	100+300	900+100
Internal Standard	C↓D↓	50µM	50µM	50µM
	D↓	500nM	500nM	500nM
	D↓C↑	500nM	500nM	500nM
Reconstitution volume (µL)	C↓D↓	100	400	400
	D↓	50	400	400
	D↓C↑	50	400	50
Injection volume (µL)	C↓D↓	10	50	30
	D↓	10	50	10
	D↓C↑	30	10	10
Estimated IFP (mmHg)	C↓D↓	+28	+28	+28
	D↓	0	0	0
	D↓C↑	+28	+28	+28
Analysing Machine	C↓D↓	HPLC	HPLC	HPLC
	D↓	HPLC	LC/MS	LC/MS
	D↓C↑	HPLC	LC/MS/MS	LC/MS/MS
Extraction method	C↓D↓	SPE	PPT	PPT
	D↓	SPE	PPT	PPT
	D↓C↑	SPE	PPT	SPE

SPE= Solid Phase Extraction, PPT= Protein Precipitation without evaporation.

7. CONFERENCE ABSTRACTS:

7.1 Abstract-1, presented in the BACR 50th Anniversary Meeting. “Hallmarks of Cancer: From Mechanisms to Therapies” held from 13th to 15th June 2010 at Heriot-Watt University, Edinburgh.

The development and evaluation of a model for assessing convective fluid flow through multicell layers in vitro

H Makeen¹, N Periasamy¹, PM Loadman¹, S Smye^{2,5}, B Sleeman³, P Jones⁴, C Evans⁵, C Twelves^{6,1}, RM Phillips¹

¹Institute of Cancer Therapeutics, University of Bradford, Bradford, West Yorkshire, United Kingdom, ²Department of Medical Physics and Engineering, Leeds Teaching Hospitals, St James's University Hospital, Leeds, West Yorkshire, United Kingdom, ³Department of Applied Mathematics, University of Leeds, Leeds, West Yorkshire, United Kingdom, ⁴Section of Molecular Gastroenterology, Leeds Institute of Molecular Medicine, University of Leeds, St James's University Hospital, Leeds, West Yorkshire, United Kingdom, ⁵Division of Medical Physics, Leeds Institute of Genetics, Health and Therapeutics, University of Leeds, Leeds, West Yorkshire, United Kingdom, ⁶Section of Oncology and Clinical Research, Leeds Institute of Molecular Medicine, University of Leeds, St James's University Hospital, Leeds, West Yorkshire, United Kingdom

One consequence of elevated interstitial fluid pressure (IFP) in solid tumours is that the normal process of convective fluid flow (CFF) through tissues is impeded. This is recognised as a major barrier to drug uptake leading to reduced drug efficacy. Studies of IFP have exclusively used in vivo models; the aim of this study was to develop an in vitro model that could be used to measure CFF. The model consists of a transwell cell culture insert which supports the growth of multicell layers (MCL) on collagen coated membranes with a pore size of 3 μm . A graduated tube is inserted into the transwell and a pressure gradient is applied across the membrane by raising the volume of medium in the tube above that of the bottom chamber. CFF is determined by measuring the weight of medium in the bottom chamber as a function of time. Using a physiologically relevant pressure gradient of 28.8 mmHg, CFF progressively decreased as the thickness of the MCL increased. DLD-1 MCL with a thickness of $47.6 \pm 11.2 \mu\text{m}$ completely impeded CFF. Using a MCL of $12.9 \pm 3.0 \mu\text{m}$ and a pressure gradient of 28.8 mmHg, CFF was 0.192 mL/min. Under these conditions, the rate of penetration of doxorubicin across the MCL was 75 fold greater

than when no pressure gradient exists. This model illustrates the pharmacological impact that reduced CFF can have on drug delivery; it also provides a model for evaluating strategies designed to restore CFF in tumours.

7.2 Abstract-2, Presented in the 5th Saudi International Conference, (SIC 2011), 23rd – 26th of June, 2011, the University of Warwick, Coventry, UK.

Influence of convective fluid flow on the penetration of anti-cancer drugs through multicell layers.

Hafiz Makeen¹, Nagarajan Periasamy¹, Paul M. Loadman¹, Pamela F. Jones², Brian D. Sleeman², Stephen W. Smye², Chris J. Twelves², Roger M. Phillips¹

¹University of Bradford, Bradford, ²University of Leeds, Leeds, United Kingdom.

Background and aims: Elevated interstitial fluid pressure (IFP) is a characteristic feature of many solid tumours. One consequence of elevated IFP is that the normal process of convective fluid flow through tissues is impeded, and this is now recognised as a major barrier to drug uptake. Therapeutic approaches designed to reduce tumour IFP with the aim of restoring convective fluid flow and hence enhance the delivery of partner therapeutics is currently of considerable interest. To date, studies of tumour IFP have almost exclusively used in vivo models. The aim of this study was to develop an in vitro model that could be used to measure convective fluid flow.

Model Design: The model is based upon the conventional transwell model for assessing drug penetration across multicell layers. This model consists of a transwell insert that is placed into 1 well of a 24 well plate (panel A). The top and bottom chamber is separated by microporous membrane upon which cells can be cultured to form multicell layers (panel B). Drugs are added to the top chamber and drug concentrations in the bottom chamber are measured as a function of time.

In the conventional apparatus, the level of medium in the top and bottom chamber is equal and no pressure gradient exists across the membrane. By inserting a graduated tube into the transwell apparatus (panel C), the level of medium in the top chamber can be raised above that in the bottom chamber and a pressure gradient across the membrane is formed, the

magnitude of which can be varied by adjusting the height of medium in the tube.

Analysis of convective fluid flow: DLD-1 human colon carcinoma cells were cultured on transwell membranes to various thicknesses and convective fluid flow was measured by weighing the bottom chamber at various time intervals after applying the pressure gradient. Following the application of a physiologically relevant (20.2 mmHg) hydrostatic pressure, convective fluid flow decreased as the thickness of the MCL increased. No fluid flow across the membrane occurred when the MCL was greater than 47.6 μm . In the absence of a MCL, fluid flow was 5.5 mL/min.

Proof of concept studies: DLD-1 human colon carcinoma cells were cultured on transwell membranes for 1 day ($12.91 \pm 4.50 \mu\text{m}$ thickness) and doxorubicin, gefitinib and imatinib at 100 μM were added to the top chamber in the presence or absence of a hydrostatic pressure gradient in individual experiments. The concentration of drugs were measured in the bottom chamber as a function of time using HPLC. At each sampling point, the medium in the top chamber was 'topped up' to ensure that both the pressure gradient and drug concentration remained constant. Similarly, medium in the bottom chamber was replaced at each time point with drug free medium. The rate of penetration of doxorubicin is significantly greater (approx 42 fold) when hydrostatic pressure of 20.2 mmHg is applied. In case of gefitinib and imatinib, the rate of penetration increased by 12 and 26 fold respectively when convective fluid flow was present.

Conclusions: The results of this study illustrate the importance of convective fluid flow for effective drug delivery. In tumours where the convective flow is reduced due to elevated tumour IFP, drug delivery is impaired. Strategies designed to enhance convective flow by manipulation of tumour cell or tumour/stroma interactions could enhance drug uptake and this model provides a 'tool' for evaluating such strategies. The limitation of the model is that it does not mimic the role played by the microvasculature in generating elevated interstitial fluid pressures in tumours.